

**INTEGRATING THERMAL ENERGY STORAGE AND NUCLEAR REACTORS: A
TECHNICAL AND POLICY STUDY**

A Dissertation
Presented to
The Academic Faculty

By

Cal Abel

In Partial Fulfillment
Of the Requirements for a Degree
Doctor of Philosophy in
Nuclear Engineering

Georgia Institute of Technology

May 2018

Copyright © 2017 by Cal Abel, Integrating Thermal Energy Storage and Nuclear
Reactors: A Technical and Policy Study is made available under a Creative Commons
Attribution 4.0 License (international)
https://creativecommons.org/licenses/by/4.0/deed.en_US

**INTEGRATING THERMAL ENERGY STORAGE AND NUCLEAR
REACTORS: A TECHNICAL AND POLICY STUDY**

Approved by:

Dr. Bojan Petrovic, Advisor
George Woodruff School of Mechanical
Engineering
Georgia Institute of Technology

Dr. S. M. Ghiaasiaan
George Woodruff School of Mechanical
Engineering
Georgia Institute of Technology

Dr. Valerie M. Thomas
H. Milton Stewart School of Industrial
and Systems Engineering
Georgia Institute of Technology

Dr. Anna S. Erickson
George Woodruff School of Mechanical
Engineering
Georgia Institute of Technology

Dr. Marilyn A. Brown
School of Public Policy
Georgia Institute of Technology

Dr. Eric P. Loewen
Nuclear Energy
GE-Hitachi

Date Approved: March 8, 2018

DEDICATION

This work is dedicated to those working for a better life and those committed to improving the lives of others.

ACKNOWLEDGEMENTS

This work would not have been possible without the tireless support of my wife, Bree Pattillo. Without her encouragement and support over the years, this work would never have reached fruition. I am grateful for the support from my academic advisor, Bojan Petrovic, for his guidance in preparing this work. To Chris Romero, who curated my research database and for filling the notes of references in this work. To Rod Adams and Will Davis who pushed back on many of the early concepts in this work, helping to steer my preliminary research. To Eric Loewen, who has been a mentor since the mid 1990's and who graciously accepted to be a member of my committee.

TABLE OF CONTENTS

Dedication	iii
Acknowledgements	iv
List of Tables	x
List of Figures.....	xii
Nomenclature	xvi
Summary.....	iii
Introduction.....	1
Part 1 – Policy Background	7
Chapter 1 Introduction.....	8
Chapter 2 Current Economic Environment.....	10
2.1 Softening Electricity Demand.....	10
2.2 Market Diversification.....	12
2.3 Shale Revolution and Monetary Policy	13
2.4 Variable Renewable Energy	16
Chapter 3 Direct Regulatory Costs	18
3.1 Linear-No-Threshold	18
3.2 Pre-Construction/Construction	21
3.3 Operational.....	23
3.4 Decommissioning	30

Chapter 4 New Nuclear Business Model.....	31
4.1 Energy Server.....	34
4.2 Limit Regulatory Liability	37
Chapter 5 Policy Recommendations	40
Part 2 – Basic Engineering Design	41
Chapter 1 Introduction.....	42
Chapter 2 Background	45
Chapter 3 Design Objectives and Approach	50
3.1 Heat Exchanger Network Design.....	51
3.2 Intermediate Heat Transport and Auxiliary Cooling Systems.....	53
3.3 Balance of Plant	60
Chapter 4 Facility Layout	64
Chapter 5 Material Selection	66
Chapter 6 Reactor Protection Systems	68
Chapter 7 Intermediate Heat Transport and Auxillary Cooling System	
Heat Exchanger Design	72
7.1 Regulatory Design Considerations	73
7.2 Intermediate Heat Transport System and Heat Exchanger Design..	74
7.3 Salt Heat Exchanger.....	78
Chapter 8 Auxiliary Cooling System Design	80
8.1 System Flow Path	80
8.2 Check Valve.....	83
8.3 Heat Exchanger Selection	86

8.4	Heat Exchanger Calculations	88
Chapter 9 System Response to Real World Data.....		91
Chapter 10 Conclusions.....		95
Part 3 – Control System Design.....		97
Chapter 1 Introduction.....		98
Chapter 2 Nonlinear System Dynamics Model		99
Chapter 3 Control System Design		103
3.1	Instrumentation and Control	104
3.2	State Equation	105
3.3	Design Specification	109
3.4	Loop Shaping and H_{∞} Synthesis	110
Chapter 4 Simulation Results		117
4.1	Open Loop Simulation without Control	117
4.2	Closed Loop Simulation with Optimal Control.....	119
Chapter 5 Conclusions.....		124
Part 4 – Safety Evaluation.....		125
Chapter 1 Introduction.....		126
Chapter 2 Background		128
2.1	Summary of Previous S-PRISM Study.....	130
2.2	Modification of S-PRISM.....	134
Chapter 3 Objectives and Approach.....		137
3.1	Transients to be Evaluated.....	138
3.2	Baseline Events	142

3.3	Modified Design Basis Event	142
3.4	Modified Bounding Events	143
Chapter 4 Computational Tools		147
Chapter 5 Computational Model.....		149
5.1	Baseline S-PRISM	149
5.2	Modified S-PRISM	168
Chapter 6 Transient Simulations		177
6.1	Comparison to Published Data.....	177
6.2	Unprotected Accidents.....	183
Chapter 7 Conclusions.....		196
Part 5 – Technological Implications		198
Chapter 1 Introduction.....		199
Chapter 2 Utility Simulation.....		201
Chapter 3 Non-conventional Applications.....		203
Chapter 4 Policy Limitations		206
4.1	Non-Light Water Reactor Licensing.....	206
4.2	Price Anderson and Liability	206
Chapter 5 Recommendations/Conclusions.....		208
Appendix A: Instructions for RELAP5-3D		210
A.1	Reference Design Initialization.....	210
A.2	nTES Design Initialization.....	211
A.3	Testing and Initialization	212
A.4	Bounding Events	213

References	214
-------------------------	------------

LIST OF TABLES

Table 1-1 Results from NRC SOARCA Using Different Dose-Response Models(NRC 2012)	26
Table 2-1 Reference design heat exchanger network parameters.....	52
Table 2-2 nTES design heat exchanger network parameters.....	52
Table 2-3 Compact intermediate heat exchanger design parameters.....	77
Table 2-4 Salt Heat Exchanger Design Parameters	79
Table 2-5 Summary of Butterfly Check Valve Design Parameters	86
Table 2-6 AHX Design Data for 40°C air inlet and T_{ave} of 432°C.....	87
Table 3-1 Core Physical and Control and Instrumentation Design Parameters.....	108
Table 3-2 Loop Design Parameters.....	108
Table 3-3 Core Reactivity Feedbacks at Various Times in Core Life	109
Table 3-4 Delayed Neutron Parameters at Various Times in Core Life.....	109
Table 3-5 Modeled Steady State to Steady State Step Response.....	117
Table 4-1 Previous Study S-PRISM Reactivity Feedbacks	131
Table 4-2 Modeled S-PRISM Delayed Neutron Precursor Data.	132
Table 4-3 Bounding Event Description	140
Table 4-4 Bounding Event Summary	141
Table 4-5 Reference S-PRISM Core Hydrodynamic Data.....	152
Table 4-6 Fuel Assembly RELAP Darcy Friction Factor Correlations	152
Table 4-7 Fuel Assembly Physical Parameters.....	153
Table 4-8 Edge and Corner Fuel Assembly Pin Heat Transfer Correlations.....	156

Table 4-9 Comparison of Various Fuel Pin Nusselt Numbers	157
Table 4-10 IHX RELAP Darcy Friction Factor Correlations	171
Table 4-11 IHX RELAP Hydrodynamic and Heat Structure Data.....	172
Table 4-12 SHX RELAP Darcy Friction Factor Correlations	172
Table 4-13 SHX RELAP Hydrodynamic and Heat Structure Data.....	173
Table 4-14 AHX RELAP Darcy Friction Factor Correlations	174
Table 4-15 AHX RELAP Hydrodynamic and Heat Structure Data	175
Table 4-16 Comparison of (Dubberley 2008) and Modeled BLE-2.....	179
Table 4-17 Reference to Model Comparison for BLE-2	180
Table 4-18 Full Power Fuel Assembly Bulk Coolant Outlet Temperatures	181

LIST OF FIGURES

Figure 1 Single channel IHTS/ACS train including safety-grade boundary	4
Figure 1-1 United States (total) electricity demand (left axis), Illinois and Pennsylvania (right)[7].....	11
Figure 1-2 PJM Fuel Adjusted Locational Marginal Price (Referenced to 1999 Fuel Prices)[9].....	12
Figure 1-3 Henry Hub natural gas spot prices January 2000 to July 2017 Source EIA[14]	14
Figure 1-4 Debt and equity investment in shale plays. Source WSJ[1].....	15
Figure 1-5 Load duration curves with different amounts of VRE[15]	17
Figure 1-6 Trends in nuclear plant construction in the United States as a result of the response to Three Mile Island accident [17].....	22
Figure 1-7 PJM Reliability Metrics [2].....	32
Figure 1-8 Conceptual energy server configuration	35
Figure 2-1 nTES conceptual site layout.....	44
Figure 2-2 PRISM reactor vessel cutaway[48].....	48
Figure 2-3 PRISM reactor vessel closure head[48]	49
Figure 2-4 T-s diagram of a concept nTES OTSG	52
Figure 2-5 Modified PRISM conceptual configuration	55
Figure 2-6 Reactor Protection System Logic.....	69
Figure 2-7 Heatric heat exchanger operational envelope from Southall and Dewson[1].	72

Figure 2-8 Intermediate Heat Exchanger (a) plate profile view (b) IHX top down view inside reactor vessel (c) IHX radial view showing salt flow path.	75
Figure 2-9 Conceptual ACS flow path.....	80
Figure 2-10 Natural circulation temperature profiles	81
Figure 2-11 Single channel ACS performance for various salt inlet temperatures to the AHX.....	90
Figure 2-12 85% Combustion Turbine Control Salt Tank Level in m ³ for BPA service area from January 1, 2007 to December 31, 2011. The red line is the minimum tank level for pump NPSH.....	92
Figure 2-13 35% Combustion Turbine Control Salt Tank Level in m ³ for BPA service area from January 1, 2007 to December 31, 2011	93
Figure 2-14 Outage schedule for BPA service area when repowered with 840 MW(t) Mod B PRISM reactors using nTES. Reactors assume an 18-month cycle and 1 month refueling outages.....	94
Figure 2-15 Histogram of power transients greater than 1%/min (0.01 on the X-axis) for BPA service area from January 1, 2007 to December 31, 2011	94
Figure 3-1 Counter-flow heat exchanger governing equations.....	101
Figure 3-2 General closed loop controller model	103
Figure 3-3 Bode diagrams for the closed loop system.....	113
Figure 3-4 Sensitivity and complimentary sensitivity graphs.....	114
Figure 3-5 Controller disturbance and noise gains	115
Figure 3-6 Final closed loop controller.....	116
Figure 3-7 Transient response to a step change in pump flow	119

Figure 3-8 Closed loop response to step change in desired power level.	121
Figure 3-9 Closed loop external reactivity response to step change in desired power. ..	122
Figure 4-1 Core RELAP hydrodynamic structures.....	154
Figure 4-2 nTES primary heat transport system.....	159
Figure 4-3 EM pump coastdown curve(NUREG)	161
Figure 4-4 Reference S-PRISM IHTS	164
Figure 4-5 S-PRISM steam generator configuration [108].....	167
Figure 4-6 'A' Train IHTS for nTES S-PRISM.....	169
Figure 4-7 nTES Salt Heat Transport System.....	171
Figure 4-8 Comparison of NUREG-1368 to the modeled plant. Figure (a) is from NUREG-1368. Figure (b) is the model in two different scenarios, the one labeled NUREG is for a direct comparison to (a) the nominal assumes an intact safety boundary.	178
Figure 4-9 UTOP BE-1A using NUREG-1368 temperature feedbacks	182
Figure 4-10 Reactivity and power response to a loss of 1 RCP without protective action	184
Figure 4-11 Fuel temperatures during a reactor SCRAM with 1 RCP failing to coastdown	185
Figure 4-12 Loss of heatsink due to sabotage.....	186
Figure 4-13 Core outlet temperature for ATWOS compared to nominal loss of both ACS channels.....	187
Figure 4-14 Hottest pin adjusted temperatures during protected transient over power ..	189
Figure 4-15 Extended UTOP with plant trip.....	190

Figure 4-16 Salt Coolant Pump overspeed transient response using [90] BOC temperature feedbacks.....	191
Figure 4-17 BE-5C Salt pump overspeed using NUREG-1368 temperature feedbacks	192
Figure 4-18 Unfaulted SBO transient Response.....	193
Figure 4-19 Core outlet temperature during a rupture of a single SHX heat exchanger	194
Figure 4-20 DBA Hot pool temperature response	194
Figure 5-1 nTES integrated with Bonneville Power Administration.....	201
Figure 5-2 Estimated process heat distribution from MECS 2006.....	204

NOMENCLATURE

ACE	AXI Coherency Extension	CDR	Cool Down Rate
ACS	Auxiliary Cooling System	COL	Construction and Operating License
AHTR	Advanced High Temperature Reactor	CRBR	Clinch River Breeder Reactor
AHX	Air Heat Exchange	CRDM	Control Rod Drive Mechanism
ALARA	As-low-as-reasonably-achievable	DOE	US Department of Energy
ALMR	Advance Liquid Metal Reactor	DHR	Decay Heat Removal
ANS	American Nuclear Society	DRACS	Direct Reactor Air Cooling System
ASME	American Society of Mechanical Engineers	EBR	Experimental Breeder Reactor
ASTM	American Society for Testing and Materials	ECCS	Emergency Core Cooling System
ATWS	Anticipated Transients Without SCRAM	EES	Engineering Equation Solver
BDBA	Beyond Design Basis Accidents	EFOR	Equivalent Forced Outage Rate
BE	Bounding Event	EIA	US Energy Information Agency
BEAR	Biological Effects of Atomic Radiation	EM	Electromagnetic
BOC	Beginning of Cycle	EOC	End of Cycle
BOP	Balance of Plant	EPA	US Environmental Protection Agency
CAPEX	Capital Expenditure	EPC	Engineering Procurement Construction Contractor
CASIO	California Independent System Operator		

ERANOS	European Reactor Analysis Optimized code System	LMP	Locational Marginal Price
		LNG	Liquified Natural Gas
ERCOT	Electric Reliability Council of Texas	LNT	Linear-No-Threshold
		LOCA	Loss-of-coolant accident
FPHX	Fin Plate Heat Exchange	LOHS	Lost of heat sink
GDC	General Design Criteria	LSF	Low Salt Flow
GE	General Electric company	LTI	Linear Time Invariant
GE-H	General Electric-Hitachi	LWR	Light Water Reactor
GEM	Gas Expansion Module	MACCS	MELCOR Accident Consequence Code Systems
HRSR	Heat Recovery Steam Generator		
HT9	is a 12Cr-1 Mo-VW steel	MATS	Mercury and Air Toxic Standards
ICP	Inductively Coupled Plasma	MECS	Manufacturing Energy Consumption Survey
ICRP	International Commission on Radiological Protection	MIMO	Multiple inputs, multiple output
ID	Internal Diameter	MISO	Midcontinent Independent System Operator
IFR	Integral Fast Reactor		
IHTS	Intermediate Heat Transport System	MFP	Mean Free Path
		MOC	Middle of Cycle
IHX	Intermediate Heat Exchanger	NC	Natural Circulation
INL	Idaho National Laboratory	NFRC	Nuclear Fuel Recycling Center
IOMP	International Organization for Medical Physics	NGNP	Next Generation Nuclear Plant
ISO	International Organization for Standardization	NI	Nuclear Instrument

NOT	Normal Operating Temperature	PRA	Probabilistic Risk Assessment
NPS	Normal Pipe Size	PRISM	Power Reactor Innovative Small Module
NRC	Nuclear Regulatory Commission	PSER	Preapplication Safety Evaluation Report
nTES	Nuclear Thermal Energy Storage	PSID	Panel Study of Income Dynamics
NTU	Nuclear Time Unit	PWR	Pressurized Water Reactor
NUREG	US Nuclear Regulatory Commission technical report designation	RCP	Reactor Coolant Pump
NYISO	New York Independent System Operator	RE	Renewable Energy
O & M	Operation & Maintenance	RELAP	Reactor Excursion and Leak Analysis Program
OPEX	Operational Expenditure	RHR	Residual Heat Removal
ORNL	Oak Ridge National Laboratory	ROI	Return on Investment
OTSG	Once through steam generator	RPS	Reactor Protection System
PCHX	Printed Circuit Heat Exchanger	RTD	Resistance Temperature Detector
PCS	Power Conversion System	RTO	Regional Transmission Operator
PHTS	Primary Heat Transfer System	RVACS	Reactor Vessel Auxiliary Cooling System
PID	Proportional Integral Derivative	SAGD	Steam Assisted Gravity Drain
PJM	Pennsylvania-New Jersey-Maryland Interconnection, LLC	SBO	Station Black Out
POAH	Point of Adding Heat	S-CO ₂	Supercritical Carbon Dioxide
		SCRAM	Safety Control Rod Activation Mechanism

SFR	Sodium Fast Reactor	UTOP	Unprotected transient overpower
SG	Steam Generator		
SHTS	Salt Heat Transport System	VRE	Variable Renewable Energy
SHX	Salt Heat Exchange		UNITS
SISO	Single input, Single output	ΔP	change in Pressure
SIV	Safety Isolation Valve	ΔT	change in Temperature
SMR	Small Modular Reactor	¢/s	cents per second
SNAP	Symbolic Nuclear Analysis Package	$^{\circ}\text{C}$	degree Celsius
SOARCA	State-of-the-Art Reactor Consequence Analyses	(e)	Electricity
S-PRISM	Super Power Reactor Innovative Small Module	β	heat transfer surface area to total volume
SS	Stainless Steel	∞	infinity
STP	South Texas Project	(t)	Thermal
STP	South Texas Project	atm	atmosphere
TES	Thermal Energy Storage	dB	decibel
TRU	Transuranic waste	GW	Gigawatt
TTD	Terminal Temperature Difference	K	Kelvin
TVA	Tennessee Valley Authority	kg	kilogram
		kJ	kilojoule
ULOHS	Unprotected loss of heat sink	KNO_2	Potassium Nitrite
		KNO_3	Potassium Nitrate
ULOF	Unprotected loss of flow	kPa	kilopascal
UNSCEAR	United Nations Scientific Committee on the Effect of Atomic Radiation	kW	kilo Watt

lm	log-mean temperature	OD	outside diameter
mils	one thousandth of an inch	pcm	per cent mille
MKS	Meter, kilogram, second	P/D	pitch to diameter
MPa	Megapascal	POAH	Point of Adding Heat
Mt/a	Metric tons per atom	psig	pounds per square inch gauge
m	meter	PW	Petawatt
mm	millimeter	rad/s	radians per second
mSv	millisievert	rem	roentgen equivalent man
MW	Megawatt	T	temperature
N ₂	Nitrogen	T _c	cold leg temperature
Na	Sodium	T _h	hot leg over temperature
Na ₂ O	Sodium Oxide	UA	overall heat transfer coefficient and heat exchanger area
NaNO ₂	Sodium Nitrite		
NaNO ₃	Sodium Nitrate		

SUMMARY

Combining Thermal Energy Storage (TES) and mid-temperature nuclear reactors is not a new concept. What has not been done is to move the combination of these two technologies past the purely conceptual phase. The primary purpose of this work is to: 1) create a detailed enough engineering design to be able to 2) propose a fully automatic plant control logic under normal operations, 3) to conduct a preliminary safety analysis consistent with what was originally done in NUREG-1368, the Preapplication Safety and Evaluation Report for the Power Reactor Innovative Small Module (PRISM), and 4) evaluate the anticipated operation using real world data.

What this work shows is that the nuclear TES (nTES) concept is achievable using existing technologies and conventional materials. It shows that fully automated plant control is achievable meeting an anticipated operational envelope defined by studying real world utility level electricity demand data. The proposed design offers a third independent safety-grade system to the design reference PRISM, improving the integrated nTES safety performance over the already impressive performance of the reference design. Finally, this work shows that the integrated design can meet a utility's entire demand profile, with the reactors operating with a capacity factor of over 90%, including planned outages.

The nTES concept successfully decouples the kinetics of the reactor from the final output of the turbine generator, allowing the facility to operate with automatic generator control and be fully compliant with 10 CFR 50 restrictions requiring only licensed operators to control reactor power. The proposed design also shows that electrical power

is not needed to ensure reactor safety because the integrated design can indefinitely passively remove decay heat without operator intervention or electrical power even under extreme accident scenarios. The combined system allows nuclear energy to expand beyond baseload electricity improving the fundamental economics.

INTRODUCTION

Nuclear energy faces significant economic hurdles limiting even the viability of current generating assets, much less future ones. The current Light Water Reactors, LWRs, are well suited to provide low cost power, but the flattening demand curve in many deregulated electricity markets is significantly reducing the marginal revenue from these facilities. Current operational restrictions and economics prevent these reactors from accessing ancillary markets to increase their revenue by supply additional services or shifting their generation to times of increased value.

While next generation nuclear facilities will be able to provide improved plant flexibility and diversification into other energy services such as process heat, they are still destined to the same fate by simple economics. Nuclear energy has an almost zero marginal cost of electricity production and a large fixed cost when compared to other power sources. This means that the reactors will need to run at maximum capacity, earning maximum income, all of the time to attain the greatest capital recovery. To address this limitation, the reactor's thermal output needs to be separated from its electrical output. One viable way to do this is to add some form of energy storage, either thermal or electrical.

Historical implementations of energy storage by a nuclear power plant was done by coupling the reactor's electrical output with pumped hydro facilities. An example of this is the Tennessee Valley Authority's (TVA) coupling of Sequoyah Nuclear Power Plant (NPP) with Raccoon Mountain pumped hydro facility. During off-peak grid-demand periods NPP-generated electricity is directed to pumps to lift water below the

hydro-plant spillway back up to the hydro facility reservoir. While effective and relatively low cost, pumped hydro is significantly limited by geography. What is needed is a low cost scalable solution. One such technology that uses thermal storage and is commercially deployed globally is solar thermal. In this application, the heat supply is variable and the output is constant. In the nuclear application, the heat supply is constant while the load is variable.

Thermal energy storage with nuclear reactors is not an entirely novel concept. What has not been shown is taking a detailed conceptual design, sizing it to meet real world needs, designing a control methodology, and evaluating the impact of such a design on reactor safety. The purpose of the present study was to answer these remaining questions. In so doing, more questions emerged and are detailed for future work.

Solar salt, a binary eutectic of potassium and sodium nitrates, was selected as the best candidate for nTES. It has an operational temperature range of 250°C to 600°C, which is well suited for sodium fast reactors – primary coolant temperatures of 360°C at the core inlet to 499°C at the core outlet. Of these designs, the one that is farthest along with the most published data is General Electric-Hitachi's (GEH) Power Reactor Innovative Small Module (PRISM). This work demonstrated the integrated concept with PRISM's larger sibling, the Super-PRISM (S-PRISM).

The PRISM Intermediate Heat Transport System (IHTS) was split into two separate and independent trains. Each IHTS train was given its own Auxiliary Cooling System (ACS). Because this design uses a compact heat exchanger to transfer heat from the IHTS, there was not enough external surface area to use it for heat transfer to the ACS, similar to how the exterior of the Steam Generator (SG) is used to transfer heat to

the ACS. This difference in arrangement from the conventional PRISM necessitated the ACS to have an additional heat transfer surface for Decay Heat Removal (DHR). Each IHTS/ACS train (Figure 1) is an entirely independent safety-grade path for DHR. The nTES design has three safety-grade avenues for DHR compared to the conventional PRISM's two. This provided an improvement in off-normal plant operations when one safety-grade path for DHR was removed/degraded. Otherwise the response of the nTES to the events considered was identical to the conventional PRISM. In the bounding events that included a Loss of Heat Sink (LOHS), the use of nTES resulted in significantly lower structural temperatures. For every bounding event considered with nTES, the primary hot pool temperature never exceeded 630°C, even for events that caused a loss of two safety-grade DHR paths.

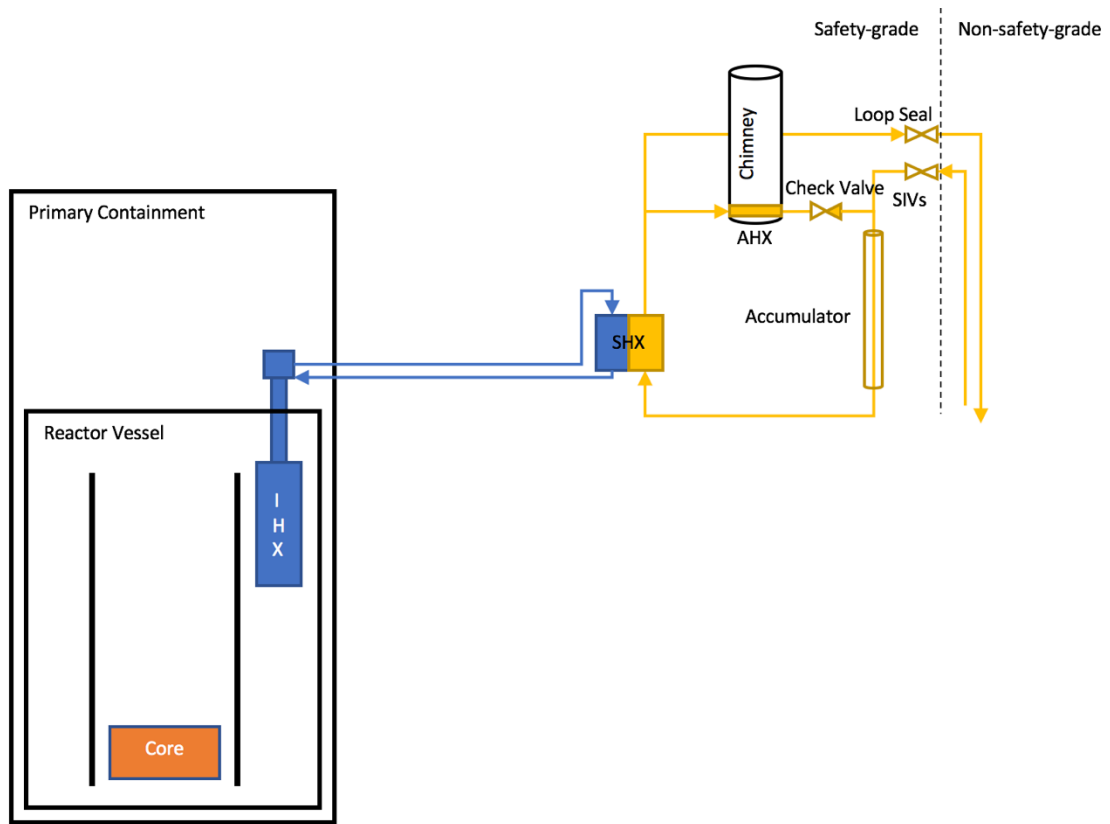


Figure 1 Single channel IHTS/ACS train including safety-grade boundary

For the scoping study, the nTES was sized to meet the entire load profile for the Bonneville Power Administration (BPA) using a study period from January 2007 to December 2011. To do this, twenty-one Mod B PRISM reactors (840 MW(t) each) were needed. For the design, two reactor modules were paired with one thermal storage system resulting in 10 independent systems. The thermal storage design for each reactor pair was sized to match the Andasol Solar Power Station in Spain. This selection was arbitrary, and was done to provide a comparison to a system that had already been built and was in commercial operation. Over the BPA study period spanning 35,064 operating hours, the largest reactor transient was 4.2%/min, with a very simple bang-bang control for salt tank level. This can easily be improved upon. This information was then used to create a modern control architecture for the nTES using H_{∞} synthesis. The plant was required to

transition from steady-state 50% power to steady-state 100% power in 10 minutes, while maintaining constant salt temperature, having zero power overshoot, and minimal control action. This design basis transient was fully achieved, the reactor reached 90% power within 3 minutes and used the remaining 7-minutes to achieve equilibrium conditions. A maximum reactivity insertion rate of 7.5 pcm/s was used, which is the design limit reported for PRISM. This control system had an effective 13.3%/min rate of power change, three times that needed for the design basis operational transient, demonstrating that fully automatic reactor plant control is achievable with this design.

This work first sets the policy and market stage in Part 1, putting the utilities' needs in perspective and illustrating how the current nuclear power business model is failing in the United States. Unfortunately, a new business model cannot be met by conventional LWR designs. That is not to say that conventional reactors won't serve a market niche in the future, just that that niche is smaller than the current generating capacity of the existing fleet of LWRs, even in regulated markets.

Part 2 of the dissertation goes through the conceptual design work for assembling a suite of technologies that meet the new business model. This begins with a survey of past work, then it shifts to merging the different technologies into a cohesive and integrated system. In doing this integration, much of the work will be on simplifying the design and collapsing the nuclear island to as small a physical footprint as possible.

Part 3 looks at how the system would function under normal operations and proposes method of integrated and automatic plant control using modern control theory under H_∞ synthesis. This part answers questions about the stability and controllability of the system. If the system is not stable or controllable, it will have serious operational

consequences that make it not suitable for a utility's needs. This part shows that not only is the plant stable and controllable, but that fully automatic control with simultaneous reactivity insertions from control rods and changing cooling flow is a viable automatic or operator assisted control architecture. This dissertation shows that the system is capable of level 0 through 3 automation, no automation to conditional automation without a human in the loop.

Part 4 shifts focus to how the plant responds to protected and unprotected off-normal operations and is divided into three portions. The first portion of this part establishes a baseline design reference. This creates a benchmark to compare the modifications made to the plant to integrate nTES.. The second portion shows that the reactor protective features both inherent and electronic are adequate to ensure plant safety. The third portion demonstrates that the inherent safety features provide adequate safety margin when the electronic means of plant protection fail. This part uses the evaluation approach of NUREG-1368, Preapplication Safety Evaluation Report of the PRISM, to provide a more direct comparison between the conventional PRISM and the PRISM coupled with nTES.

Part 5 then answers, "Why should this concept be built?" It does this by illustrating what a utility can expect from this power station, what regulatory advantages it offers, what potential regulatory hurdles it could face, and what can be done to address those regulatory challenges.

PART 1 – POLICY BACKGROUND

CHAPTER 1 INTRODUCTION

Nuclear energy is facing significant challenges in the market regarding the construction of new power plants and the continued operation of existing units. Many of these challenges can be grouped into three main areas: direct regulatory costs, changing market conditions, and general energy policy. If we are to consider a more effective design approach, we must consider these fundamental constraints in our design methodology. Here an effective design is one that can receive the financial backing to be built, can be built in a meaningful and economic timescale, and can operate providing adequate payment to those providing the financing.

In the early part of last decade, the existing nuclear plants were being spun off from vertically integrated utilities into the new deregulated electricity markets.[2] Nuclear at the time had one of the lowest marginal prices of any generator. The utilities that spun off these reactors were able to capitalize on the high Locational Marginal Prices, LMP, creating a significant windfall and return for their shareholders.[3] This set the stage for what was going to be a nuclear renaissance, which abruptly ended in 2011. While the accidents at Fukushima Daiichi certainly put a damper on the hopes for new nuclear builds, other than some modifications to the existing units, the fallout, wasn't significant.[4] What drove the end of the renaissance in the United States were predominantly economic forces.

While regulation is certainly a factor it serves more to inhibit certain economic opportunities, some intentionally and most as an unintended consequence. By restricting specific operational activities, certain business activities are correspondingly restricted.

This tends to exacerbate negative economic forces making marginal economic activities no longer viable.

This part will first discuss the economic environment that the nuclear industry is facing. It will then discuss historical factors, including regulations that have impacted the construction and operational costs associated with nuclear reactors. It will then shift to how these economic and policy constraints are causing the current business model, baseload generation, to fail and to propose a new business model.

CHAPTER 2

CURRENT ECONOMIC ENVIRONMENT

2.1 Softening Electricity Demand

The role of energy in the economy is something that is not well understood by economists in general. It is generally relegated to the role of a simple exogenous input.[5] It is much more than this. Energy is what allows capital to move when directed by labor. To give an example of the scale of this consider some food, a shovel, and a laborer. How quickly can they dig a ditch? Now, change that to be diesel fuel, an excavator, and the same laborer. Comparatively, in which are capital and labor more productive with increased economic activity? The latter case has the greatest economic activity, the worker's productivity is orders of magnitude higher. But what drove that productivity?

Energy is not an end it is the means to the ends. Energy when properly considered in economic activity is 80% of GDP.[5] More specifically, exergy, useful work, is 80% of GDP. Electricity is basically pure exergy, electrical components have such high conversion efficiencies, that conversion from electricity to the useful output is effectively 1:1.

Since 2008, electricity demand nationally has been relatively flat. In fact, 2016 had lower total electricity demand than did 2008 and demand has been relatively constant since 2010, Figure 1.1.[6] Using Ayers and Warr's work, this suggests that there was a rebound from the recession in 2010 and that there has been little to no economic growth since.

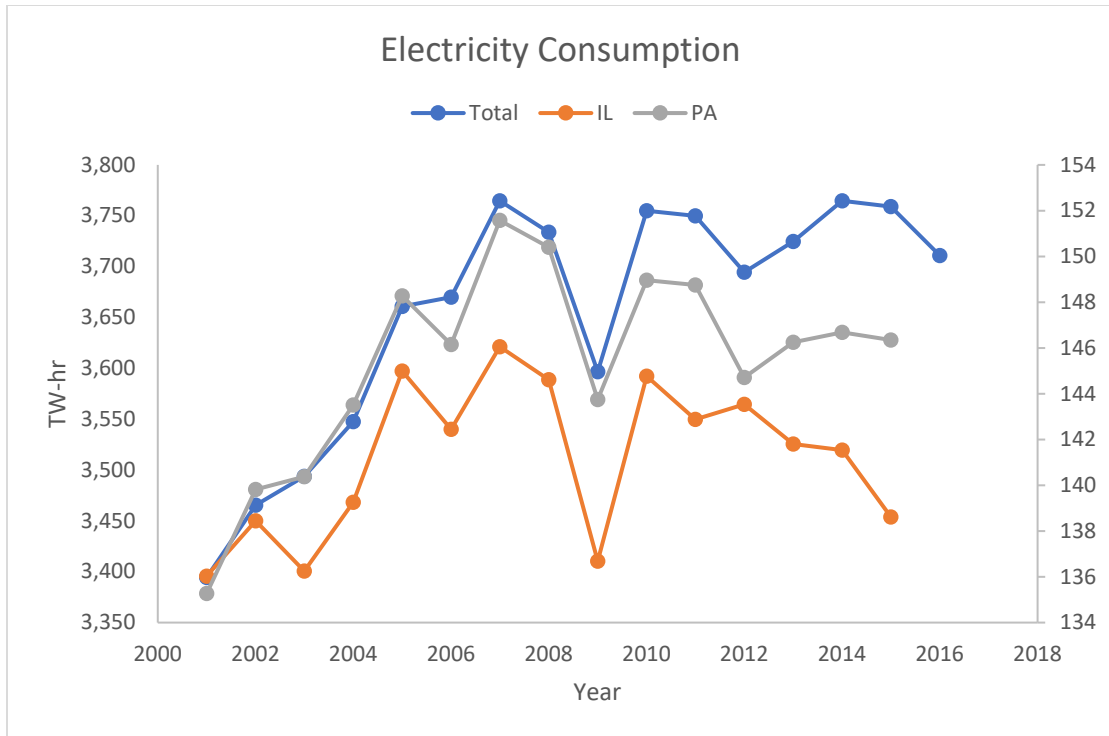


Figure 1-1 United States (total) electricity demand (left axis), Illinois and Pennsylvania (right)[7]

If we consider the two states with the largest nuclear generation portfolios, Illinois and Pennsylvania, their electricity markets are shrinking in size.[8] This suggests an overall reduction in economic activity in these states, and growth of economic activity in other states. Their declining electricity market is putting downward pressure on the capacity and LMP.[8] Based on the structure of the PJM market, there are two markets in which nuclear can participate, capacity and LMP. The LMP price history shown in Figure

1.2 shows the downward trend in LMP for the PJM market since 2007.[9]

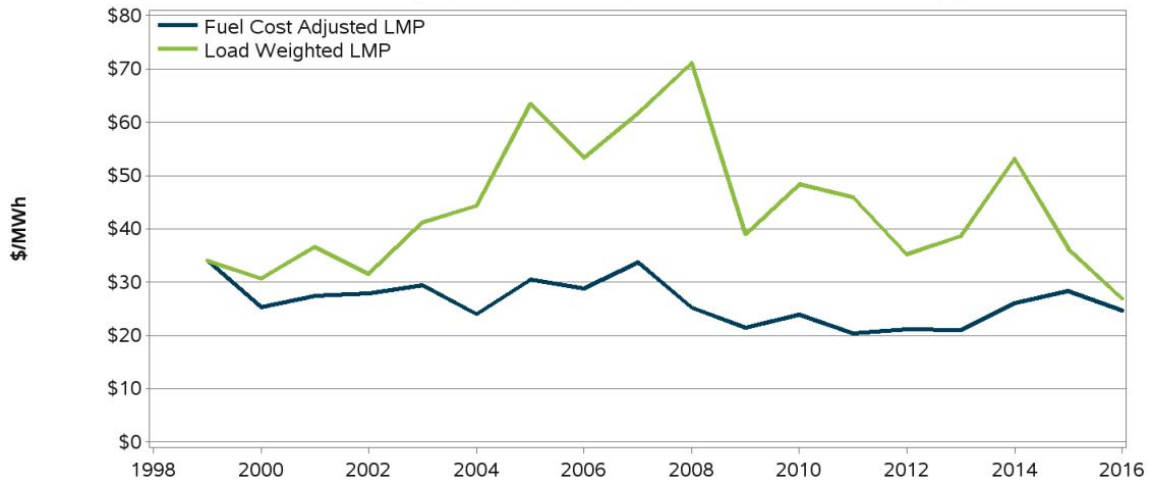


Figure 1-2 PJM Fuel Adjusted Locational Marginal Price (Referenced to 1999 Fuel Prices)[9]

2.2 Market Diversification

The deregulated markets initially launched as very simple markets, focusing on creating LMP. Since this time, they have implemented capacity and other ancillary markets, such as regulatory mileage and reserve markets. The increased market diversification allows for better pricing to consumers. It does this by differentiating the services and specifically compensating those services provided in a competitive market. Markets with low diversification will tend to have higher average prices, due to paying for services not rendered. This gradual market creation/diversification leads to revenue insufficiency for those plants which provide the service but are not appropriately compensated.[2] By creating other markets those that can diversify will and those that can't are even more constrained and susceptible to market upsets.

Nuclear can only effectively participate in the LMP and capacity markets. This is due to regulatory and technical issues.[10] As a result, prior revenues that included

services that weren't rendered through aggregation, are now segregated resulting in an effective loss of revenue.

The markets do not adequately compensate for services such as resilience, and fuel security.[2] An example of the importance of resilience is the performance of the South Texas Project nuclear generating station during the recent hurricane Harvey. STP accounted for 50% of the generation operating margin during and shortly after the Harvey. Other generators were forced to shut down as a result of the storm.[11]

Much of nuclear plants' resilience comes from the regulatory requirements to ensure a means of decay heat removal. This translates into significantly hardened sites that are resistant to flooding and worst case natural disasters. This makes nuclear plants more expensive, a cost that is not currently accounted for in the markets and represents "revenue insufficiency" for these generators.[2]

2.3 Shale Revolution and Monetary Policy

The shale revolution has had a tremendous impact on the overall supply of natural gas in the United States. It has significantly increased market supplies of natural gas, so much so that significant investment has been made in building LNG export capacity, when only a few years ago, it was an increase in LNG import terminals. This has had a corresponding increase in natural gas electricity generation and has suppressed prices in markets like PJM.[8]

Oil and gas exploration/production is a high risk/high yield business. It has benefited significantly from investors seeking yield.[1] These investors have been driven to seek yield because of the protracted low interest rates, forced to gamble for returns. It

is particularly driven by the fixed income groups, insurance and pensions.[12] Other investors face similar constraints to those of the fixed income category.

Investment in the shale revolution has been and continues to be a money losing proposition.[1] As the initial hedges that occurred when oil prices declined from their previous highs in 2012 start to expire. Oil and gas producers will face further losses as market prices are below the expiring hedges.[13]

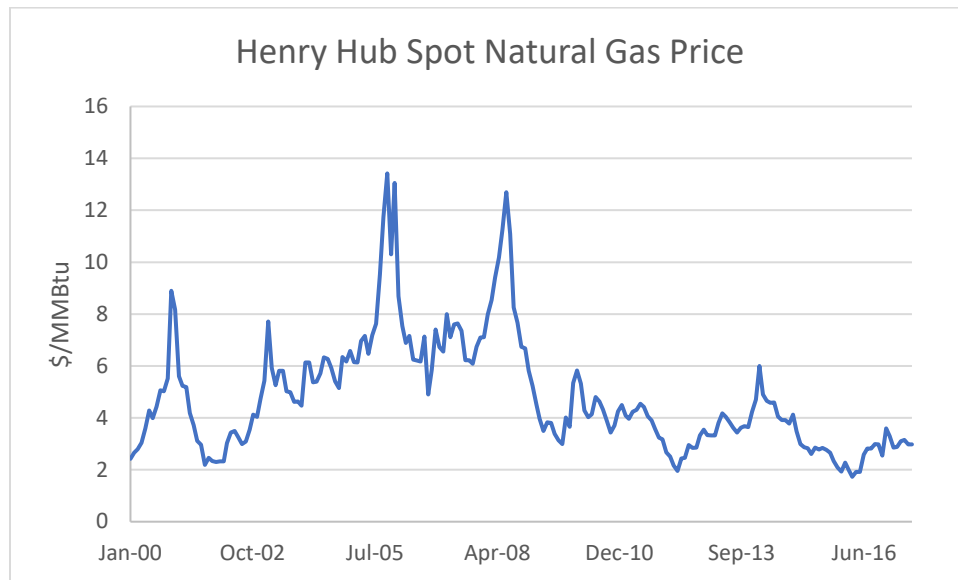


Figure 1-3 Henry Hub natural gas spot prices January 2000 to July 2017 Source EIA[14]

Betting on Shale

U.S. drillers have been awash in Wall Street cash, though that funding has begun to slow down.

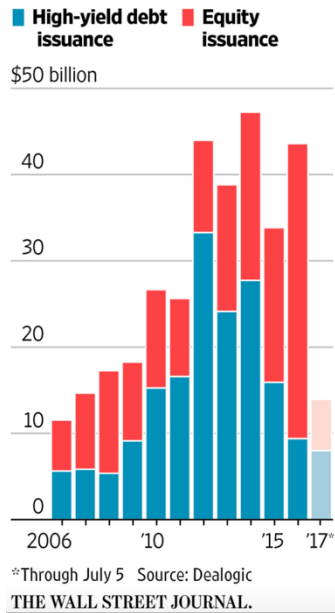


Figure 1-4 Debt and equity investment in shale plays. Source WSJ[1]

Figures 1.3 and 1.4 show how debt and equity investment have followed price expectations in the shale plays. The recent decline in investment suggests that yield returns are not consistent with price rebounding to higher levels to be able to support current production levels.

The current production of shale has for the first time allowed natural gas to displace coal as the primary source of energy for electricity production.[2] This change over, was due to multiple factors including increased regulatory costs, e.g. MATS, but was predominantly driven by low natural gas prices leading to more favorable conditions for natural gas production. This is accelerated by the fact that natural gas plants are highly modular and can be constructed in under two years.

2.4 Variable Renewable Energy

Renewable energy has seen significant incentives for increasing production in the past two decades. This has been mainly driven by a policy goal of electrical grid decarbonization in response to concerns over Anthropogenic Global Warming, AGW. The policy support has come in two major forms. First is through renewable portfolio standards, mandated consumption, and through tax incentives such as production and investment tax credits, price supports. This has created a set of incentives for the inclusion of VRE in the grid that are not sensitive to market pricing.

VRE is treated as a fungible commodity to electricity. However, it is not. Looking at the historical development of deregulated markets the initial markets just looked at marginal prices and did not include certain desirable features that led to revenue insufficiency for some generators. With the inclusion of VRE on the grid under current market structures there is a new revenue insufficiency for dispatchable generators, which creates a revenue surplus for VRE. This is a policy induced market failure. The variability of VRE increases the variability in remaining load not serviced by VRE. The net load duration curves from Denholm et al., Figure 1.5, show how VRE acts to increase this variability, by effectively eliminating baseload energy with as little as 30% market penetration. To be entirely fungible with the current grid VRE needs to have 100% backup capacity, MW for MW. This is not done so the cost of the uncertainty of the VRE is passed onto other generators in the form of an externality.

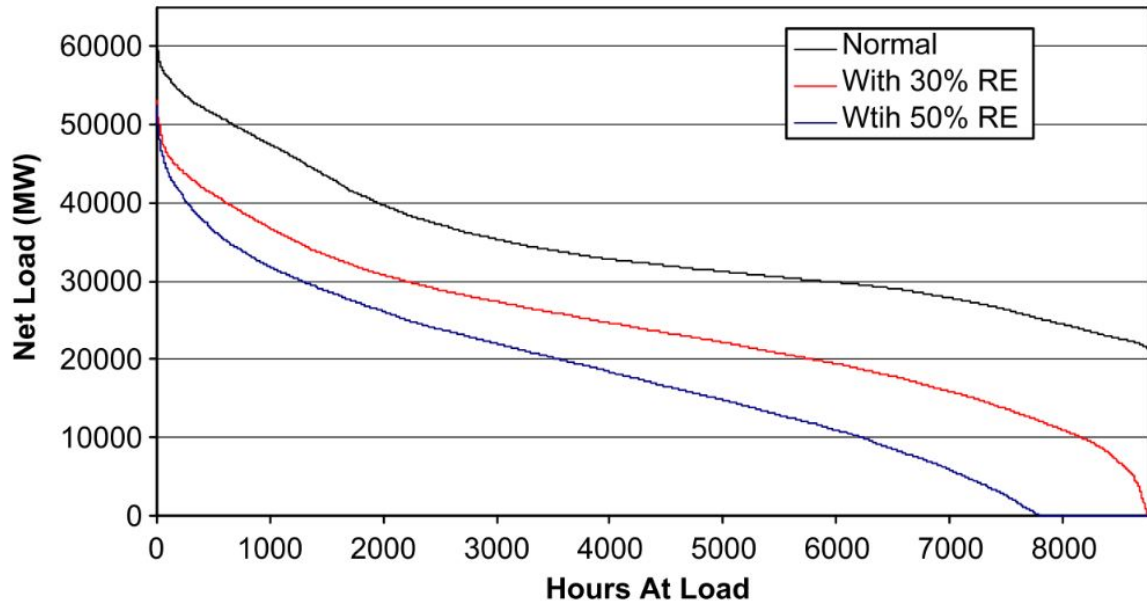


Figure 1-5 Load duration curves with different amounts of VRE[15]

The current markets have responded to the inclusion of VRE through a reduction in the capacity market prices and an increase in the regulatory mileage and needed reserve capacity margins to be able to balance the VRE. This effectively places a premium on flexibility over stability.[2]

While the markets of PJM and MISO have not had significant VRE penetration ERCOT and CAISO have. The proposed closure of Diablo Canyon Units 1 and 2 cited declining market conditions. Indian Point 2 &3, Nine Mile Point, Ginna, and Fitzpatrick, all within the NYISO, cited economic conditions for plant closure.[2] NYISO has 23% of its power come from VRE, with 3,737 of wind generating capacity in 2016.[16] The inability of nuclear to operate in a more flexible manner has led to the planned closure of all remaining nuclear generating assets in the state. The impact of VRE in PJM has been relatively small due its small market share.[8]

CHAPTER 3 DIRECT REGULATORY COSTS

Regulation has significant impact on the overall construction costs and has been identified as an impediment for the construction of new nuclear reactors in the United States.[2] It has led to a more than 2x cost and project timeline for reactors in the United States.[17] Pertinent federal regulations come from two sources: the EPA, established in 1971 and the NRC established in 1975. The regulatory warrant for these two agencies is fundamentally based on the premise of no-safe-dose, or the Linear-No-Threshold model of dose response.[18]

This chapter will go through the historic evolution and adoption of LNT, as well as considering the negative impacts to human life due to its continued use. The next parts show how application of LNT in practice creates costs at each stage of a nuclear plant's life.

3.1 Linear-No-Threshold

The LNT dose response model has been controversial since its inclusion in BEAR-I in 1957. The prevailing understanding and informal basis of radiation dose response was based on a concept of tolerance dose.[19] Tolerance dose is the concept that to a certain point the human body can tolerate radiation exposure, much like how we can tolerate ultraviolet radiation from the sun. This was based on practical experience over the previous 60-years since the discovery of radiation in 1896.

LNT is based on the concept of the “genetic effect” which relies on three presuppositions [20]

- *That the mutagenic effect of a given radiation dose to the gonads is independent of the dose rate*
- *That the relationship of the mutation-rate to accumulated dose is linear*
- *That the spectrum of radiation-induced mutation is similar to the spectrum of spontaneous mutation*

The inclusion of the genetic effect and suppression of research that provided contradictory evidence was undertaken by Dr. Herman Mueller, who in his 1946 Nobel prize acceptance speech stated that there was no evidence to contradict the genetic effect, when at the time he was reviewing the work of a study that actually did find evidence to the contrary.[21, 22] Mueller was unequivocal in his objection to nuclear weapons. He was a signatory of the Einstein-Russel Manifesto. He saw with his longtime collaborator Curt Stern, the use of the Nobel platform to use Mueller's theory of the genetic effects of radiation to limit nuclear weapons testing.[21, 22]

Mueller had an opportunity to make a successful impact and with his credibility from his recent Nobel prize was able to be on the panel for the BEAR-I report where he was able to introduce the genetic effect into the protection standard. Until this time, radiation protection standards for radiation workers and civilians had been based entirely on the threshold model of Cantril and Parker. Their work served as the basis of the radiation protection standards for radiation workers, but the genetic effect was included for the general population. This was able to provide a sufficient policy justification to limit atmospheric weapons testing with the Limited Test Ban treaty in 1963.

What the genetic effect created was the concept of collective dose. Collective dose is used in evaluating the impact of radioactive source plumes for design and beyond

design basis. It serves as the justification for emergency planning zones around reactors, limiting radionuclide concentrations in water, and for the concept of As Low As Reasonably Achievable, ALARA. ALARA is perhaps the most impactful, because under the concept of having no-safe-dose, any marginal reduction in exposure saves lives. LNT gives the regulator unlimited regulatory warrant. Any regulatory decision becomes justified, regardless of the cost, because each incremental improvement can use imagined lives saved to justify the cost calculations.

The concerted act of a small group of individuals to implement a policy for the greater good which they knew was contrary to good science has resulted in a serious human toll. Not only has nuclear power been limited through increasing regulator action based on LNT, so has nuclear medicine, radium needles once used to treat tumors became too expensive for hospitals to use in cancer treatment due to regulatory compliance.[23] As a result, cancer treatment with radiation has to rely on large doses of external ionizing radiation spread out over the entire body causing increased damage to adjacent tissue. Doctors are unwilling to give Emergency Room X-rays to children, and as a result broken bones and other easily treatable events go undiagnosed and untreated.

More impactful though is the Japanese response to the Fukushima disaster. An estimated 1,600 people died in the evacuation.[24] Those survivors of the evacuation continue to face stigmatization, that they are now somehow flawed.[25]

In 2012 UNSCEAR completed a study began in 2006 regarding policy guidance for evaluating low doses of radiation[26]:

Therefore, the Scientific Committee does not recommend multiplying very low doses by large numbers of individuals to estimate numbers of radiation-induced health

effects within a population exposed to incremental doses at levels equivalent to or lower than natural background levels [100 mSv].

The radiation levels proposed by UNSCEAR are consistent with those of tolerance dose from Cantril and Parker, who placed the recommended number at 5 rem/yr, 50 mSv/yr. The difficulty identified by UNSCEAR is that measurement at levels consistent with background is difficult to distinguish potential effects from the radiation exposure from that of natural background radiation. Shortly after, the International Organization of Medical Physicists issued a policy statement that radiation exposure from medical imaging less than 100 mSv/yr should not be of a concern for increased risk to the patient—that the patient faces increased risk from not having the imaging. They go further echoing the UNSCEAR statement that any adverse effects are not identifiable from conventional epidemiological methods.[27]

As recently seen, taking an overly conservative model can cause more harm than adopting one that more closely matches what has been observed. The risks inherent in our world need to be taken in context with each other. Methods of assessing risk such as collective dose and genetic effects need to be removed from public policy for evaluating radiation exposure risks. The reality facing nuclear plant operators is that their regulators under the current regulatory regime can act without restraint. The current regulatory paradigm holds immeasurable risk from any radiation exposure justifying complete and arbitrary regulatory action.

3.2 Pre-Construction/Construction

Population exposure from radiation and the consequences thereof are the proper justification of the design of the power plant. They incorporate many measures that are

reasonable and sound. However, they can be taken too far. During the regulatory shift to the EPA and NRC in the 1970's there was a considerable shift in the construction costs and construction schedules, particularly to those plants that had yet to be completed.

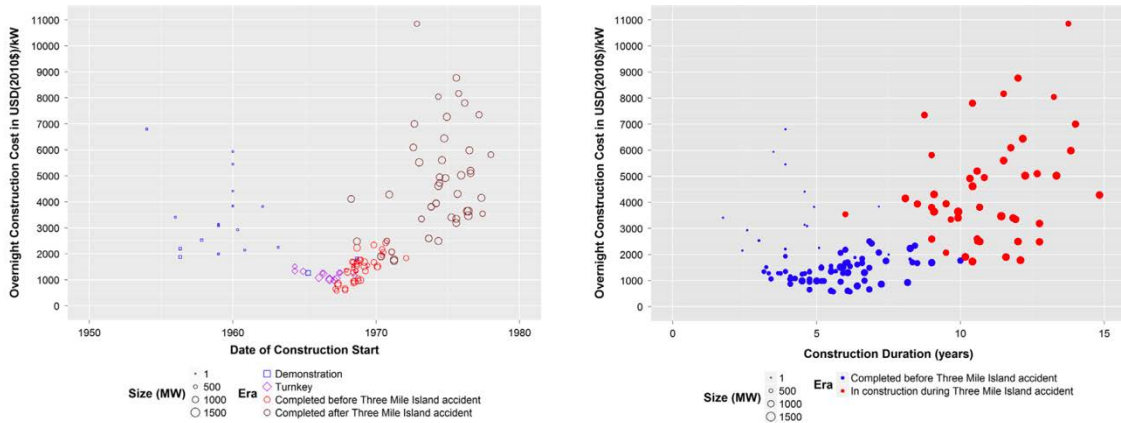


Figure 1-6 Trends in nuclear plant construction in the United States as a result of the response to Three Mile Island accident [17]

The additional costs associated with construction as a result of complying with the additional measures effectively doubled the construction timeline and cost for the reactors that did not have their operating license. Additionally, Figure 1.6 does not show the number of reactor projects that were abandoned because of the increased costs of regulatory compliance. With large multi-year infrastructure projects, delays carry significant risk to the company due to the amount of debt needed to finance the project. Servicing the debt can force companies into bankruptcy.

To hedge these risks due to the sheer magnitude of the projects, utilities will either be very large, e.g. Southern Company, and/or share the risk of the project with the rate payers, SCANA and Southern Company.

There are other methods for causing delays with reactor projects, some intentional and others unintentional. A recent example was from NRC Chairman Gregory Jaczko delaying the COL for Vogtle 3 and 4 and VC Summer 2 and 3. He was the lone

dissenting vote on the Aircraft impact assessment, which was previously determined as not applicable to the (4) AP1000 projects by the NRC under a different commissioner. Chairman Jazcko made the determination that it was applicable and forced a two and a half year delay while the primary containment structures were redesigned.[28]

An example of a non-intentional delay was a difference in interpretation of the specifications for the rebar in the concrete basemat of the primary containment structure. This caused a several-month delay in the two projects in Georgia and South Carolina while it was resolved.[29]

3.3 Operational

The NRC advances new regulation often without thought associated with the cost. This was observed by the DOE as needing to be addressed to prevent future nuclear plant closures.[2] It is not entirely the NRC, the EPA is capable of inserting additional costs, e.g. the recent regulations for condenser circulating water requiring plants to have closed loop cooling systems. This regulation forced the planned closure of Oyster Creek and was a considering factor in the announcement of Indian Point 2 and 3 closure.[2]

3.3.1 ALARA

Perhaps the most insidious cost comes from the NRC regulations for ALARA. Significant planning and costs are added to the maintenance on any system. In some instances, maintenance items are deferred to another outage due to not having sufficient time or man-rem budget left in the outage to address the new items. The trend of increasing ALARA standards is not new. ORNL published a report in 1981, “What is ALARA?” The report noted that the codification of it in the Federal Register allows a continual regulatory ratchet.[30]

Some disturbing trends have been identified in recent years. Regulatory agencies seem to have rediscovered and redefined ALARA to meet whatever ends they may wish to serve. This is doing a disservice to radiation protection programs and may even be counterproductive. The time has come, in our regulatory process, to apply the brakes to these trends. First, the trends must be identified and revealed for the frauds they actually are.

One consuming passion of regulatory agencies is to ratchet dose limits forever downward whether scientific evidence for justifying the change exists or not. Much of this is done in the good name of ALARA.

An example of the creeping regulatory ratchet is from my personal experience. As an undergraduate nuclear engineering student in the 1990's I toured Point Beach Unit 1's primary containment for about an hour and a half; walking underneath the reactor vessel, around the ECCS accumulators, and over the refueling bridge. 20-years later as a developmental Senior Reactor Operator, such a tour was prohibited as it was not in the outage's man-rem budget. There were defined no go areas outside of the primary containment where entrance without a man-rem plan were prohibited. Thus, walking down all of the primary components for operator training was prohibited.

UNSCEAR and IOMP both consider exposures to populations of less than 100 mSv as to have no measurable increase in risk. When coupled with historic data from nuclear shipyard workers and from exposure of residents in a Taiwanese apartment building, that show "significantly lower mortality" with increased low-level radiation exposure, the justification for maintaining LNT as a regulatory basis is untenable.[31-33] Evidence and experience show that further reductions in exposure do not provide any

measurable betterment to an individual. And, that concepts such as collective dose, upon which ALARA is based are inaccurate at best and malicious at worst.

What is the benefit of following ALARA if it provides no measurable benefit to the workers in a nuclear power plant? The amount of cost and time added serve no benefit to the workers, no benefit to the utilities shareholders, and all of the cost is passed onto the consumer. What is the impact to the nation by artificially increasing the cost of electricity generated? The cost of energy is the single biggest factor in determining economic growth.[5] Economic growth is significant portion of what leads to long healthier lives.[34]

One can argue that all that is needed to be done is a cost benefit analysis of each maintenance evolution to determine the optimal ALARA amounts. It is reasonable after all. Auxier and Dickson[30] properly note that the actual dollar cost of computing such dose benefit analysis are inherently time consuming and expensive. One that is plagued by the information problem noted by Hayek.[35] Information, Hayek notes exists locally and that in the process of aggregation, information is inherently lost. As a result, one-size-fits all solutions like ALARA will always lead to sub-optimal solutions.

3.3.2 Security

The NRC Published SOARCA in 2012[4]. It used various dose truncation levels in its calculation it noted the following:

The LNT model provides a viewpoint that is consistent with the NRC regulatory approach, and past analyses using the MACCS2 code have assumed an LNT dose-response model. The NRC is neither changing nor contemplating changing radiation protection standards and policy as a result of an approach taken in the

SOARCA study to characterize offsite health consequences for low probability events. Still, the NRC can use different approaches for different applications.

The adoption of different dose response models resulted in 1-2 orders of magnitude reduction in radiation risk. Former ANS President Eric Loewen, hypothetically postulated three different kinds of radiation, green or natural radiation, yellow or medical radiation, and red radiation from nuclear power operations, and then asked, why are each of these treated differently?[36] The NRC in SOARCA stated that only LNT was consistent with the current practice. It is not however consistent with logic. What is the increased risk from red radiation if the levels do not affect the combined total red and green levels? Why is it that the regulators adopt LNT which is 2 orders of magnitude more conservative (costly), when the effects are entirely indistinguishable from background radiation? Why is the red radiation quantitatively different?

Table 1-1 Results from NRC SOARCA Using Different Dose-Response Models[4]

Table 8 Peach Bottom Results for Scenarios without Successful Mitigation for LNT and Alternative Dose-Response Models

Scenario	Scenario-specific risk of latent cancer fatality for an individual located within 10 miles (per reactor-year)		
	Linear No-Threshold	Background	Health Physics Society
Long-term SBO	3×10^{-10}	2×10^{-12}	1×10^{-12}
Short-term SBO	6×10^{-11}	4×10^{-12}	4×10^{-12}
Short-term SBO with RCIC Blackstart	2×10^{-11}	2×10^{-13}	9×10^{-14}

As a result of the terrorist attacks of September 11, 2001, there was a significant change in the NRC’s policy toward security. It revised the Design Basis Threat rule in 2005 and had a series temporary measures as an immediate response to the attacks.[37]

The rules are based on revised source terms to the general population similar to those assessed in the SOARCA. The NRC treats an attack on a nuclear reactor in a similar manner as a Radiological Dispersal Device, a.k.a. dirty bomb. The assessment of risk from such attacks is based on utilizing collective dose and the LNT dose-response model to large populations surrounding dirty bomb sites—attacked nuclear power plants, contrary to the recommended guidance from UNSCEAR and ICRP.

The overestimation of risk from the use of collective dose and the genetic effect adds considerable cost to the production of power from nuclear power plants for no measurable benefit. The Nuclear Energy Institute published a white paper discussing the trends in the marginal cost of production from nuclear power plants.[38] These increased marginal costs, while not directly attributed to plant closures certainly did not facilitate their continued operation.

3.3.3 Post Fukushima

Another source of regulatory cost were the compliance items with the post Fukushima plant upgrades for extended station blackouts. While these events were serious and catastrophic, various lessons can be learned from them. First is that the decision to vent the primary containments was delayed until after the evacuations were started.[39] This ignored the thermodynamics involved eventually leading to the containment vessels venting themselves, there was a bang followed by a drop in the containment vessel pressure and equalization with reactor vessel pressure.[39] With the now compromised containment vessels establishing core cooling became more difficult and was eventually not possible due to a series of cascading events that prevented the operators from acting.[39] While early venting would have released some particulate

fission products, it would have primarily been short lived fission product gases and hydrogen.[40] The addition of hardened vents would have helped, however, using the non-hardened vents when prescribed by procedure would have been more helpful. Instead it appears that concerns over exposure to the general population caused an even larger release of radioactive contamination into the atmosphere and directly into the near surface ground water. This has led to the stigmatization of an entire population, 160,000 evacuees from the prefecture.[25]

There is an entire lack of exploring why the operators elected not to follow the procedures at the facility. By not questioning this and focusing on capital expenditures as a means of solution, the NRC missed an opportunity to help. Instead a reactionary action was taken in lieu of a more thoughtful approach. If our fundamental tenants on radiation and risk are flawed and drive us to increase the risk of those charged with operations and to the general population, then it is imperative to reassess those tenants.

3.3.4 Load Following

Some nuclear reactors, e.g. Sequoyah nuclear generating station, were designed for the capability for automatic generator control including both voltage and frequency regulation. While this capability still exists in the control room, they are prohibited from operating in that mode by the NRC. It places control of reactivity and transitioning power levels into the hands of unlicensed remote operators, which is contrary to the plant's operating license and federal regulations.[10]

New PWRs like the AP-1000 have special control rods called "gray rods" with reduced worth (appearing grey to the neutrons) to allow the reactor to adjust power levels without requiring changes in boric acid concentration, reducing the need for primary

water treatment/disposal. BWRs can adjust power much more simply by changing the recirculation flow rate.[10] The ability to change power levels without having to process large volumes of water gives BWRs their reputation for being able to load follow much better than PWRs.

In France, where nuclear generation is approximately 75% of total generated electricity, the reactors operate in load following and frequency regulation modes. Load following typically has a swing of 5-10% power, while primary frequency regulation is in the range of 1 to 2% and has a duration of 2 to 30 seconds.[10]

However, this type of operational profile, in either type of reactor, is no longer considered due to self-imposed fuel conditioning limitations on power transients.[41] This type of voluntary operational restriction prevents the plants from operating in any mode other than as baseload generators. There is no apparent need to limit leaking fuel other than to minimize the costs associated with handling these fuel elements. In all phases of plant operations, from operation, fuel handling, fuel storage, dry storage, and reprocessing, there are adequate means for handling leaking fuel assemblies.[42]

Nuclear reactors in Europe, France and Germany, operate in load following modes and do not observe the fuel conditioning guidance set by EPRI with typical transients in the range of 3-5%/min and do not report an increase in fuel failures due to load following transients.[10] Because the European reactors were built using the design and operational experience with US reactors,[43] there is no technical reason why US reactors cannot load follow. Additionally, European reactors are capable of frequency regulation, which is expressly prohibited by the NRC in federal regulations.[10]

3.4 Decommissioning

Nuclear plant owners when faced with adverse market conditions, could potentially shut down the operating reactor and wait for market conditions to improve. This option is not economically viable for them to do so as they continue to carry the fixed costs of maintaining the operating license, which includes staffing, security, and regulatory compliance. The operational costs for an average reactor in 2016 were \$164.5 million.[38] This does not include fuel which is purchased years in advance. The cost for operating the reactor are fixed whether the reactor is operating or shut down.

Utilities, when faced with a money losing reactor, can face significant losses to maintain the operating license or they can shut down and shift the license to a decommissioning license.[3] This in effect removes the reactor from the books as the decommissioning fund is now funding the decommissioning efforts at the plant, not the utilities operational accounts. As most utilities are publicly traded companies, they have fiduciary obligations to their shareholders. As such, decommissioning a reactor is a decision that they can easily justify to their shareholders.

CHAPTER 4

NEW NUCLEAR BUSINESS MODEL

Assuming no change in future policy at best and potentially worse conditions in the future, how can new nuclear plants be built in the United States?

The simple answer is, not with the current business model. The current business model works well in predictable and more centrally controlled electricity markets, associated with the more traditional vertically integrated utilities. It does not port well into deregulated electricity markets that can undergo significant market shifts within only a few years, as exemplified by the number of plant closures in those markets and the absence of plant closures in the conventional regulated markets. To create a new business model, the risks associated with building and operating the power plant need to be fully considered, otherwise it will be doomed to fail for the same reasons as the current business model is failing.

What does the ideal business model look like? A good starting point is that it satisfy most if not all of the reliability attributes developed by PJM, Figure 1-7.[2] Doing this would differentiate it from all other generator/fuel business models. It would be a disruptive technology and would create significant market potential for utilities that adopted it and provide a better quality of service to its customers at a lower price.

Figure 4.13. Mapping Reliability Attributes Against Resourcesⁱⁱⁱ 301

● = Exhibits Attribute
 = Partially Exhibits Attribute
 = Does Not Exhibit Attribute

Resource Type	Essential Reliability Services (Frequency, Voltage, Ramp Capability)					Fuel Assurance		Flexibility			Other		
	Frequency Response (Inertia & Primary)	Voltage Control	Ramp			Not Fuel Limited (> 72 hours at Eco. Max Output)	On-site Fuel Inventory	Cycle	Short Min. Run Time (< 2 hrs.) / Multiple Starts Per Day	Startup / Notification Time < 30 Minutes	Black Start Capable	No Environmental Restrictions (that Would Limit Run Hours)	Equivalent Availability Factor
			Regulation	Contingency Reserve	Load Following								
Hydro	●	●	●	●	●	○	●	●	●	●	●	●	●
Natural Gas - Combustion Turbine	●	●	●	●	●	○	●	●	●	●	●	●	●
Oil - Steam	●	●	●	●	●	●	●	○	○	○	○	○	●
Coal - Steam	●	●	●	●	●	●	●	○	○	○	○	○	●
Natural Gas - Steam	●	●	●	●	●	●	○	●	○	○	●	●	●
Oil/ Diesel - Combustion Turbine	●	●	○	●	○	○	●	●	●	●	●	○	●
Nuclear	●	●	○	○	●	●	●	○	○	○	○	●	●
Battery/ Storage	●	●	●	●	○	○	○	●	●	●	●	●	●
Demand Response	○	○	●	●	●	●	●	●	●	○	○	○	●
Solar	●	●	○	○	●	○	○	●	●	●	○	○	●
Wind	●	●	○	○	●	○	○	●	●	●	○	○	●

Conventional generation sources—particularly hydroelectricity, combustion turbines (natural gas and oil), and steam turbines (oil, coal, and natural gas)—performed very well against most of PJM’s reliability requirements. Nuclear units are not optimized for significant flexibility or ramping capability, but do exhibit strong fuel assuranceⁱⁱⁱ attributes. Batteries and storage meet all flexibility requirements, and DR offers high flexibility and ramping management capability. Wind and solar are highly time dependent and do not offer fuel assurance on their own, but can offer good flexibility if they have the proper controls and contractual arrangements.

The Electric Power Research Institute (EPRI) summarizes how regional grid operators use centrally-organized markets to procure specific reliability attributes from generators:

Figure 1-7 PJM Reliability Metrics [2]

The first step in evaluating the business model is to start with construction.

Merchant generators cannot pass the construction risk onto their customers as vertically integrated utilities can. This will limit the size of the projects. Instead of a single large infrastructure project, it will need to be smaller incremental capacity additions over time. By breaking up the increments of the project similar capacity additions can be made with

much more manageable risk profiles. It may even allow Engineering Procurement and Construction Contractors, EPCs to return to turnkey projects, where the construction firm takes the risk (profit) of the project. But for this to happen the construction time line has to be predictable and the plant needs to be licensed under 10 CFR 52[44] with a combined Construction Operation License. Additionally, during construction very few design changes can be made. It is imperative that the designs for each project be finalized before construction starts.[45] Several vendors have developed reactors that were purposely built to fulfill this need. These are the Small Modular Reactors.

Looking at the current business model in Figure 1-7, nuclear completely fulfills the Voltage Control, Not Fuel Limited, On Site Fuel Inventory, and Equivalent Availability Factor. It partially fulfills Frequency Response, Load Following, and No Environmental Restrictions that Limit Run Hours. The new business model must do everything that the current nuclear business model fulfills. These are valuable services and at a minimum need to be met. To be able to grow in the future, the business model needs additional capability. It needs to be able to provide full frequency response capabilities, regulation services, contingency response and fully follow load. It also needs to be able to cycle and be black start capable. A new plant under this business model needs a very large and flexible operating envelope that separates the generator's transient response from the dynamics of the reactor. Most importantly, the plant needs to be able to maintain its profitability over time, with a high enough capital recovery to justify the capital expenditure to build the unit in the first place, much less follow-on units.

As the SMR market stands, not a single design can fulfill this need. Of the most mature designs of the SMRs, none of them can fulfil this market need as the Power

Conversion System is directly coupled to the reactor, meaning that power transients due to changing the steam turbine throttle position will have a direct feedback to the control of the reactor. This means that to add new capability, new technology is needed.

If we consider Natural Gas – Steam in Figure 1-7 it provides the remaining services that nuclear does not, additionally nuclear provides the services that Natural Gas – Steam does not. There are two reliability metrics that neither fulfill due to the limitations of steam cycles and those are short minimum run time and startup/notification time < 30 minutes. Only Combustion Turbines, Diesel Generators, Hydro and Batteries/Storage have those capabilities.

Solar and wind, while considered by PJM to satisfy many of the reliability metrics, are not considered because they are not dispatchable. Solar is available only when the sun shines. Based on the physics of photovoltaic cells, once the sun is shining you can't turn them off. Wind is subject to the vagaries of the wind, and can only provide reliability services at something that is as poets describe, fickle.[46]

4.1 Energy Server

Combining the dispatchable technologies into a more cohesive package requires a coupling method that allows independent parallelization. The best comparative analogy here is of a server farm where multiple parallel servers provide processing and data storage sharing a common communications bus(es). Applying this analogy directly to energy, consider an energy server, where components are hot swappable complementary modules. To do this the common bus should allow some sort of energy storage. This allows the buffering of load response with nuclear reactor response, allowing automatic generator control of the PCS. The energy storage also allows a different paradigm where

the owner can conduct price arbitrage on the electricity market capitalizing on the inherent volatility induced by VRE and one where the PCS can act as a semi-infinite inertial mass. The former requires no modifications to policy, the latter needs the addition of an inertial mass ancillary market for primary frequency regulation. A completed energy server block would look something like Figure 1.6.

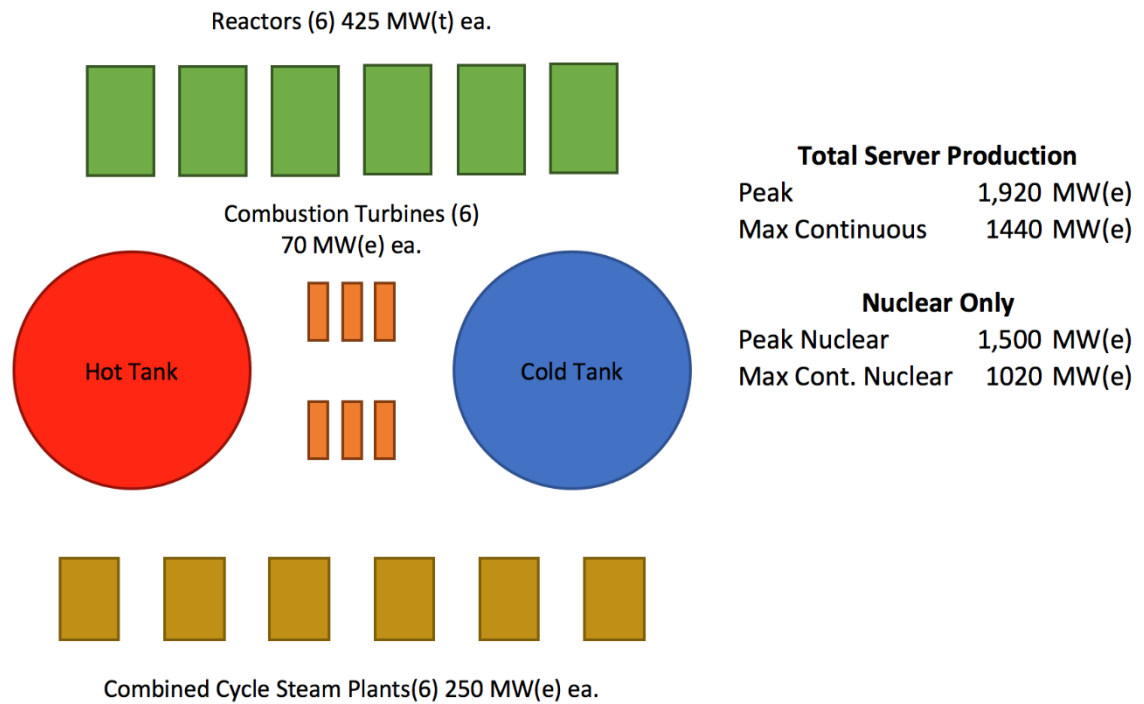


Figure 1-8 Conceptual energy server configuration

Figure 1.8 shows multiple reactor modules in parallel with each other and a number of combustion turbines. During operation, the reactors and combustion turbines heat salt from the cold tank for storage in the hot tank and the steam plants, conventional combined cycle steam plant modules, take the hot salt and convert it into electricity when needed. This concept even without the addition of the combustion turbines fully satisfies all of the PJM reliability requirements of Figure 1-7. The addition of combustion turbines, allows the combustion turbines to operate in simple cycle mode with combined

cycle efficiency. The cost of the storage and additional heat exchangers needed for the system are not justifiable with the combustion turbines by themselves but is justifiable when combined with the nuclear reactors.

The production and construction of the combined cycle steam plants, combustion turbines and storage tanks are all well understood. Typical construction time for a combined cycle plant is on the order of 2 years.[47] Thus the reactors represent the long lead item. Using a design like GE-H Mod A PRISM, 425 MW(t), the largest single component, the reactor vessel, is rail shippable to the site.[48] This allows for very little onsite construction compared to conventional reactor designs.

The massive parallelization of the server allows for incremental capacity additions as needed by the utility, a lower Forced Outage Rate, predictable construction costs and schedules, and flexible maintenance and outage planning (a single component can be taken offline without affecting any others). A COL can be for a number of modules expandable to a total final number. For example, a utility can plan the site to contain 12 reactor modules with integrated storage and obtain a COL for this. Once the COL is obtained. The utility can build the first two storage tanks and place the first reactor module. Once that is operating additional modules can be built as needed. Because of the separation of the reactor from the load, only the cold tank salt pumps supplying an individual reactor can affect that and only that reactor's power. For this reason, the cold salt pumps are controlled by the reactor operators. If the salt tanks become damaged and inoperative the reactors would shut down on their own even without operator action. Because of this, everything else at the site is outside of the scope of NRC regulations and

only requires state, local, and EPA permitting for water and environmental emissions like a conventional combined cycle plant.

4.2 Limit Regulatory Liability

Segregating the energy server as outlined above, creates a compartmentalized and limited regulatory scope through design. As shown earlier, arbitrary regulatory action is the single largest liability that is hindering the expansion of nuclear power. By separating the PCS from the reactor, much of the limitations that hinder the current fleet of generators is eliminated. By using a reactor that has a robust fuel, e.g. PRISM's metallic fuel, the reactors can operate at various power levels without concern. By adding the storage, the reactors can operate at near maximum power, ensuring profitability, even as the PCS cycles to meet demand and access every available ancillary market and provide a hedge against market volatility. This allows the utility to now profit off of the inherent volatility of VRE.

If market conditions change, or if policy continues to be arbitrary, the server can operate in the mode that best allows maximal capital recovery. Additions can be made as new technology becomes available and is economic, allowing the server to change and evolve with time. Individual units can be retired if they are no longer economic and not affect the remainder of the facility.

Because of PRISM's compact nature and its coolant's chemical reactivity, it needs to be segregated from the atmosphere, this limits operator exposure. Contamination is always contained and has increased shielding and distance from the operators. This is done without adding any special operating procedures or additional equipment. This minimizes regulatory risk/cost associated with radiation protection. There are no valves

or pump seals that need to be replaced/repared. There is not the myriad of associated contaminated subsystems needed to operate the reactor. There is no boric acid to cause corrosion, the sodium doesn't corrode the structural metal or fuel assemblies.[49] For these reasons continued regulatory ratchet associated with ALARA are almost completely eliminated.

By relying on the regulatory framework of other technologies, nuclear is less insular and susceptible to "Bootlegger and Baptist" types of regulation.[50] Bootleggers and Baptists is a theory developed by Bruce Yandle to explain how environmental regulations have their structure. In his theory, different groups can have the same policy goal, e.g. prohibition, but for different reasons. The bootleggers like prohibition because their business model depends on the restricted markets created by it. The Baptists like it because "demon liquor" is outlawed. This forms an informal policy alignment between two disparate groups.

By relying on the same regulatory base as every other generator out there and even on much of the same technology, the incentives for the "bootleggers" to block through a selective regulatory regime are minimized as they would be blocking themselves from the market and their product by itself is not as competitive. For this reason, they are disincentivised to implement restrictive policy and are keen to lobby for less restrictive policy to preserve their market share. The "Baptists" alone do not have the capital resources to affect policy, by eliminating the "bootlegger" funding, prohibition fails. A recent example of the "bootleggers" funding the "Baptists" was the Sierra Club's initiative "Beyond Coal" funded by Chesapeake Energy, a natural gas producer.[51] A historical one for nuclear can be seen in Roger Stone's "Pandora's Promise" where

opposition to Shoreham Nuclear Power Station was in part “sponsored in the public interest by the Oil Heat Institute”.^[52]

CHAPTER 5 POLICY RECOMMENDATIONS

There are two main types of policy recommendations from this study. First is to allow the deregulated electricity markets to continue to function and innovate. Second is to restrict the roll of LNT in regulation, as recommended by UNSCEAR. The former appears to have significant traction, the latter is a Sisyphean task and likely not to occur in any meaningful timescale.

The Regional Transmission Operators and Independent System Operators have been and continue to innovate to provide the best service to their customers. Even the partial market liberalization that occurred with their creation has shown significant positive benefits for consumers. Many of the RTOs and ISOs are creating additional markets to improve reliability and grid stability, e.g. CAISO and MISO implementing ramping reserve markets, and ERCOT designing markets for frequency responsive and inertial response reserve markets.[2] Markets are incredibly resilient things, as long as they are allowed to have price discovery they can function. Once price controls are implemented, the markets fail to find solutions because the distortion of the price controls distorts the information of availability that is included in the price.[53] Allowing the markets to continue to evolve without enacting price controls will ensure that they will eventually find the best possible outcome as a function of the applied policy constraints, e.g. RPS.

PART 2 – BASIC ENGINEERING DESIGN

CHAPTER 1 INTRODUCTION

Nuclear power plants generate energy with life-cycle near-zero emission of greenhouse gases and particulates.[54] However, there is over one trillion dollars stranded in infrastructure related to coal transportation and mining and to fossil power plants,[55] and irrespective of nuclear power advantages it is economically not viable to simply abandon this infrastructure. The purpose of this study will be to explore the idea of repowering existing infrastructure with nuclear power. The goal is to validate the proposed approach of effectively decarbonizing electricity production by reusing as much of existing infrastructure as possible. The hope is that by reusing existing capital assets to the maximal extent possible, regulatory compliance costs can be minimized, particularly the proposed rules on greenhouse gas emissions.[56]

The existing fleet of Light Water Reactors (LWR) are only economically effective at high capacity factors acting as baseload energy.[57] Their complexity and size precludes many utilities from even considering a new reactor project. Additionally, their large size forces utilities without expansive networks to build surplus transmission capacity in the event of a forced outage with a large LWR. Grid limitations also impact the adoption of renewable energy sources because of the construction costs and difficulty in obtaining adequate right of way for the new transmission lines.[58] The remaining choice for addressing the changes in environmental regulation is natural gas, but here too there are problems such as limited pipeline capacity, volatile natural gas market prices with significant fluctuations due to supply and seasonal affects.[59, 60]

The focus was to develop a solution that reuses existing infrastructure and relies upon technologies already commercially deployed or at least demonstrated at commercial scale (e.g. pool type Sodium Fast Reactors, SFR, ready for commercial deployment). The design needs to be able to integrate with coal, combustion turbines, and combined cycle plants. The reactors need to also operate at a high capacity factor to have favorable capital recovery. To be able to load follow, integrate with existing infrastructure, and have the reactors operate at a high capacity factor, thermal energy storage is needed. In the past, the Nuclear Regulatory Commission, NRC, was reluctant to consider allowing even advanced reactors from connecting directly with Power Conversion Systems that were not considered during the licensing of the reactor without implementing additional measures.[61] Figure 2-1 shows the intended concept that will be evaluated in this study.

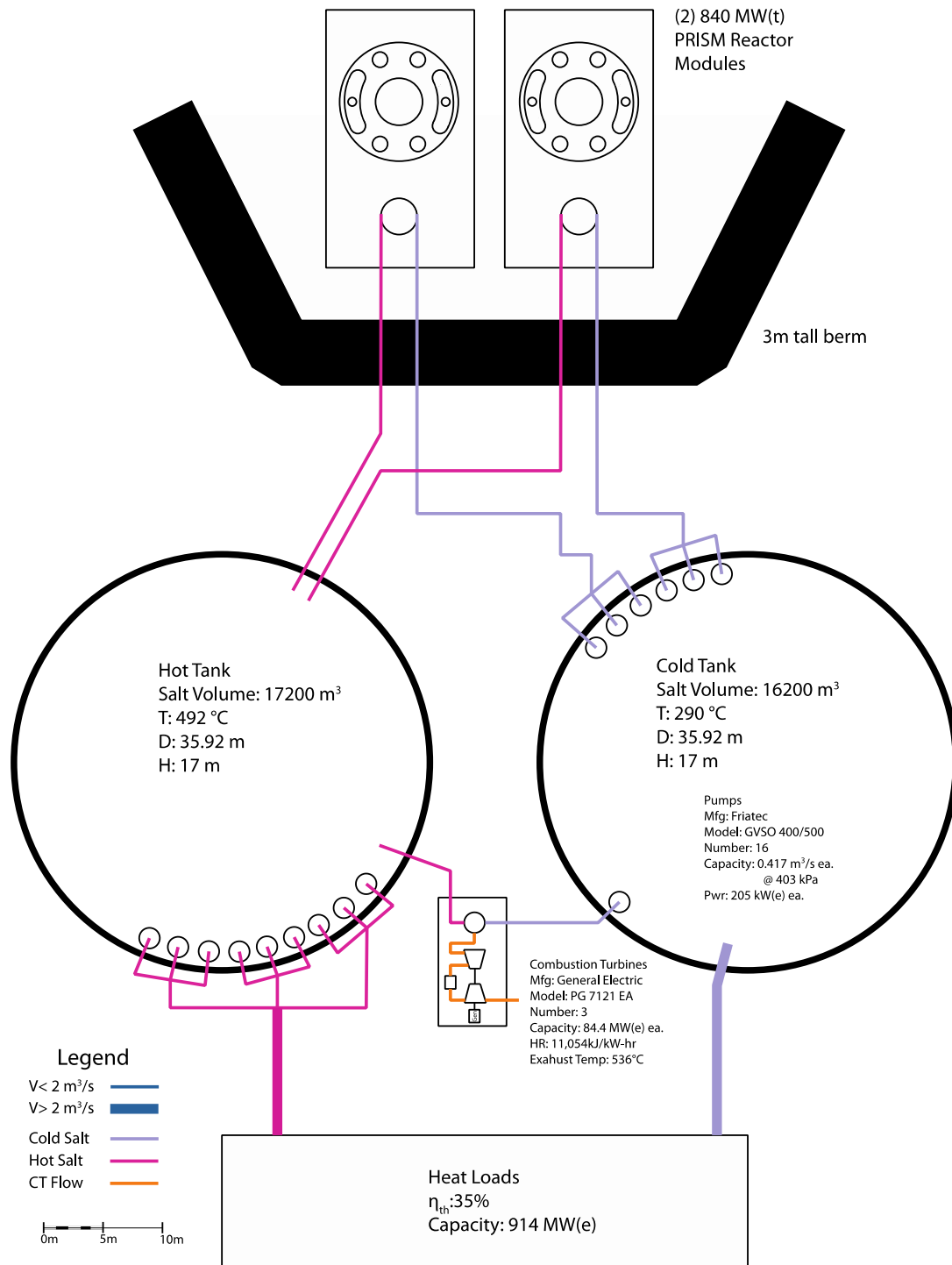


Figure 2-1 nTES conceptual site layout

CHAPTER 2 BACKGROUND

There are several strategies of energy storage to consider.[62] Historically, pumped hydroelectric storage has been successfully integrated with nuclear power plants, the TVA's Sequoyah/Raccoon Mountain is an example of this approach. Other storage systems are dictated by the considerations of selecting the reactor design. These methods usually involve storing sensible heat, but this is not always the case. There has been some work in storing chemical energy, sometimes involving electrolysis or other easily reversible approaches, where high reactor temperatures, $\sim 800^{\circ}\text{C}$, reduce the Gibbs potential to minimize the thermodynamic loss of such a conversion approach. Even for more conventional sensible heat storage approaches, heat from LWRs is not sufficient to be useful. The lower reactor outlet temperatures preclude lower cost inorganic fluids. While there are suitable organic compounds that will not breakdown at 260°C , the volume required for the relatively small ΔT across the core, $\sim 50^{\circ}\text{C}$, and the fluid cost, makes this technology prohibitively expensive.

The most promising storage design is the storage of sensible heat. Some approaches use geologic formations and others use high temperature salts.[63, 64] Geologic formations were not considered due to additional siting difficulty and the scope of those projects limit feasibility, especially when salt storage is already commercially available. One of the most cost effective salts is solar salt, $60 \text{ NaNO}_3 - 40 \text{ KNO}_3$. [65] It has an operational temperature range of $250^{\circ}\text{C} - 630^{\circ}\text{C}$ and is already commercially deployed, e.g. Andasol Project in Spain.[66, 67] This provides an adequate operational envelope for mid temperature reactors especially the SFR.[15] There has been some work

looking at using the less expensive inorganic salts as a storage means for bottoming cycles of AHTR.[68] This approach can similarly be coupled with other advanced high temperature reactors involving salt or gaseous coolants. If storage of the high temperature is desired, more expensive higher temperature salts will be needed.

In selecting a reactor technology, a more holistic look at the reactor as part of a national/global system was taken. If we are considering reactors for meeting future energy demand, we need to consider the supply of fissile material as an inevitable future constraint.[69] Uranium mining and enrichment has seen significant technological improvement in the last 30-years, in-situ leaching and gaseous centrifuges respectively, significantly reducing the needed energy and environmental impact of extraction and enrichment. This downward price pressure and softening uranium demand due to conversion efficiency improvement and post Fukushima nuclear plant shutdowns lead to historically low enriched uranium costs in constant dollars.[70] What has been seen is that changes in demand can have immediate and significant impacts on price. At one point in history, nuclear vendors had included the fuel cost as part of the capital cost of the projects. They subsequently defaulted when fuel prices rose in the mid 1970's.[71] Compared to other fuel markets and because of the incredible energy density of nuclear fuel, the uranium market has very low volume and therefore high volatility.

If we consider for the moment the size of the global electricity market, roughly 20.9 PWh/yr for 7 billion people, and then imagine a simple scaling where average electricity use increases from 2.97 MWh/yr-person to 10 MWh/yr-person, consistent with the energy demand of the developed world, and the population increases to 10 billion. This equates to global electricity demand increasing to 100 PWh/yr. This would result in

a 5x increase in the entire supply chain for all fuel sources assuming constant fuel mix distribution. For coal, this is a change in supply from ~7,876 Mt/a to 39,300 Mt/a. Natural gas infrastructures will have to increase similarly as would oil. The total global energy sector investment in 2016 was \$2 trillion in 2016.[72] To place this in perspective, nuclear uses about 75 Mt/a of U_3O_8 and with no changes in technology would require 375 Mt/a of production. Using an open fuel cycle will become prohibitively expensive and limit potential market opportunities for a reactor grade plutonium market.

As can be seen from this simple exercise, the cost of increasing the scale of fossil fuel extraction and transportation will not be trivial, especially when compared to the fixed cost of increasing the fissile material supply through breeding with a combination of thorium and uranium cycles. When fissile breeding is adopted on a global level, it will cap the growth in uranium mining/enrichment at the breakeven cost for fissile material from breeding.[73]

It is thus for purely economic reasons and looking at global energy trends, that the reactor technology considered for this project is a breeder. Utilities can hedge the cost of future fuel cost as a component of CAPEX during construction. Subsequently, the fissile material hedge can be turned into an active market or used to fund internal growth.

Considering the need for breeding and a mid-temperature reactor, the most mature of the Gen-IV reactor types is the Sodium Fast Reactor, with global operational experience spanning over 60-years and a unit in commercial operation, no other Gen IV reactor technology is as developed or even commercially deployed.[73] The GIF roadmap estimated that the SFR would be commercially deployed by 2015, the Beloyarsk Unit 4 BN-800 achieved commercial operation Q4 2016.

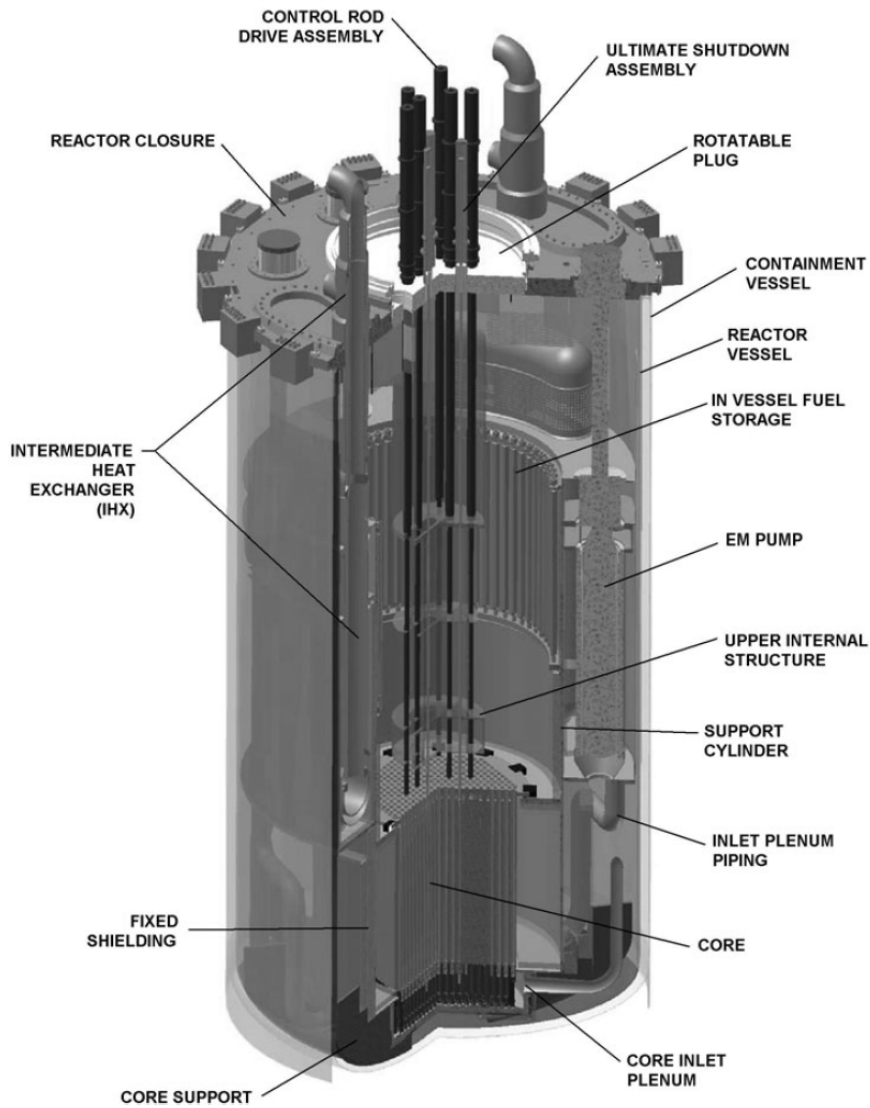


Figure 2-2 PRISM reactor vessel cutaway[48]

The slate of SFR designs that are available or have been deployed over the years is manifold. The SFR falls into two general categories, loop and pool design. Because of the inherent safety features demonstrated by EBR-II, the pool type reactor was selected as being the best fit as it eliminates LOCA as a part of the design basis.[61] For this reason and the availability of published data, we selected the PRISM, Figure 2.2 and 2.3, as the most mature design.[2, 16] Because the reactor is a GE-H design and GE is a major

vendor of combined cycle plants, we used GE's extensive line of combustion turbines as they would be likely candidates in any contracted project.

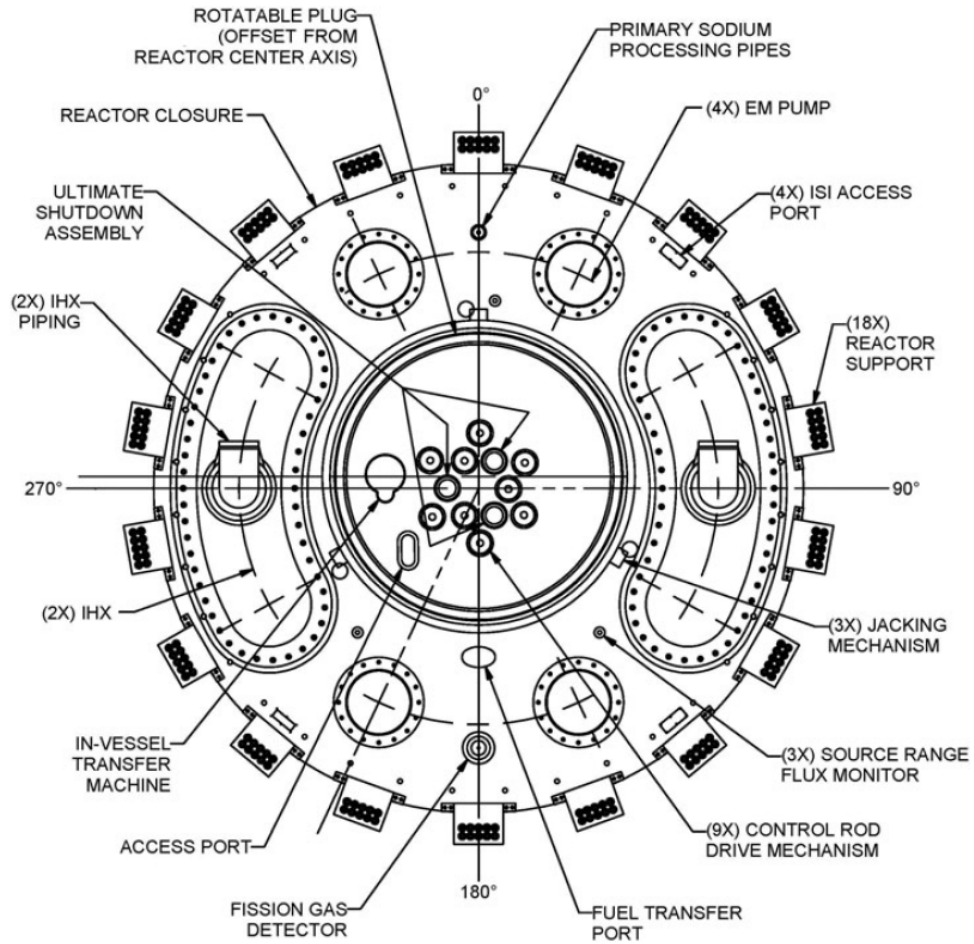


Figure 2-3 PRISM reactor vessel closure head[48]

CHAPTER 3 DESIGN OBJECTIVES AND APPROACH

The fundamental objective of the design process was to make the design as simple and as robust as possible. While the inherent safety aspects of the S-PRISM make it a significant improvement in existing reactor designs, the design changes needed to either improve safety or do no worse than the baseline S-PRISM.

To aid in ensuring the design changes did not adversely affect safety, NUREG-1368[61] was extensively referenced for the specific components that were affected in the design modification. This study did not include a change in the risk magnitudes, but where appropriate indicated the direction of impact on safety margin and an estimate magnitude. Because of the limited documentation and regulatory guidance on SFR design evaluation, NUREG-1368 was taken as the primary regulatory reference on this subject, even though it doesn't provide formal licensing guidance.

For simplicity, a simple single pressure Once Through Steam Generator, OTSG, was assumed for the purpose of steam generation on the PCS side of the salt storage tanks. There is no technical reason why a multi-pressure steam couldn't be used, and there are several economic reasons why one would want to use one. Multi-pressure steam generators are commonly used in Heat Recovery Steam Generators, HRSG. Because the salt and water have benign reactions, water is a solvent of the salt with only a dissociation reaction at low temperatures, the cost of creating a multi-pressure steam generator is reduced, allowing for lower exergy loss in the steam generator. The increased exergy recovery is done by creating multiple pinch points instead of one, allowing the steam temperatures to more closely follow those of the salt, increasing plant thermodynamic

performance. Second, it will allow a lower salt outlet temperature, down to 290°C, which was considered as the lowest desired operational temperature. This is also 10°C below the operational temperature limit of carbon steel, which is used for the construction of the cold salt tank. If the final design uses a higher salt outlet temperature, more expensive stainless steel will need to be used to make the cold tank. For engineering and design purposes of this study, the lowest salt temperature was based on a 25°C pinch point ΔT for a OTSG. The resultant salt outlet temperature was 313.8°C. Because of the economic incentives to have as large ΔT of a salt within the operational temperature bounds of 290°C-500°C, having the highest possible salt outlet temperature carries a significant premium.

3.1 Heat Exchanger Network Design

The heat exchanger network was designed to have the highest outlet salt outlet temperature possible, while minimizing the pressure loss in the PHTS and the IHTS. Table 2-1 and Table 2-2 show the design parameters for the reference PRISM and the revised nTES design. The steam conditions were set to be the same. The only difference in the design of the steam generator is the PRISM has pinch point ΔT of 29.4°C. Other proposed SFR S/G have pinch points of 21.3°C. (Conceptual Design of a Helical Steam Generator with 750 MWt for an SFR). An arbitrary pinch of 25°C was selected for the nTES design and can be seen in Figure 2-4, which shows the T-s diagram of the simplified single pressure OTSG.

Table 2-1 Reference design heat exchanger network parameters

	Reference Design		
	PHTS	IHTS	SGS
T_h [°C]	499	477	452
T_c [°C]	360	326	216
ΔT_{lm} [°C]		27.6	57.4

Table 2-2 nTES design heat exchanger network parameters

	nTES Design			
	PHTS	IHTS	SSS	SGS
T_h [°C]	499	490	480	452
T_c [°C]	360	326	316	216
ΔT_{lm} [°C]		19.1	7.0	60.4

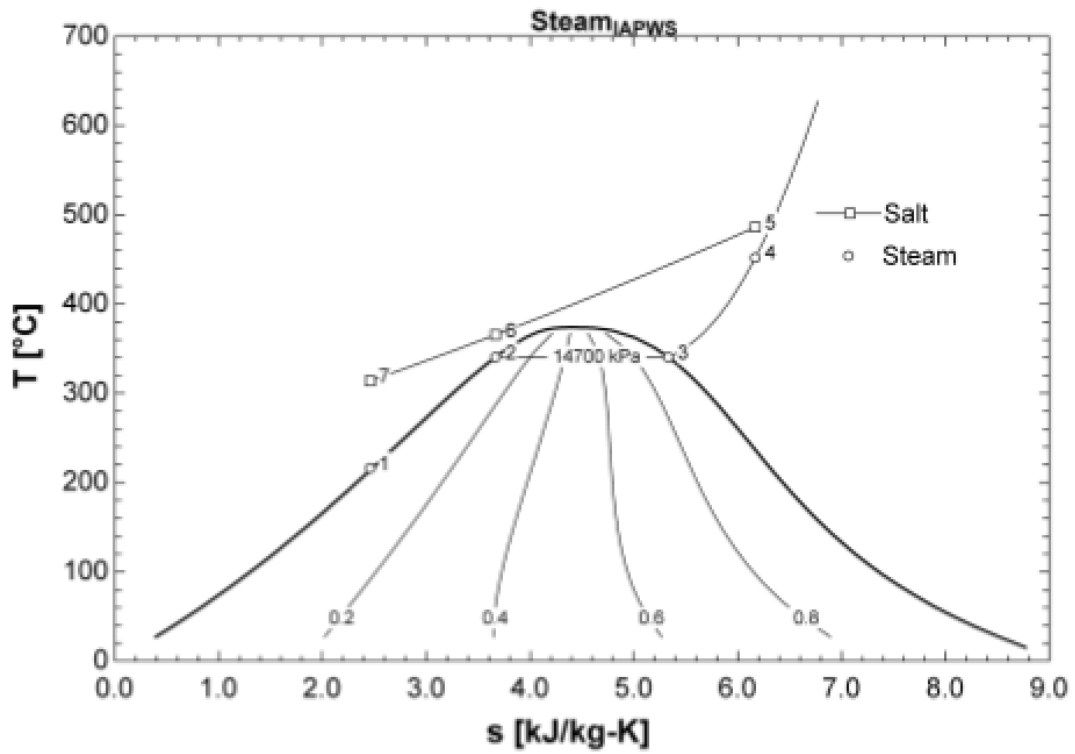
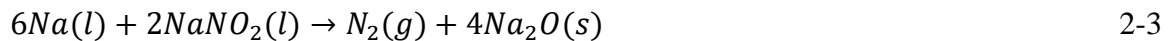
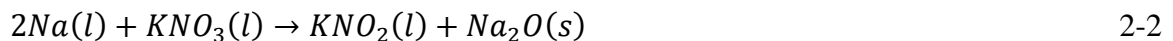


Figure 2-4 T-s diagram of a concept nTES OTSG

Because of the induced thermal stresses in heat exchangers based on the temperature differences. The IHTS cold-leg temperature was set to that of the reference design. The approach temperatures and the resultant log-mean temperature differences ΔT_{lm} were estimated to be consistent with other liquid-liquid compact heat exchangers. Because of the desirability of keeping the IHX relatively short, increasing natural circulation pressure differential and minimizing sodium pressure drop, the IHX was not aggressively sized, and used the reference design's SS304 as the structural material. Correspondingly the SHX, was not aggressively sized due to limiting the amount of P91 steel in the heat exchanger. A more detailed, exergetic analysis of the entire system needs to be done to optimize the size of each of these heat exchangers and this is not worth doing unless done in conjunction with a detailed design of the multi-pressure OTSG and plant cost optimization. The numbers selected here assume more expensive materials compared to the value of the power produced, thus a desirability to limit plant CAPEX.

3.2 Intermediate Heat Transport and Auxiliary Cooling Systems

Solar salt has three potential chemical reactions with sodium,



The reaction of 2.1 supplies the reactants for 2.3. All three reactions will occur spontaneously and are strongly exothermic. For this reason, the intermediate loop needs to remain in the system. The original concept had hoped to find a chemically compatible salt, but the sodium proved to be too reactive, with every candidate salt. The solar salt, while reactive with sodium, will add the least to the overall capital cost of the project. The design focus of the intermediate loop is to minimize entropy generation and system

size. High efficiency heat exchangers with low pressure loss will be used. Because all of the heat transfer will occur liquid to liquid, the heat exchangers will be much more compact and with lower head loss. This will provide for increased natural circulation during off normal events.

The sodium to salt heat exchanger will need to have rupture bellows similar to those of the reference design's steam generator. It will not have enough external heat transfer surface to provide a secondary cooling function of the ACS. As a result, we designed a purpose-built ACS system. Similar to the S-PRISM and the most recent PRISM this ACS will be included in the safety boundary.

Due to the lack of substantive changes to the PHTS and IHTS, the existing design basis of the PRISM will not be affected by this design change. Part 4 will look at the thermal-hydraulics under various accident and operational scenarios. The specific changes in natural circulation will also be assessed in Part 4.

Figure 2-5 shows the design for the ACS system. The use of compact heat exchangers reduces the total system weight that is supported by the seismic isolations. The sodium-water reaction mitigation becomes a sodium-nitrate reaction mitigation, those reactions will produce sodium oxide, but will not produce hydrogen. Instead inert nitrogen is created, which can create a personnel hazard by displacing oxygen, but is not an explosive risk. Further design consideration will need to be given to the exact configuration of the chemical suppression tanks and their venting system.

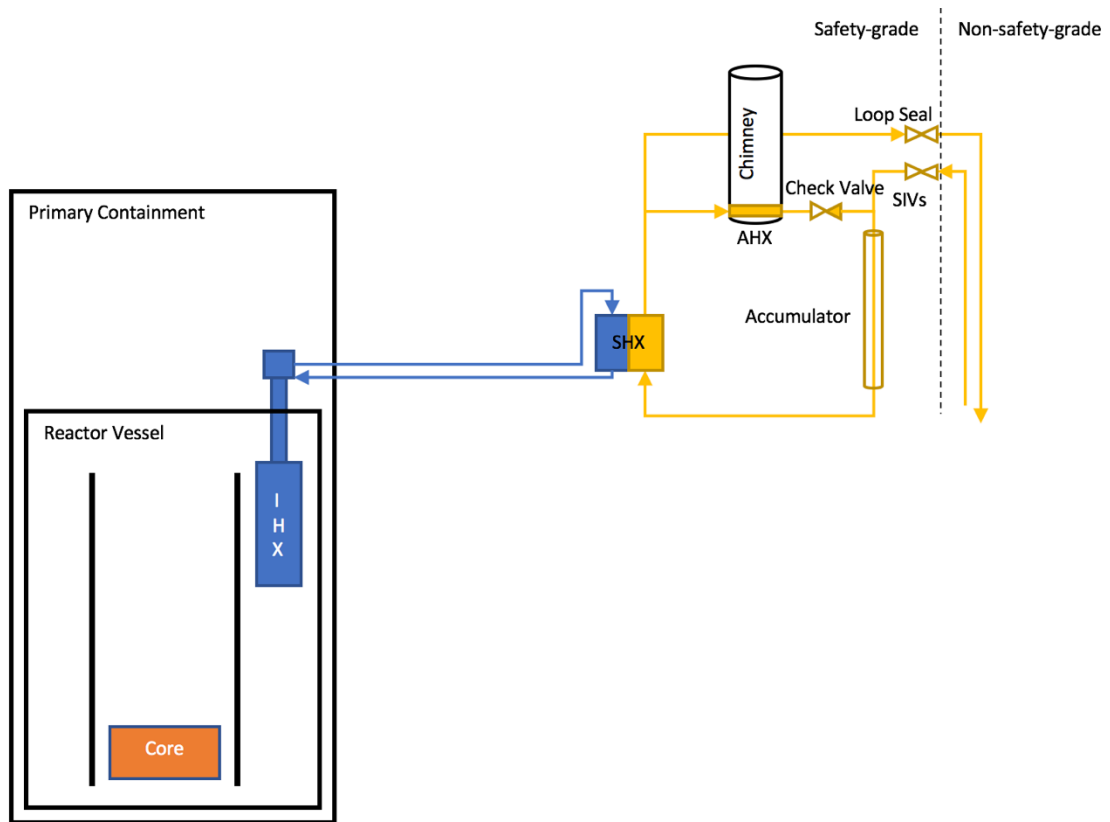


Figure 2-5 Modified PRISM conceptual configuration

The safety-grade boundary is the salt tank side of the Safety Isolation Valves, SIVs. The previous ACS had one steam generator attached to both IHXs. This will have two separate ACS trains, one for each of the two sodium IHX. Each ACS train is sized to passively remove 1% of reactor power, with a design basis ambient temperature of 40°C, the entire plant in natural circulation, and natural draft through the AHX.

3.2.1 Decay Heat Removal

In the redesigned ACS, the heat removal capacity is based on the heat transfer surface area provided in the ACS air heat exchanger, AHX. A single AHX is sized to provide enough DHR capability to cool the reactor down from NOT to refueling conditions at a nominal Cool Down Rate, CDR, of 2.5°C/hr 3-days after shutdown in

natural circulation without forced draft cooling, notionally 0.3% reactor power from decay heat, 0.2% reactor power for the desired cooldown rate, and 0.5% reactor power margin. The plant cooldown can be accelerated by the use of forced draft fans located in the ACS chimney.

As conceived, the ACS can remove 1% reactor power. A single train can maintain PHTS temperature under natural circulation 45 minutes after full power operation under natural circulation and natural draft conditions. Two trains can achieve the same threshold in 11 minutes. This will limit primary temperature excursions. This also limits ACS temperatures below the thermal decomposition temperature of the salt, 630°C.

Solar salt has a freezing temperature of 220°C. The ACS will need to have freeze protection to keep the salt at least 10-15°C above freezing, providing a minimum salt return temperature of about 235°C. Typical SFR refueling temperatures are about 200°C. The modified PRISM will require adjusted procedures to allow refueling at about 250°C.

3.2.2 *NUREG-1368 Considerations*

Chapter 3 of NUREG-1368 proceeds step by step through the General Design Criteria, GDC, providing a justification and basis for how the NRC would likely interpret the existing rule structure. To be able to meet the NRC's standards to license a new unit, we need to first go through their logic. While the design isn't complete, if it is at least logically consistent with the regulator's published interpretations of the existing rules it will greatly simplify final approval.

One immediate consequence is an improvement to GDC 2-Design Basis for Protection Against Natural Phenomena, specifically with response to seismic events, as the material mass associated with the ACS and IHTS is greatly reduced. GDC 3-Fire

Protection has no changes other than the mass of sodium outside of the primary containment is considerably reduced. GDC 4-Environmental and Dynamic Effects Design Bases is not significantly affected. The salt and the sodium react exothermically and require similar systems to the reference plant. Pipe breaks in the salt system, while high temperature, do not pose the same risks as steam breaks. The salt is at atmospheric pressure and is chemically inert, so mechanical whipping forces are limited. Thus, the consideration remains with sodium piping breaks.

GDC 14- Reactor Coolant Pressure Boundary requires a high integrity of the reactor coolant pressure boundary. The elevated salt freezing temperature, 220°C, is well above the sodium freezing temperature, 98.8°C. Preventing salt freezing in the SHX will help to maintain the reactor coolant pressure boundary. This will require heat tracing of the ACS and electric heaters in the PHTS to prevent the ACS portion of the salt loop and bulk sodium temperatures respectively from falling below 220°C.

GDC 16 Containment Design offers a marginal improvement due to limiting the amount of sodium outside of the reactor pool. The containment boundary acts as a second pressure boundary to the reactor coolant pressure boundary. In this regard, the entire IHTS is a part of the containment boundary and the SHX needs to be rated to the pressure of that boundary. There are Safety Isolation Valves (SIVs) that isolate the ACS from the remainder of the non-safety-grade salt loop. This is to prevent the salt loop from interfering with the safety operation of the ACS, e.g. a restoration of pump flow can cause the AHX to solidify as reverse salt flow through the ACS check valve is not adequate to prevent freezing with un restricted airflow across the AHX. The ACS will require a means of pressure control and over pressure protection, similar to the IHTS,

using an accumulator and relief valves/rupture bellows. The accumulator would be normally online, and appropriately heat traced. It would also benefit from being within thermal contact with the remainder of the ACS piping to delay the need for power restoration to prevent freezing. A novel approach for the accumulator would be to have the accumulator as an annulus around a vertical portion of ACS piping. In this scenario, as long as the IHTS was above 230°C, there would be a positive and entirely passive means of pressure control in the ACS.

The increased DHR capability of the ACS allows increased margin to fuel damage in events where there is a station blackout. The inclusion of the ACS in the safety boundary allows inclusion in the design basis. GDC 17-Electric Power Systems requires extremely reliable power to the systems and components that are important to safety. The reliance on natural circulation and natural draft along with the ACS dampers that fail open ensures that the system provides additional safety margin even in the event of a SBO without a SCRAM. The design basis for the plant will be slightly modified, reactor SCRAM with a loss of a single ACS train. The inclusion of the loss of both ACS trains is not considered reasonable.

GDC 20-Protection System Functions covers the RPS initiation. GE-H stated in the PSID that RPS actuation would result in the following: “(1) release of all control rods and operate rod drive-in motors, assuring full rod insertion, not exceeding the design fuel limits and (2) initiate primary sodium coolant pump coastdown, containment isolation, and plant control system adjustments to respond to the reactor trip.” This defines the sequence of events for a reactor trip which we will use to assess the transient and accident response in RELAP. On a plant trip, once the SCRAM has been confirmed with a stable

negative period of ~80s, the SIVs will close. With a time delay set at the SIV stroke time, the ACS dampers will open, and the ACS fans would start. In the event of a SBO the CRDM would disengage as they would in a SCRAM. The SIV's would close after a time delay to allow system pressure to stabilize as the salt pumps coastdown. The ACS dampers would fail open after a time delay drop out to allow the SIVs to actuate. The purpose of the SIVs closing before allowing airflow through the AHX is to ensure that an inadvertent restoration of salt flow would close the ACS check valve securing natural circulation flow through the AHX and causing it to freeze.

Because of the GEMs, rod latching would not be allowed until the RCPs were at 100% flow. This is also a measure to mitigate any potential blockages in a fuel assembly.[61] This will ensure that GDC 28- Reactivity Limits will be met. The reactivity feedback from the salt system is buffered by the minimum tank volume in the cold salt tank resulting in near constant temperature from the salt tank. Additionally, the worst-case reactivity initiation would be maximal salt flow with reactor critical with power just above the source range. Such worst-case events can be handled with procedures such as not opening the SIVs until the reactor is above the point of adding heat. Once above the Point of Adding Heat, POAH, any reactivity insertion will have prompt fuel Doppler feedback mechanisms ensuring immediate negative reactivity insertion compensating for the positive reactivity from fuel cooling. The coolant Doppler results in a positive temperature coefficient of reactivity, thus cooling coolant causes a negative reactivity insertion, lagged by the more positive reactivity insertion of the fuel doppler. Ensuring that the reactor is above the POAH will ensure that a fuel thermal limit will not be exceeded.

GDC 29-Protection Against Anticipated Operational Occurrences requires that the RPS and reactivity control systems perform their functions with high reliability. A more detailed consideration of the events needing consideration is given in Part 4.

GDC 34 Residual Heat Removal has a third independent DHR path. This will be specifically addressed in Part 4.

3.2.3 IHX Design

The IHX is a critical component and many heat exchanger improvements have occurred over the last decade, including the commercial availability of ASME ‘N’ stamped compact heat exchangers.[74] Because of the importance of natural circulation in the PHTS and the IHTS/ACS using high NTU low pressure drop will greatly improve overall plant safety by increasing safety margins.

3.3 Balance of Plant

The BOP can be divided into the Power Conversion System, the energy storage system, and the auxiliary site power. Being able to bootstrap the grid is a critical feature for the facility and needs to be allowed for in the design. The site has tremendous quantities of stored energy in the salt tanks which can be used to start up the reactors. Because the reactors don’t require any electrical power for RHR, the need to have power available for RHR is obviated. Also, with multiple independent sources of power onsite, there is designed redundancy in power supplies that should assuage any argument against operating the reactors in island mode.

3.3.1 Power Conversion System

The PCS should consist of multiple smaller independent steam plants. This has two operational benefits: reduced EFOR due to a trip in one PCS not affecting another

and increased capacity factor due to taking out a smaller unit for a planned outage, instead of the entire facility. The design also decouples the reactor outages from PCS outages providing increased flexibility to the owner in planning and executing scheduled maintenance. From the grid operator's perspective, this type of arrangement with smaller generators will limit the impact of forced outages improving grid stability. It lessens the rolling reserve requirements because one single trip of a 250 MW unit is far less than the impact of the trip of a 1,250 MW unit. An additional benefit is that the storage system acts like an energy RAID that is hot swappable. One component of the server might fail but that can be addressed without affecting the server's availability, only a slight reduction in capacity. Independence between the reactor and the PCS prevents a trip from either affecting the other.

The PCS would likely be a Rankine cycle because S-CO₂ Brayton cycles are not currently available in the size needed for this facility. With smaller power packages, the owner can change them out as economics dictate. For the Rankine cycle, the steam generator can be similar to the S-PRISM S/G, which is a single pass helical design. It would be slightly smaller, for a 250 MW(e) PCS, the steam generator would be about 625 MW(t), larger than a 425 MW(t) Mod A PRISM and slightly smaller than the 840 MW(t) Mod B variant. Additionally, the SG would be better suited for multiple pressures, consistent with the SG's used in solar thermal applications. This will minimize the effects of the pinch points, by going from one to two to three spread out over the salt's temperature profile. This will allow lower overall cold tank temperatures, 290°C which is common in solar thermal applications.

Each PCS would be an adaptation of the bottoming cycle of a combined cycle plant, with the only significant changes being the replacement of the Heat Recovery S/G with the single pass helical salt S/G. The modularity of this approach allows nearly infinite customization in a site even after the facility is operational. This can allow an owner to adjust to long term market trends and technological availability.

The independence of the PCS from the reactors allows the PCS to be operated with Automatic Generator Control, providing voltage and real-time frequency response, improving the power profile on the network. This opens all of the ancillary markets to the owner, who can then specify regulating reserve, rolling reserve, and standby capacities to the ISO that will result in the highest ROI on the assets. The regulating reserve and associated regulating mileage offers perhaps the greatest market opportunity. The Rankine PCS can respond nearly instantly to changes in operational set points, when attached to a semi-infinite constant temperature energy supply. Being quick to respond to Area Control Error, ACE, signals gives the owner access to the mileage before competing energy sources.

3.3.2 Energy Storage System

The energy storage system needs to be sized to meet the operational profile specified by the operator. While there are multiple types of salt thermal storage systems, the two-tank variant will result in the greatest cycle efficiency and consistency of temperatures to the PCS and to the reactors. As with the redundancy needs of the overall project, each salt tank needs to have multiple redundant pumps, sized so that a pump can be taken off service, removed and refurbished and reinstalled without affecting the remaining operational pumps.

3.3.3 *Auxiliary Site Power*

The salt system has a comparable temperature range to the exhaust gas temperatures from a combustion turbine. This allows the bulk of the thermal energy recovered by a conventional combined cycle plant to be recovered by the salt. Placing simple cycle combustion turbines in parallel with the reactor provides additional generating capacity and redundancy from different fuel sources and an additional source of heat for the salt tanks. These combustion turbines can provide simple cycle response time with combined cycle efficiency. Because the cost of the natural gas is the main cost of the power from the combustion turbines, their duty cycle can be varied to follow fuel prices and electricity prices.

The simple cycle combustion turbines, when coupled with a pony diesel can provide blackstart capability allowing the startup of a reactor and the PCSs. A larger pony diesel can be used to start up a hot tank salt pump and PCS which can then bootstrap a reactor. The second approach would be used to blackstart with an outage in the gas supply pipeline. The first approach would be used in a “normal” blackstart situation.

CHAPTER 4 FACILITY LAYOUT

Figure 2.1 nTES conceptual site layout shows the proposed layout of the integrated storage system. A simple way of understanding the modularity of the nuclear Thermal Energy Storage, nTES, is to think of it as an energy bus much like an electrical switchboard. The salt storage tanks act like a battery buffering the temperature (voltage) variation of the bus. The heat from the reactors and the heat recovered from the combustion turbines act like electrical generators. Everything attached to the bus is in parallel. This allows a component (load or generator) to be removed from service through either forced or planned outage without affecting the entire system. It also allows scaled capacity additions, increasing the utilities' flexibility in adding/retiring smaller steps of capacity with demand fluctuations, helping to increase capital utilization without impacting grid stability.

The intention for salt tank operation is to not take the tanks out of service. For this reason, there are at least two reactors, multiple combustion turbines, and several Rankine Power Conversion System, PCS, attached to each set of tanks. Refueling outages are used to adjust for major fluctuations in seasonal demand. With at least one reactor on service the tanks will always have a means of restoring their level. Similarly, the PCS are redundant allowing seasonal adjustment and continued operation with a forced outage. The combustion turbines are another level of redundancy. The site can at some level always maintain electrical power and can restore power quickly after a station blackout without the need for offsite power. The redundancy and the ability to restore plant operation from on site is a critical design feature allowing the plant to bootstrap the grid.

The use of a berm between the reactors and the salt tanks provides a barrier to direct the salt around the reactors in the event of a salt tank catastrophic failure. This can be extended further to provide a missile barrier from any remaining BOP components.

The missile criteria is the one remaining source of “feedback” from the BOP that can affect the nuclear island. Other approaches include using distance, thus creating exclusion zones where non-NRC regulated components cannot be placed.

CHAPTER 5 MATERIAL SELECTION

The storage system is constrained in its material selection due to the chemical interactions of the salt with the metal. Careful consideration was needed to find materials that are compatible with coolants. The materials had to exhibit low general corrosion rates and prevent localized corrosion, e.g. crevice corrosion cracking. Additionally, materials need to withstand duty cycle and transient temperatures without failure.

Carbon steel exhibits adequate corrosion resistance (5mils/yr) at 460°C.[75] In solar thermal applications, carbon steel is limited to 300°C.[67] Carbon steel in nTES similarly has an operational and transient limitation of 300°C. Stainless Steel (SS316) has corrosion rates of 0.03-0.04 mils/yr at 600°C.[75] SS316 is one of 5 alloys; SS304, SS316, 2.25Cr-1Mo, Alloy800H, and ASTM A213 Grade T91, allowed for structural applications under ASME Code Section III Subsection NH for high temperature structural integrity in nuclear applications.[76] SS316 exhibits low corrosion rates, <0.02 mils/yr, in the temperature range of the heat exchanger, < 500°C, and has low rates of decarburization in this temperature range.[77, 78] 9Cr-1Mo at 600°C has corrosion in salt < 0.9 mils/yr.[75] 9Cr-1Mo (ASTM A213 Grade T91) is widely used in combined cycle heat recovery steam generators.[79] T91 could also be used in the PCS steam generators.

The cold tank is made out of carbon steel ASTM-A516-70.[67] The cold tank piping is not made out of ASTM A106 carbon steel, recommended by Moore et al., due to issues of galvanic corrosion between stainless and carbon steels. All salt supply and return piping and the hot tank are SS321 or SS347. There needs to be galvanic protection where the cold pipes interface with the cold tank.

The IHX is made out of SS304 similar to the design reference IHX. The SHX and AHX are T91, however, SS316 and SS304 were considered as viable candidates, but require stricter chemistry controls on the salt increasing capital costs along with O&M. Selecting slightly more expensive materials in favor of reduced operational costs over the life of the plant appeared to be more prudent. Any final material determination is going to need careful engineering and cost consideration. The combustion turbine heat exchanger is T91, with supply and return piping made out of SS321 or SS347. The cold supply piping, in this application, being made out of SS321 or SS347 prevents degradation of the pipe due to the frequency of back flow initiation from cycling the combustion turbines. All of the components and piping outside of the SIVs are non-nuclear using conventional ASME codes. Figure 2.4 shows the safety grade boundary. The system configuration of the ACS prevents carbon steel from being exposed to higher temperatures seen in natural circulation decay heat removal.

SS304 and SS316 are susceptible to crevice corrosion cracking in the presence of impurities in the salt. For this reason, Moore et al recommend using SS321 or SS347 in every application where SS304 and SS316 are used. This is an economic choice, does the increased structural material cost off set the lower cost of the salt.

CHAPTER 6

REACTOR PROTECTION SYSTEMS

The reactor protection system's primary purpose is to ensure that an adequate means of DHR is on service. Because of the inherent reactivity feedback effects associated with the metallic fuel and low stored thermal energy in the fuel, tripping the reactor is not necessary to show protection and limit temperature excursions. Instead, securing coolant flow and establishing natural circulation are what is needed to show protection and limit temperature excursions.

The RPS has three means of providing protection, over power SCRAM, primary hot pool over temperature SCRAM, and a low salt flow SCRAM. The first limits heat generation, the second provides protection against loss of decay heat removal, and the third limits temperature excursions. The LSF SCRAM may not be needed for protection, as the T_h SCRAM provides protection for a loss of salt flow. Instead, the LSF may be a cutback, driving the rods in at normal rod speed until reactor power is less than the protective action's set point. To make this determination one of the more challenging loss of salt flow transients evaluated in Part 4 will be used for comparison of the resulting temperature excursion.

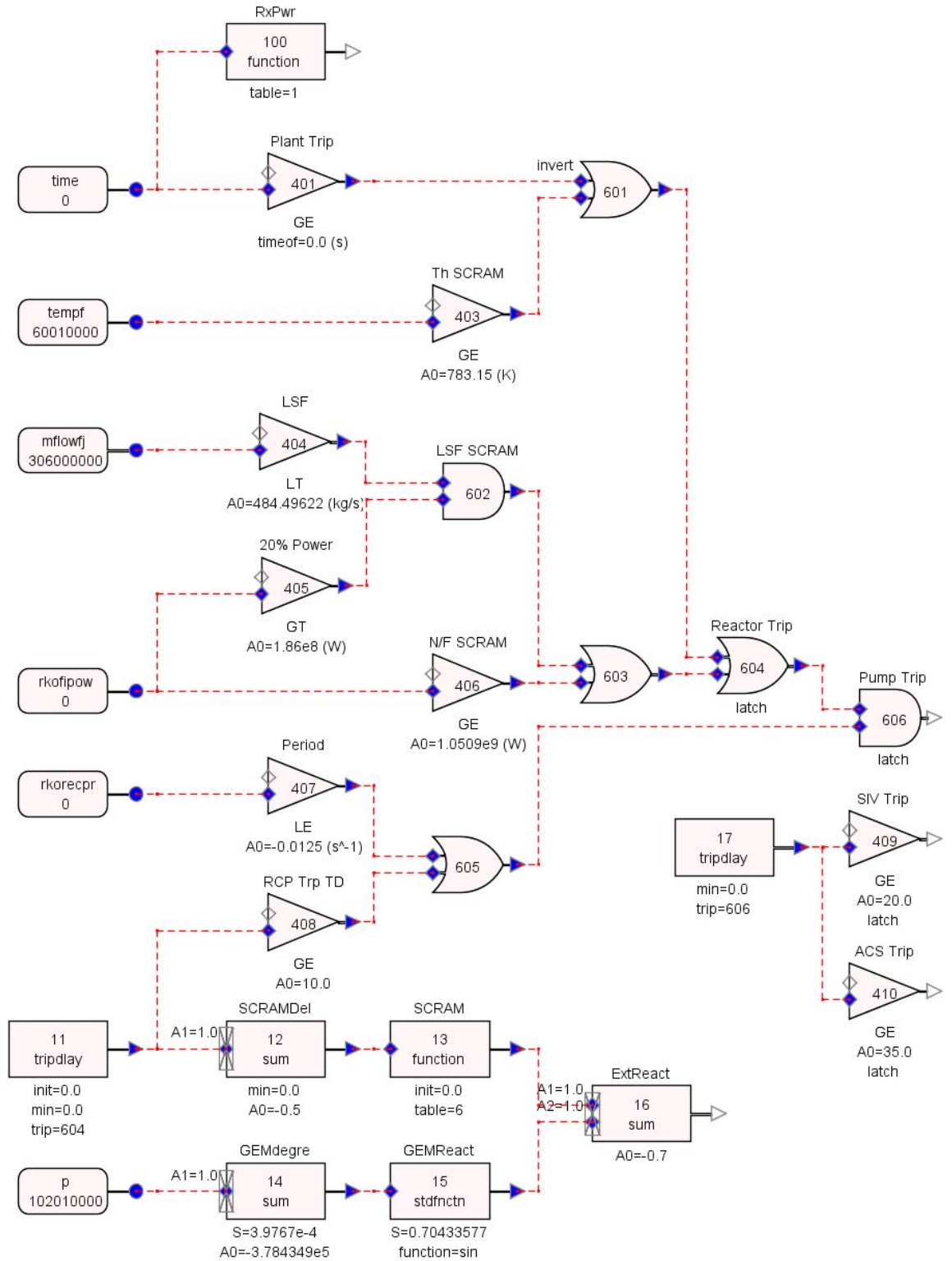


Figure 2-6 Reactor Protection System Logic

Figure 2.6 shows the ladder logic implemented in RELAP for the RPS. The plant trip, **401**, is for manual trips. The T_h SCRAM, **403**, uses the thermocouples in the lower portion of the hot leg riser as its input signal. The LSF SCRAM, **602**, relies on two inputs, that fission power is greater than 20% and that cold inlet salt flow just upstream of the branch supplying the two SHXs is less than 10% of the design flow rate. The over power SCRAM, **406**, is based on a fission power that is greater than 113% of rated indicated reactor power.

The pumps will trip based on the following logic (reactor period shorter than -80 seconds, **407**, OR 5 seconds since a reactor trip, **408**) AND a reactor trip, **604**. The SIVs close 20 seconds after a pump trip, **409**. The ACS dampers open 15 seconds later, **410**. This sequence is to ensure inward rod motion before removing forced circulation and then provide a stately transition to natural circulation conditions. The reactor SCRAM is delayed 0.5 seconds, **12**, from a reactor trip signal, **604**. This is to account for instrumentation, processing, and actuation delays.

The control rods are assumed to have an integral rod worth of \$17.[80] and follow the SCRAM response testing of [81]. The assumed zero reactivity point of the control rods was assumed to be 650 mm corresponding to [81]. Total rod travel was assumed to be the active fuel height of 1.016m with a differential rod worth that followed a cosine function, this left around \$14 for shutdown. Unfortunately, the previous work did not provide data on the rod worth and full power control position to allow more accurate modeling.

The Gas Expansion Modules use the grid plate pressure to provide for their reactivity feedback mechanism. The gas was assumed to be isothermal, temperature does

not affect reactivity. This is significant simplification, but without the heat structure data of the GEMs a more accurate model is not possible. The GEMs were assumed to have an integral worth of \$1.4 with a cosine shaped differential worth. Normal operating conditions were set at a level of 95% of design compression. Minimum static pressure was calculated at a hot leg of 499°C and was 442 kPa. Maximum design pressure was 796 kPa. The GEM reactivity was calculated using Equations 2.4 and 2.5.

$$\theta = 180^\circ \frac{P_{grid\ plate}}{P_{max} - P_{min}} - 90^\circ \frac{P_{max} + P_{min}}{P_{max} - P_{min}} \quad 2-4$$

$$\rho_{GEM} = \$0.7 \sin \theta - \$0.7 \quad 2-5$$

CHAPTER 7 INTERMEDIATE HEAT TRANSPORT AND AUXILLARY COOLING SYSTEM HEAT EXCHANGER DESIGN

Preliminary sizing was done to estimate the configuration of the IHX. Several different configurations of heat exchangers were considered, from conventional shell and tube, Printed Circuit Heat Exchangers (PCHX), and Fin Plate Heat Exchangers (FPHX). The conventional PRISM design uses a shell and tube design rated to the operating pressure of the steam generator, 14.7 MPa.[48, 61] This significantly increases the weight and complicates the design. Additionally, the heat exchanger requires special design to accommodate thermal expansion.[61] We examined PCHX, however, these are unsuitable for applications with sodium because of its high thermal conductivity can cause channel clogging.[82] Because the salt system is vented to atmosphere, the

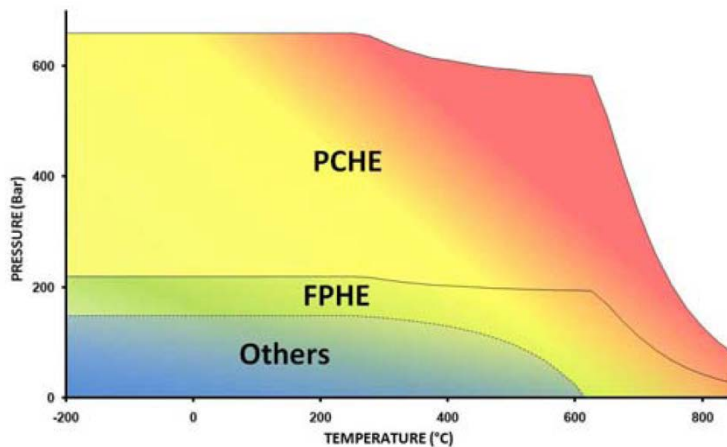


Figure 2-7 Heatric heat exchanger operational envelope from Southall and Dewson[1]

discharge pressure of the AHX, and the remainder of the IHTS, under normal operations can at most be 60.9 kPa due to design pressure loss in the pipe, 5.5 kPa, and the static head of the pipe leading to the hot tank, 55.4 kPa. Assuming a

blockage downstream of the AHX the peak pressure is the shut off head of the cold tank salt pumps, 1.24 MPa. Because the pressure limit on the design reference was set to the normal operational pressure of the steam plant and in the modified design the steam plant

is replaced with salt, 1.24 MPa is new design pressure for the IHX, well within the operating envelope for FPHX.[82] This will also serve as the design pressure for the AHX and SHX.

7.1 Regulatory Design Considerations

The NRC based the review characteristics of the IHX on GDC 15, 30, 31, and 32:[61]

- *GDC 15, “Reactor coolant system design”: Design conditions of the PHTS [Primary Heat Transport System] shall not be exceeded under normal operation or anticipated operational occurrences.*
- *GDC 30, “Quality of reactor coolant pressure boundary”: The PHTS shall be designed to the highest practical quality standards and shall provide a system for leak detection of sodium and cover gas.*
- *GDC-31, “Fracture prevention of reactor coolant pressure boundary”: The reactor coolant pressure boundary shall be designed with sufficient margin to assure that when stressed under operating, maintenance, testing, and postulated accident conditions (1) the boundary behaves in a non-brittle manner and (2) the probability of rapidly propagating fracture is minimized. The design shall reflect consideration of service temperatures and other conditions of the boundary material under operating, maintenance, testing, and postulated accident conditions and the uncertainties in determining (1) material properties, (2) the effects of*

irradiation on material properties, (3) residual, steady state and transient stresses, and (4) size of flaws.

- *GDC-32, “Inspection of reactor coolant pressure boundary”: The PHTS shall be designed to permit periodic inspection and testing of components to assess structural and functional integrity.*

Because of the reduced pressure requirements, GDC-31 is satisfied with a heat exchanger designed for lower operational pressures, allowing a reduction in mass and simplification in design. However much more detailed design analysis will be required to fully satisfy GDC-31. Verifying the IHX integrity through a pressure drop test and weld inspections or other testing satisfies GDC-32. Using an approved high temperature nuclear code and placing a nuclide trace cover gas in the primary coolant and monitoring the cover gas of the hot salt tank for that isotope satisfies GDC-30. Designing the IHX to withstand pump shutoff head satisfies GDC-15.

The separation of the primary system to the steam generator with a vented intermediate system creates an air gap. The air gap makes it physically impossible for the water to be introduced into the IHX. If any leakage occurs in the steam generator it will enter the cold salt tank (290°C, 1 atm) where it will evaporate and leave the tank vents.

7.2 Intermediate Heat Transport System and Heat Exchanger Design

Taking into account the regulatory considerations of 2.2.1.1 and the limitations of sodium requiring larger channel sizes, we determined the FPHX would give the best performance characteristics. We settled on using the Kays and London’s *wavy plate-fin surface 17.8–3/8W* for both sides of the IHX. The sodium side of the AHX used *plain plate-fin surface 12.00T*. These combinations maximized the compactness of the IHX and

minimized PHTS and IHTS pressure drops. The primary pressure drop across the IHX is 218.6 kPa, roughly half of the 430 kPa across the core. The secondary side has a pressure drop of 157.8 kPa. At lower natural circulation flow rates, the secondary pressure drop will be very little, allowing for a reduced elevation difference between the AHX and the IHX. The heat exchanger has a total compactness of $1,538 \text{ m}^2/\text{m}^3$ resulting in significant performance improvements.

Figure 2.8 shows the flow configuration of the IHX and how each IHX is assembled. Table 1 lists the pertinent design parameters for the IHX. Each IHX assembly consists of 4 counter-flow FPHX modules, two modules on either side of the salt supply pipe. We selected an approach temperature of 9°C between reactor core outlet and the IHTS hot-leg. This was done to limit the overall pressure drop across each side, and to

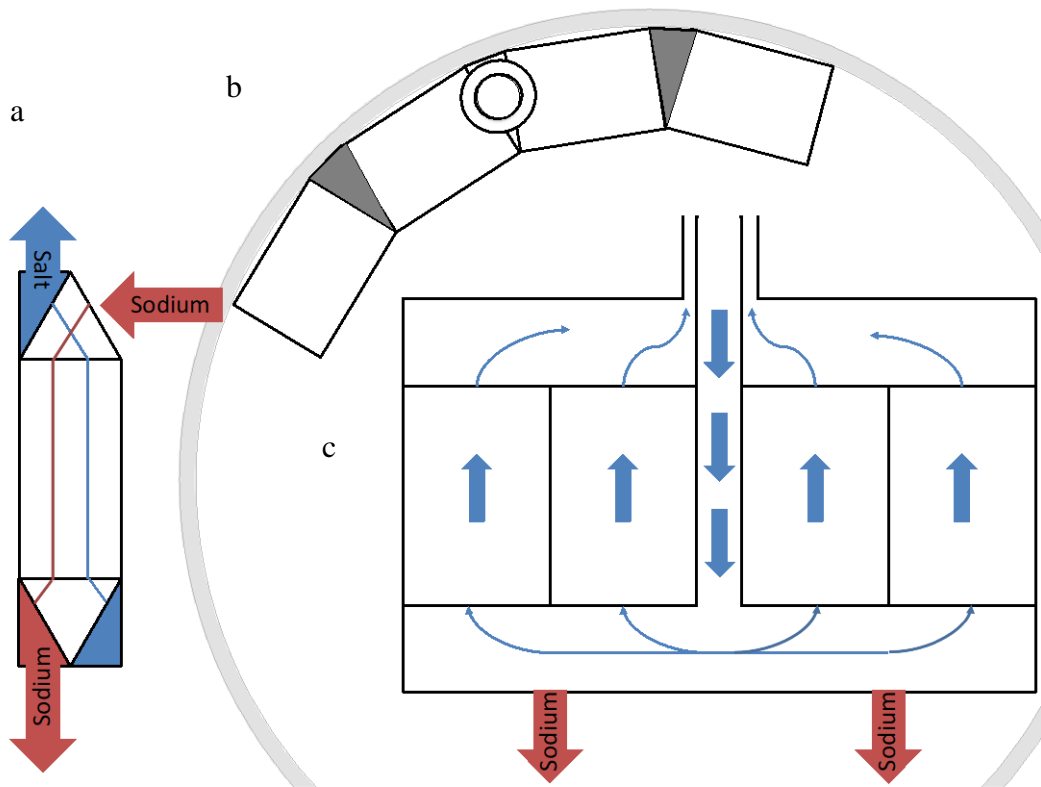


Figure 2-8 Intermediate Heat Exchanger (a) plate profile view (b) IHX top down view inside reactor vessel (c) IHX radial view showing salt flow path.

raise the center of the heat exchanger. The higher heat exchanger center of volume and the relatively low pressure drop improve the PHTS natural circulation flow rate, lowering the core's ΔT and thus fuel peak temperatures. Each IHX spans $\frac{1}{4}$ of the circumference of the reactor vessel. This posed a maximum heat exchanger module width of 1.478 m and a thickness of 0.618 m, assuming the annulus outside of the core rise is 0.626 m wide. Each IHX was sized to remove half of the net heat input into the primary. The RCP thermodynamic efficiency was assumed to be 35% with 100% of the heat and work being transferred to the primary system. Also for design purposes, RVACS was assumed to remove 1.4 MW of heat during normal operation. The net heat removal of each IHX is 424.9 MW and the corresponding length was 3.432 m. Based on the experience of EBR-II fouling of the IHX heat transfer surfaces was not considered, as the machine marks were still visible on the reactor vessel internals during decommissioning. [

Using the exact same IHX support structure as the conventional PRISM, the center of the IHX moved higher 1.66 m. Coupled with the reduced pressure drop and increased elevation, primary natural circulation is greatly enhanced.

Table 2-3 Compact intermediate heat exchanger design parameters

Reactor power [MW(t)]	840	
IHX Design Power [MW(t)]	424.9	
# IHX/Reactor	2	
# Modules/IHX	4	
Module Dimensions		
Length [mm]	3,432	
Width [mm]	1,483	
Thickness [mm]	618	
Surface Area Density [m ² / m ³]	1,538	
	Primary	Secondary
Plate Type	17.38 3/8W	17.38 3/8W
Fin Type	wavy sine	wavy sine
Plate Divider Thickness [mm]	1	1
Plate Thickness [mm]	10.49	10.49
Fin Pitch [fins/m]	701	701
# Plates/Module	65	64
Re	12,546	10,248
Pr	0.00544	0.00544
Heat transfer coefficient	325.5	299.2
Totals for IHX		
Flow Area [m ²]	1.500	1.489
D _H [m]	0.002123	0.002123
Total Heat Xfer Area [m ²]	9,767	9,617
ΔP @ 100% Flow [kPa]	218.6	157.8
Flow [kg/s]	2,391	2,022
IHX inlet Density [kg/ m ³]	866.7	874.2

The original heat exchanger was 6.75 m long. While entirely possible to make the new design having the same length and a much closer approach temperature, we would lose the benefit of the 1.66 m higher heat exchanger center, create a larger pressure drop, and increase heat exchanger manufacturing costs. The pressure drop across the PHTS is what limits the RHR capability of the ACS.

Raising the displacement of the IHX center of volume will have a significant positive impact on the natural circulation and passive Decay Heat Removal (DHR) characteristics of the PRISM, higher elevation differences between the heat source and

heat sink increases loop differential pressure, increasing natural circulation flow, which in turn increases DHR of the ACS, limiting plant temperature perturbations in various accident scenarios, increasing the margin to sodium voiding improving plant overall safety especially for Anticipated Transients Without SCRAM (ATWS).

7.3 Salt Heat Exchanger

As the Salt Heat Exchanger, SHX, is within the safety-grade boundary it needs to meet the same qualification requirements as the IHX. To do this and ensure maximum compatibility with the salt, P91 was selected as the structural material. The SHX is designed to have minimal pressure drop with close approach temperatures. The minimal pressure drop is to facilitate natural circulation flow with minimal elevation change. We took the reference design cold leg piping as is. The hot leg piping was shortened because the SHX is located 2 m above grade and the heat exchanger is only a few meters in height, 3.533 m. The elevation difference between the SHX and the IHX is 9.959 m. A consequence of raising the IHX center 1.66 m to improve PHTS natural circulation, is that the SHX needed to be raised similarly to keep the IHTS temperature difference lower.

The SHX is composed of two different plate types, *plain plate-fin 12.00T* for the sodium side and *wavy plate fin surface 17.8 3/8W* for the salt side. The high heat transfer coefficient of the salt side did not require the additional surface area provided by the wavy plate fin and the IHTS is much more sensitive to pressure drops than the ACS. The ACS is a very compact system and the salt undergoes a much larger density change than the sodium reducing needed elevation differentials. Table 2.4 provides the design parameters for the SHX.

Table 2-4 Salt Heat Exchanger Design Parameters

Reactor power [MW(t)]	840	
SHX Design Power [MW(t)]	426	
# SHX/Reactor	2	
# Modules/SHX	4	
Module Dimensions		
Length [mm]	3,553	
Width [mm]	2,397	
Thickness [mm]	1,065	
Surface Area Density [m ² / m ³]	1,373	
	Secondary	Salt
Plate Type	12.00T	17.38 3/8W
Fin Type	Plain Triangular	wavy sine
Plate Divider Thickness [mm]	1	1
Plate Thickness [mm]	6.35	10.49
Fin Pitch [fins/m]	472	701
# Plates/Module	127	128
Re	6,449	334.1
Pr	0.00544	8.724
Heat transfer coefficient	84.94	3.615
Totals for AHX		
Flow Area [m ²]	3.182	5.091
D _H [m]	0.00287	0.002123
Total Heat Xfer Area [m ²]	15,760	34,080
ΔP @ 100% Flow [kPa]	10.52	18.65
Flow [kg/s]	2,022	1,718
IHX inlet Density [kg/ m ³]	874.2	1,888

CHAPTER 8 AUXILIARY COOLING SYSTEM DESIGN

The ACS is designed to maximize natural circulation and to reject approximately 700 kW at 40°C ambient air conditions for each ACS heat exchanger. It is designed for passive initiation with or without isolation from the remainder of the IHTS. The primary function of the ACS is to function as a Direct Reactor Air Cooling System (DRACS), but by relying almost entirely on equipment used by other systems. Figure 2.7 shows the conceptual ACS flow path that will be evaluated in Part 4.

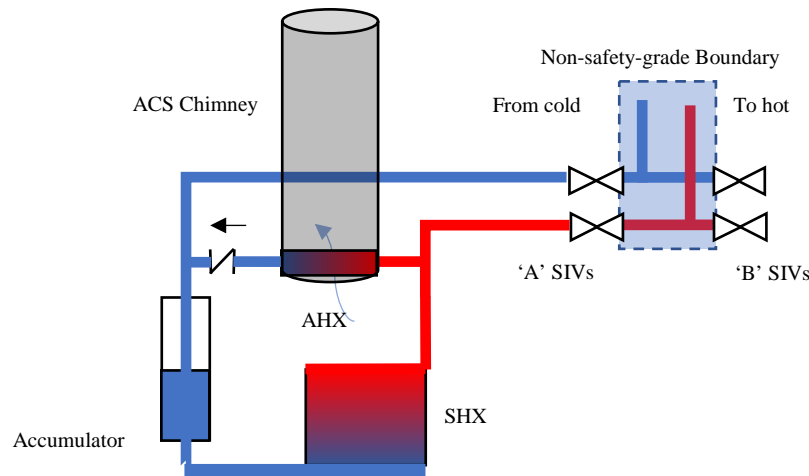


Figure 2-9 Conceptual ACS flow path

8.1 System Flow Path

The ACS heat exchanger (AHX) for each train is located directly above its associated SHX, e.g. the 'A' train AHX is located directly above the 'A' SHX. The AHX is outside of the primary containment and at an elevation of 6.631 m above grade. This is

about 6 m below the mid-point elevation of the helical S/G in the conventional S-PRISM design. This elevation difference was set to provide a 40°C salt ΔT at a design heat removal capacity of 700 kW(t) with 40°C ambient conditions. It can be lowered or raised as necessary to adjust the outlet ΔT . The three systems, PHTS, IHTS and ACS have corresponding ΔT s of 57.7°C, 67.1°C, and 40°C respectively. Figure 2.9 shows the natural circulation temperature profile.

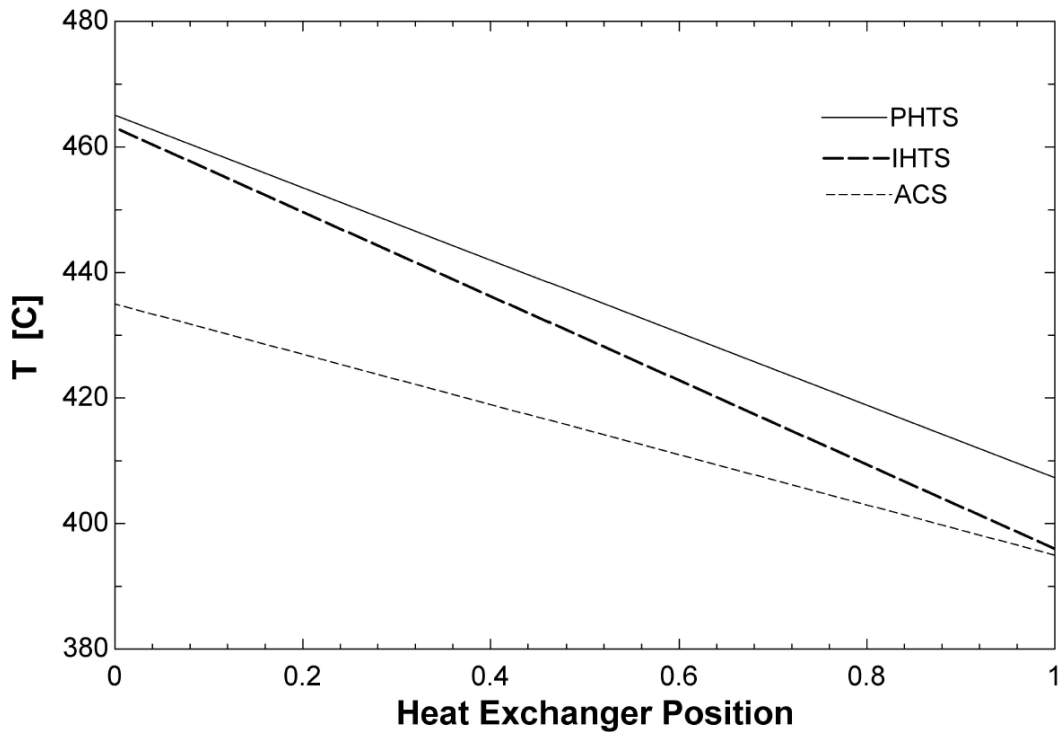


Figure 2-10 Natural circulation temperature profiles

Position changes have a significant impact on the natural circulation driving head and careful consideration needs to be given to heat exchangers and piping system head loss. The downcomer from the AHX is a straight vertical pipe that goes directly to the inlet plenum of the associated SHX. The riser pipe from the SHX only extends a few meters above the SHX to the AHX, and uses long radius pipes as much as possible. The tee's

from the SHX module discharge and supply headers going to the AHX use radiused tee's to promote natural circulation.

The SIVs are located at the top of the IHX inlet and outlet pipes. The remainder of the Salt Heat Transport System, SHTS, salt piping returns to normal grade from the respective common salt header. This elevation change acts as a loop seal in the event of any pipe ruptures in the non-safety grade piping located outside of the ACS and SIVs. The SIVs are the defining boundary between safety and non-safety grade components. The SIVs also form the system boundary for their respective train to keep the trains independent. The SIVs close automatically on a loss of power or on a reactor trip. They have additional features that allow local operation either to open or close them.

Local operation of the SIVs allows restoration of forced circulation to the ACS to allow additional DHR capability via the cold salt tank to the IHX. This additional redundancy will help to limit any accident's temperature transient and aid in plant stabilization. However, shifting to forced circulation requires closing the air dampers of the AHX prior to initiation of forced circulation to prevent salt freezing.

The butterfly check valve will actuate passively based on the system pressure differential. The valve can have external penetrations or it can be designed to have no external penetrations. The simpler design is to have no external penetrations as there is no packing to seize and prevent operation. However, this removes the ability to have an opening assist, e.g., a spring plunger with a hold open solenoid, and removes the ability to verify valve position. These features need to be considered in a more thorough PRA. One can replace the check valve with a fluidic diode. This will increase system reliability,

but reduce performance. Further evaluation needs to be made on which technology is more appropriate in this application.

The ACS chimney extends 11m above the AHX and is 2.5m ID. For conservatism, the surface was assumed to be bolted steel, with a 2mm absolute roughness. The redesigned chimney extends approximately 1.5m above the elevation of the original helical S/G ACS chimney and should pose no additional design challenges.

There are forced draft fans in the chimneys. These are only needed for normal operations during plant cooldown for maintenance and refueling. The safety related dampers open automatically on a loss of power and on a reactor trip and are the ‘normal’ means of DHR. During an accident, the fans can provide additional DHR capability provided electrical power is available.

Pressure is maintained in the ACS when the SIVs are closed by using a gas accumulator attached to the ACS downcomer. The accumulator is an annulus with the central part of the annulus being the downcomer. Nitrogen is used as the cover gas.

8.2 Check Valve

At the outlet of the AHX natural circulation flow path, there is a butterfly check valve. These valves are used in Chinese naval nuclear power plants to prevent loop backflow and allow natural circulation primary coolant flow at power.[83] The check valve will allow better leakage protection and offer a lower natural circulation pressure drop than a fluidic diode. Fluidic diodes are being developed for work in the AHTR, but have non-trivial forward pressure drops and reverse flow rates.[84] While fluidic diodes provide a more reliable initiation solution, they are better indicated for situations where there is no ability for remote access, e.g. inside the PHTS pool. Because the check valves

are located outside of the primary containment, they are accessible for inspection and repair. With two independent ACS systems, one can be taken offline, drained and serviced including replacement/repair of all components. This allows periodic component inspection to satisfy safety related design basis criteria.

The check valve needs to have a design backflow to keep the AHX warm and passively prevent salt freezing. We estimated this to be around 1% of the total salt flow to the IHX without significantly impacting outlet salt temperatures. A full system design of the ACS is needed to obtain the actual number and is beyond the scope of this work.

To have a check valve for modeling in Part 4 a simple non-optimized one was designed according to Rao.

$$\Delta P = 0.5(a + b\theta + c\theta^2 + d\theta^2)\rho v^2 \quad 2-6$$

where the terms a , b , c , and d are constants with the values 26.184, 0.091, -0.014, and $1.11 \cdot 10^{-4}$ respectively. The other terms are valve angle (from vertical), θ , fluid density, ρ , fluid velocity, v , and pressure drop across the valve, ΔP .

The various torques associated with the valve in the system are given by the following equations where T_P is the torque from the pressure gradient across the valve, T_V is the hydrodynamic torque from flow impingement, T_G is the gravitational torque, and T_F is the frictional torque.

$$T_P = \Delta P(A_2L_2 - A_1L_1) \cos \theta \quad 2-7$$

$$T_V = \rho v^2(A_2L_2 - A_1L_1) \cos \theta \quad 2-8$$

$$T_G = (m_2L_2 - m_1L_1)gB \sin \theta \quad 2-9$$

$$B = \frac{\rho_{disc} - \rho_{fluid}}{\rho_{disc}} \quad 2-10$$

$$T_S = 0.02 + 2k\theta \quad 2-11$$

$$\sum T = T_P + T_V - T_G + T_S + T_F \quad 2-12$$

A_i , L_i , and m_i are the respective valves areas, moment arms from the pivot, and masses. 1 denotes the portion that is above the pivot, 2 the portion below the pivot. B is the density ratio to account for buoyancy from the valve's displacement of the working fluid. k is 0.005 for $\theta \leq 16^\circ$, 0.0045 for $16^\circ < \theta \leq 50^\circ$, and 0.00335 for $\theta > 50^\circ$.

The frictional torque was found using the following conditions:

$$\text{For } \frac{d\theta}{dt} \neq 0, T_F = -C_d \frac{d\theta}{dt} \quad 2-13$$

$$\text{For } \frac{d\theta}{dt} = 0 \text{ and,}$$

$$\begin{aligned} T_P + T_V - T_G + T_S < -T_{FS}, T_F &= T_{FS}, \text{ or} \\ T_P + T_V - T_G + T_S > T_{FS}, T_F &= -T_{FS}, \text{ or} \\ |T_P + T_V - T_G + T_S| \leq |T_{FS}|, T_F &= -(T_P + T_V - T_G + T_S) \end{aligned}$$

where C_d and T_{FS} are experimentally determined constants, 0.01 and 0.12 respectively.

All units for the respective terms are MKS, degrees and Pascal.

To determine the valves equivalent orifice opening relative to the upstream pipe, ε_T , and the *vena contracta* area, ε_c , relative to the downstream pipe the following equations were used. ε is the ratio of the downstream to upstream flow areas, taken here to be 1.

$$\Delta P = \frac{1}{2} \rho \left(1 - \frac{\varepsilon}{\varepsilon_c \varepsilon_T} \right) v^2 \quad 2-14$$

$$\varepsilon_c = 0.62 + 0.38 \varepsilon_T^3 \quad 2-15$$

$$0.62 \varepsilon_T + 0.38 \varepsilon_T^3 = \frac{1}{1 + \sqrt{a + b\theta + c\theta^2 + d\theta^2}} \quad 2-16$$

The resulting design is summarized in Table 2.5.

Table 2-5 Summary of Butterfly Check Valve Design Parameters

Material	SS 347
ID _{pipe} [m]	0.7176
OD _{disc} [m]	0.7176
Δ _{disc} [m]	0.009525
Axis offset [m]	0.06396
I [kg-m ²]	1.211
A ₁ [m ²]	0.1662
A ₂ [m ²]	0.2599
L ₁ [m]	0.1205
L ₂ [m]	0.1802
m ₁ [kg]	12.43
m ₂ [kg]	19.44
Design flow [kg/s]	138.3
Design Open Angle [°]	42.26
Design ΔP [Pa]	426.6
Orifice Area [m ²]	0.001647

The disc will have an orifice in it to allow 0.5% of nominal salt flow, 8.59 kg/s, to bypass the SHX and back flow through the check valve orifice which has an area of 0.001647m². Thus, total salt flow into the ACS during normal full power operation is 1,726.63 kg/s.

8.3 Heat Exchanger Selection

The conventional helical coil ACS S/G has an outside surface area of approximately 253 m², with an estimated UA of 6.17 kW/K. The final selected AHX should have an air surface area and UA of at least this much. When conducting the natural circulation calculations this was too large of an area. 1% heat removal was achieved with a heat exchanger of roughly half the surface area, 148 m², with an airside UA of 5.777 kW/K.

The heat exchanger should have a maximal cross section for air flow with a minimum thickness. Because of the difference in the volumetric heat capacities of the salt and the air, 2,746 kJ/m³-K and 0.635 kJ/m³-K respectively, the air is the limiting fluid in

designing the heat exchanger, which is further complicated by the desire to minimize the pressure drop across either side under NC conditions. For these reasons, the crossflow heat exchanger is the best and most commonly used for liquid-gas heat exchange.

To select the most appropriate heat exchanger fill, we opted on using a compact fin plate heat exchanger. We evaluated 57 different geometries from Kays and London and selected the plain plate-fin surface 2.0 (Figure 10-19) for each side by evaluating the total heat removed from the PHTS under NC with the primary coolant at 434.15°C. For each side the plain plate-fin surface 2.0, trapezoidal geometry, performed the best.

Table 2-6 AHX Design Data for 40°C air inlet and T_{ave} of 432°C

AHX heat removal [MW(t)]	8.65	
# AHX/Reactor	2	
# Modules/IHX	4	
Module Dimensions		
Length [mm]	1,250	
Width [mm]	1,250	
Thickness [mm]	200	
Surface Area Density [m ² / m ³]	237	
	Salt	Air
Plate Type	2.0	2.0
Fin Type	plain	plain
Plate Divider Thickness [mm]	1.02	1.02
Plate Thickness [mm]	19.05	19.05
Fin Pitch [fins/m]	78.74	78.74
Plate width [mm]	200	200
# Plates/Module	124	125
Re	4,731	4,224
Pr	4.50	6.12
ΔT [°C]	26.13	372
Heat transfer coefficient	1,070	38.92
Totals for Single AHX		
Flow Area [m ²]	0.428	2.67
Total Heat Xfer Area [m ²]	148	148
ΔP @ 100% Flow [Pa]	231.3	62.5
Flow [kg/s]	217.7	21.0
AHX inlet Density [kg/ m ³]	1,804	0.5038

The indicated heat transfer surface characteristic data is in Table 2.6. To provide an initial size estimate of the heat exchanger, the β (heat transfer surface area to total volume) is $249.672 \text{ m}^2/\text{m}^3$ for a given channel. Thus, the salt side should have a volume of at least 1 m^3 to keep the surface area similar to the conventional ACS. Assuming the final heat exchanger will be 0.2 m thick on the air side, this results in approximately 82 salt plates sandwiched between 83 air plates. We took the plate thickness to be 1.02 mm. The heat exchanger was sized to be square for simplicity and was 3.3 m on a side and 0.2 m thick. This is a workable size and can be broken up into smaller sections in a folded core arrangement.[85] fig 2-42) The size of each panel if breaking the heat exchanger into fourths is 1.6 m on a side and is easily fabricated and shipped. The footprint of the foldable unit, assuming a 30° tilt on the panel from vertical results in a form factor of 1.6 m x 4 m x 1.4 m.

The actual designed unit was much smaller than the one indicated in the rough sizing. The heat transfer for the given conditions would be about 13.9 MW(t). This is much greater than what is needed for the design specification. This shows how easily heat transfer area can be scaled and not have a significant impact on the form factor of the AHX. The folding of the heat exchanger will introduce additional pressure drops into the air system from inlet and outlet ducting. Simply increasing the surface area can bring the pressure drop back to within that needed for the desired airflow.

8.4 Heat Exchanger Calculations

Using the methods of Hesselgreaves[86] and Kays and London[85], we conducted a steady state natural circulation evaluation of the ACS. Piping fixture head loss, including IHX and AHX end effects were estimated using the equivalent length method,

with a resulting salt piping length of 737.1 m of a nominal 29.25” ID schedule 40s pipe. The piping surface was assumed to be adiabatic and axial conduction was neglected in each heat exchanger. Fin efficiencies and all thermophysical properties were calculated using EES internal built in functions.

The test loop heat exchanger network was then simulated in RELAP consisting of one IHX, one SHX, and one AHX, their associated piping and ACS check valve. The system’s boundary conditions were: IHX primary wall temperature was held constant at 456.9°C and the ambient dry bulb temperature was 40°C. This resulted in the test channel removing 1.03 MW(t) with corresponding steady state conditions listed in Table 2-7. Note, the salt was simulated using sodium as the working fluid.

Table 2-7 ACS Performance for Uniform Primary Wall Temperature of 456.9°C and Ambient Temperature of 40°C

	\dot{m} [kg/s]	T_c	T_h	ΔT
IHTS (Na)	66.57	443.91	456.84	12.93
ACS (Salt)	35.98	434.36	456.36	22.00
UHS (Air)	8.902	40.0	154.05	114.05

The performance of the system with a uniform primary wall temperature checks with the observed performance during actual simulations. Figure 2-11 shows a single channel ACS performance over a wide range of salt cold leg temperatures.

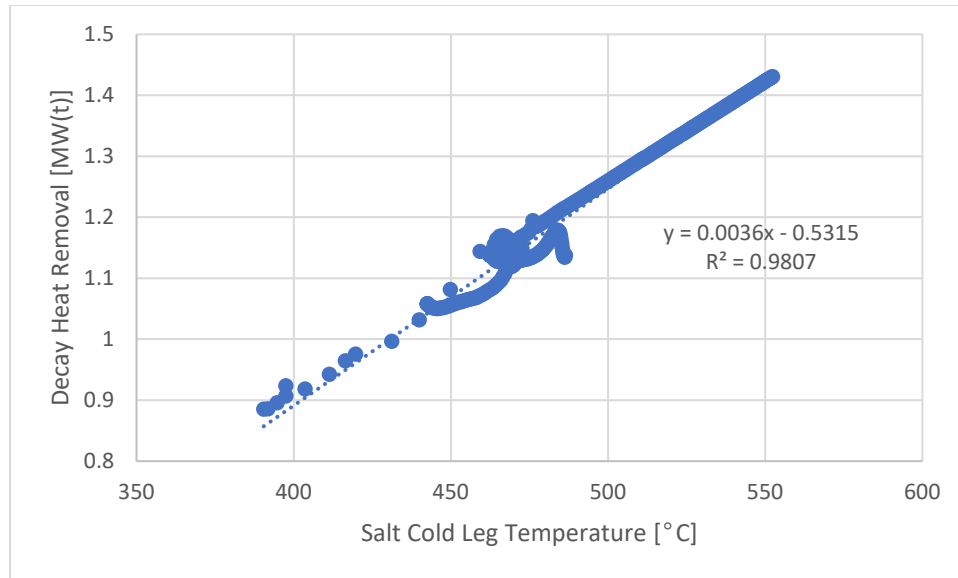


Figure 2-11 Single channel ACS performance for various salt inlet temperatures to the AHX

CHAPTER 9

SYSTEM RESPONSE TO REAL WORLD DATA

The system proposed in Figure 2-1 was evaluated using data from the Bonneville Power Administration.[87] This data set contained 5-minute service area load and generator data. The concept was to have (21) 840 MW(t) Mod B PRISM reactors fulfill 100% of the load profile of the BPA service area to see if a) this was conceptually possible, b) what sort of transients could be expected, and c) to understand how the integrated system would respond.

The control system for the combined sites was greatly simplified. The combustion turbines were set to operate in a bang-bang mode. They were either all on or all off. This system had roughly 60 combustion turbines, and could easily scale output even with individual turbines running at 100%, thus the model is quite contrived and in no way, represents actual operations. The reactors were assumed to operate at full power whenever salt levels were below full capacity and then to modulate their output once the salt tanks were full. There were no predictive capabilities assumed, even though the BPA service area can be reasonably modeled to account for weather, which drives a large portion of the daily variability in load. An actual system would likely use some form of model predictive control to optimize the overall system for a specific service area and market conditions. Such consideration is well beyond the scope of this work and was not done.

The starting and stopping of the combustion turbines was controlled by the hot tank's salt level. Two scenarios were considered, the CT starting at a salt tank level of 85% and lowering stopping once the salt tank was at full capacity, and the CT starting at

a salt tank level of 35% and lowering stopping once the salt tank was full. The results from each control logic is shown in Figure 2-12. The 85% CT control was able to prevent salt tank level from falling below the minimum level, while the 35% CT control was not. This shows that more effective controller design will easily accommodate this system in real life allowing the user to control the overall system more elegantly.

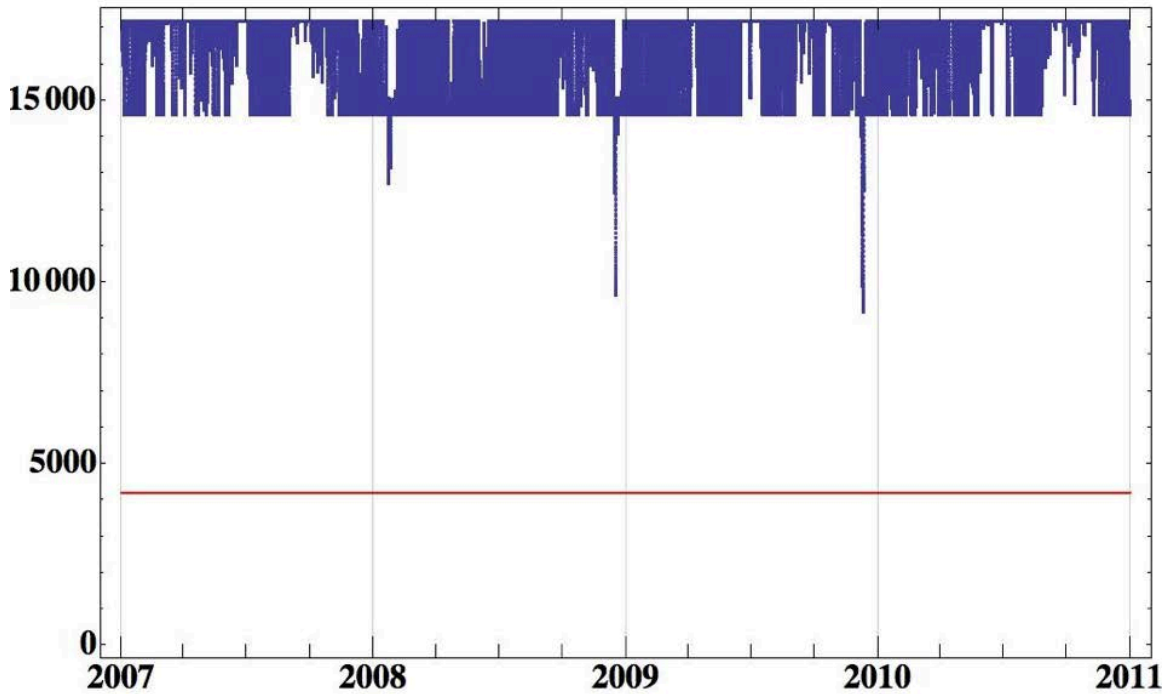


Figure 2-12 85% Combustion Turbine Control Salt Tank Level in m^3 for BPA service area from January 1, 2007 to December 31, 2011. The red line is the minimum tank level for pump NPSH

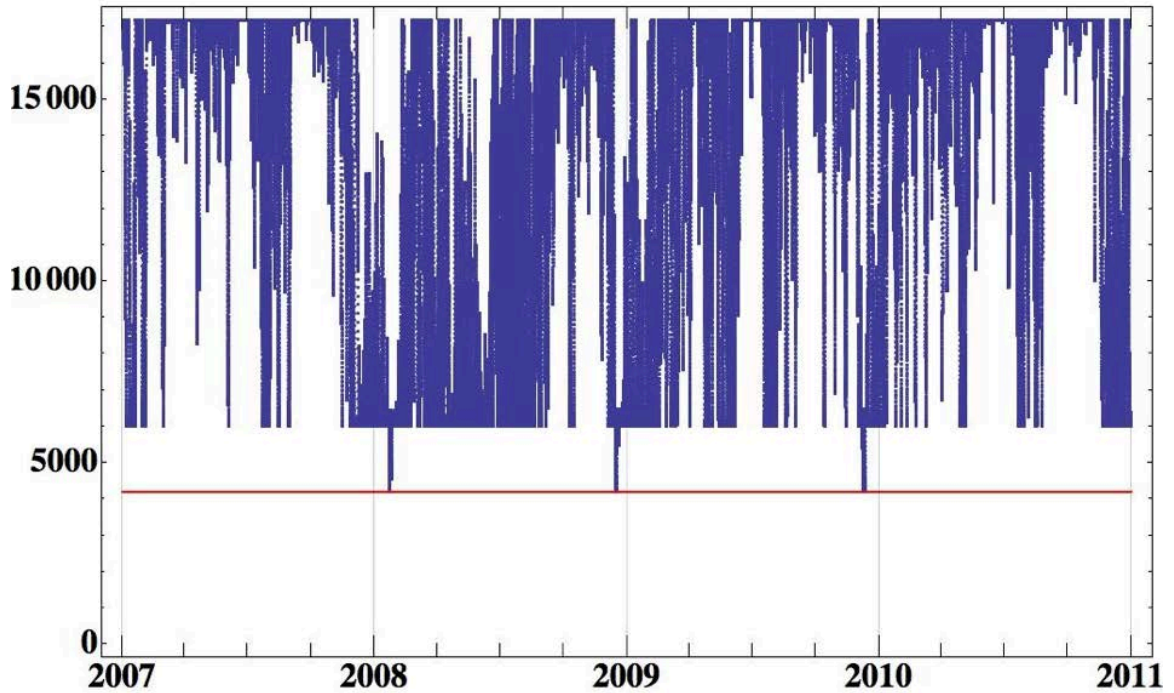


Figure 2-13 35% Combustion Turbine Control Salt Tank Level in m³ for BPA service area from January 1, 2007 to December 31, 2011

For purposes of defining a transient response from the reactor the 35% CT control was selected as it would more closely match the ultimate implementation. This resulted in a reactor capacity factor of 90%, Figure 2-13 even when accounting for planned plant outages, Figure 2-14. Taking this data the histogram of reactor transients in each 5 minute integrating period above 1% per minute was < 0.2% of all 5 minute periods over the 4-year study period, Figure 2-15. The peak rate power change was 4.2%/minute and was used to define the minimum rate of power change for the control system developed in Part 3.

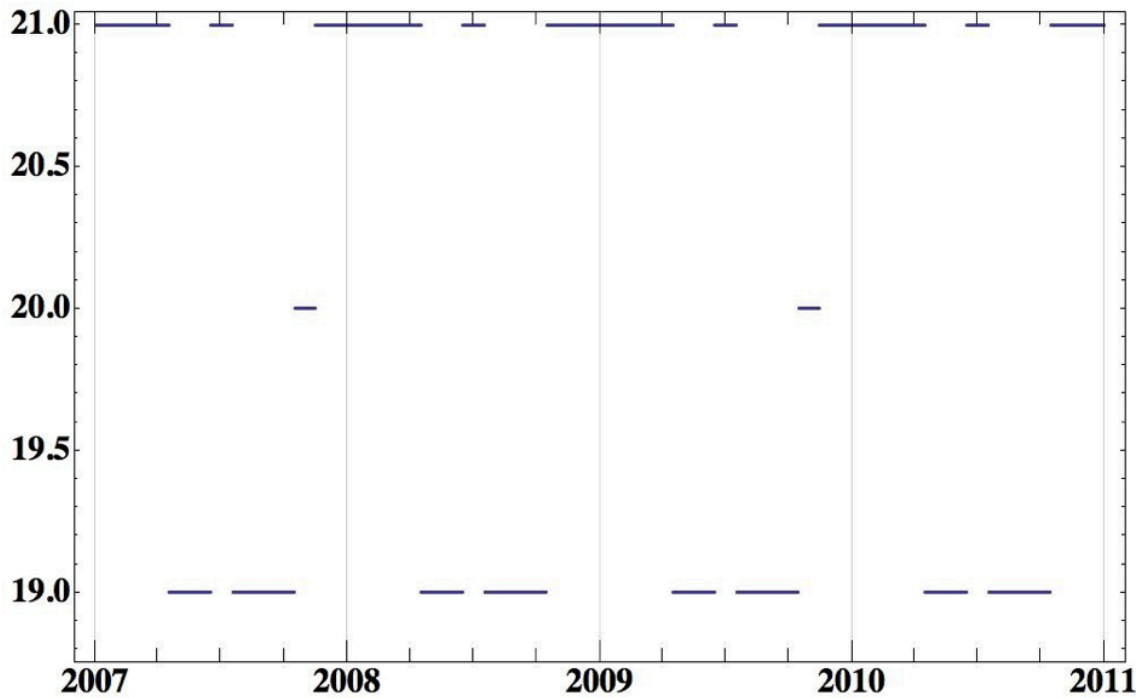


Figure 2-14 Outage schedule for BPA service area when repowered with 840 MW(t) Mod B PRISM reactors using nTES. Reactors assume an 18-month cycle and 1 month refueling outages.

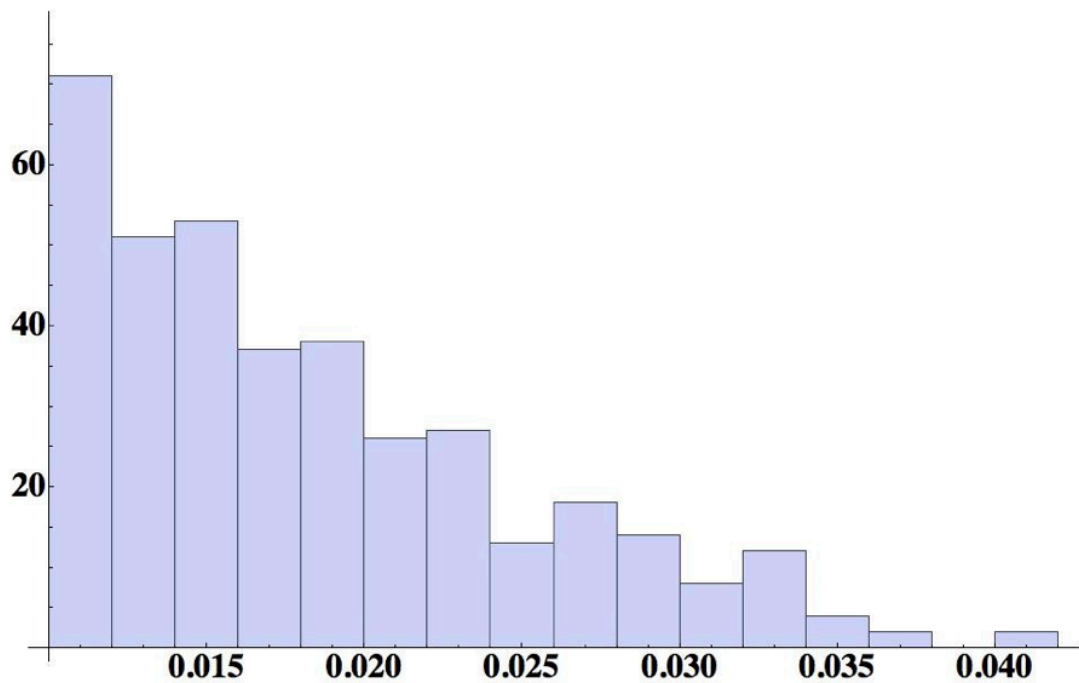


Figure 2-15 Histogram of power transients greater than 1%/min (0.01 on the X-axis) for BPA service area from January 1, 2007 to December 31, 2011

CHAPTER 10 CONCLUSIONS

One of the challenges with S-PRISM and that which has limited core outlet temperatures is maintaining fuel temperatures within the desired margins during various accident scenarios. The approach taken here allows one train of the ACS to always be considered in limiting fuel temperatures, and as importantly salt temperatures. The conventional PRISM only has one ACS system increasing the likelihood of having it unavailable during deterministic design scenarios.

This capability will be specifically evaluated in subsequent RELAP calculations as it improves the economics of storage and the overall thermodynamic efficiency of the PCS improving total plant economics. What will limit the final core outlet temperature is that solar salt begins to undergo thermal decomposition at temperatures above 630°C. Accident scenarios need to limit the time above decomposition temperatures to prevent the evolved gas from gas binding the AHX and preventing natural circulation. It may be necessary to add a gas trap near the AHX. The temperature response of the ACS to various off normal transients was evaluated and is discussed in Part 4 and normal operational transients in Part 3 as a part of designing the control system.

Overall the compactness of this design as well as the introduction of a third independent pathway for DHR represents a significant improvement in the overall design of the nuclear island. The simplification of the ACS portion of the SHTS piping provides significant improvement in the natural circulation capability of the ACS over the conventional PRISM.

The integration of energy storage creates an opportunity for the entire system to be able to access all portions of the electricity market including the entire ancillary market. We will explore the economics of the integrated system in Part 5.

PART 3 – CONTROL SYSTEM DESIGN

CHAPTER 1 INTRODUCTION

The proposed control system is intended to be condition based autonomy within a defined operational envelope. The control synthesis simultaneously adjusts reactor power to a directed power level while maintaining a stable salt outlet temperature to the hot tank. It does this by controlling external reactivity through control rod position and salt mass flow rate into the system. To simplify the controller and reduce the risk of a prompt reactivity insertion from the gas expansion modules, the primary sodium flow rate will be constant. An additional simplification to the design is to neglect the time delays associated with the intermediate loop and to treat the system as if it were just the PHTS and the SHTS.

The model is a linearization of a nonlinear system. The two nonlinear components are the reactor and the IHX. While the reactor linearization introduces small errors for $\rho(t) \ll \bar{\beta}$, the IHX has an 8% error with system power of 20% from the linearization point, worsening farther away from it. For this reason, the controller needs to have an integrating capability around the desired 0 dB crossover frequency. It also needs to have a strong roll off at frequencies above cross over to attenuate the model errors.

We use H_∞ control theory to determine an optimal controller that will exhibit the desired error cancellation at low frequencies and robustness at high frequencies. The approach taken here is based on Suzuki et al[88] work on designing a linearized H_∞ controller for nonlinear instabilities in BWRs at low flow and high power. Because our approach here is so heavily based on their work, we chose to present the material in a similar fashion. In Chapter 2, we present the nonlinear model of the nTES and discuss its

linearization. Chapter 3 presents the design of the controller design, beginning with the basic Linear Time Invariant, LTI, model and adding in instrumentation and control delays to form a complete system. We then present the desired loop shaping to create an augmented model that will be what the controller is based upon. In chapter 4 we simulate the non-controlled/non-augmented model to show basic control input transients and then show how the controlled plant functions in a closed loop to the specified command inputs.

CHAPTER 2 NONLINEAR SYSTEM DYNAMICS MODEL

For simplicity, the underlying model for the reactor is based on the single group delayed neutron precursor zero power point kinetic reactivity model. The S-PRISM has a very large neutron mean free path relative to the size of the core providing a strong leakage term. This leakage strongly shapes the flux distribution. This distribution is relatively constant over the entire power profile, neglecting control rod flux perturbation and changes in leakage due to varying axial and radial sodium densities, of the reactor allowing the separation of variables from the time dependent and the spatial dependent portions of the flux. The core is modeled by equations 3.1-3.5.

$$\frac{dn(t)}{dt} = \frac{\rho(t) - \bar{\beta}}{\Lambda} n(t) + \lambda_{eff} c(t) + \frac{1}{\Lambda} \rho(t) \quad 3-1$$

$$\frac{dc(t)}{dt} = \frac{\bar{\beta}}{\Lambda} n(t) - \lambda_{eff} c(t) \quad 3-2$$

$$\frac{d\Theta_F(t)}{dt} = \frac{Q_0}{V_F \langle \rho_{CP} \rangle_F} n(t) - \frac{2h}{r_F \langle \rho_{CP} \rangle_F} (\Theta_F(t) - \Theta_C(t)) \quad 3-3$$

$$\frac{d\Theta_C(t)}{dt} = \frac{2hr_F}{(r_C^2 - r_F^2) \langle \rho_{CP} \rangle_C} (\Theta_F(t) - \Theta_C(t)) - \frac{2U_{11}r_C}{(r_C^2 - r_F^2) \langle \rho_{CP} \rangle_C} (\Theta_C(t) - \Theta_{ave}(t)) \quad 3-4$$

$$\frac{d\Theta_{ave}(t)}{dt} = \frac{2\pi r_C L_{core} U_{11}}{V_{Na} \langle \rho_{CP} \rangle_{Na}} (\Theta_C(t) - \Theta_{ave}(t)) - \frac{\dot{m}_1 \langle C_P \rangle_{Na}}{V_{Na} \langle \rho_{CP} \rangle_{Na}} (\Theta_{core,out}(t) - \Theta_1(t)) \quad 3-5$$

Where $\Theta_i(t) = T_i(t) - T_i(0)$, $T_{ave}(t) = \frac{1}{2}(T_{core,out}(t) + T_1(t))$, $n(t) = \frac{N(t)-N(0)}{N(0)}$, and $c(t) = \frac{c(t)-c(0)}{c(0)}$ are the reduced temperatures, average coolant temperature, reduced power and reduced delayed neutron precursor concentrations respectively. The system of ordinary differential equations is entirely linear except for the first term of equation 1.a. By keeping $\rho(t) \ll \bar{\beta}$, the nonlinearity can be removed with only small prompt neutron effects observable at the initiation and termination of control rod motion. These high frequency terms can be removed by the controller's strong attenuation of noise above the cutoff frequency. The linearization of Equation 3-1 around $n(0)$ leaves us with equation 3.6.

$$\frac{dn(t)}{dt} = -\frac{\bar{\beta}}{\Lambda}n(t) + \lambda_{eff}c(t) + \frac{1}{\Lambda}\rho(t) \quad 3-6$$

The remainder of the PHTS is modeled by using a first order delay model based on Roetzel's [89] linear approximation of a network of heat exchangers. In their model, the transport of the fluid in adiabatic portions is best is a first order time delay. To approximate the IHX we use the log mean temperature approximation of a counter-flow heat exchanger. This results in equations:

$$\frac{d\Theta_1(t)}{dt} = \frac{1}{\tau_5}(\Theta_{h,out}(t) - \Theta_1(t)) \quad 3-7$$

$$\frac{d\Theta_2(t)}{dt} = \frac{1}{\tau_4}(\Theta_{core,out}(t) - \Theta_2(t)) \quad 3-8$$

$$T_{h,out}(t) = \left(1 - \frac{\gamma - w_3(t)}{\gamma - w_3(t)e^{-\frac{UA}{c_{Na}w_3(t)}(\gamma - w_3(t))}}\right)T_{salt,in} + \frac{\gamma - w_3(t)}{\gamma - w_3(t)e^{-\frac{UA}{c_{Na}w_3(t)}(\gamma - w_3(t))}}T_2(t) \quad 3-9$$

Where $\gamma = \frac{c_{Na}}{c_{salt}(t)}\Big|_{t=0}$ and $w_3(t) = \frac{\dot{m}_3(t)}{\dot{m}_3(0)}$ are the ratio of heat capacities multiplied

by the mass flow rate and the ratio of the mass salt mass flow rate to nominal flow. γ is not unity because of the larger temperature rise across the salt side of the heat exchanger

compared to the flow rate of the salt. This will contribute to an exergy loss in the system, but allows for a lower cost energy storage system.

Renaming the terms in equation 3.9 we have the following:

$$T_{h,out}(t) = f(w_3(t))T_2(t) + T_{salt,in} g(w_3(t)) \quad 3-10$$

and plotting $F = f(w_3(t)) - f(w_3(0))$ and $G = g(w_3(t)) - g(w_3(0))$ in Figure 3.1

we can see the nature of the nonlinearity. This nonlinearity when linearized will introduce a low frequency noise, particularly from $G(x)$. Because the controller is designed to have a low frequency integration term, it will be able to handle this particular modeling error.

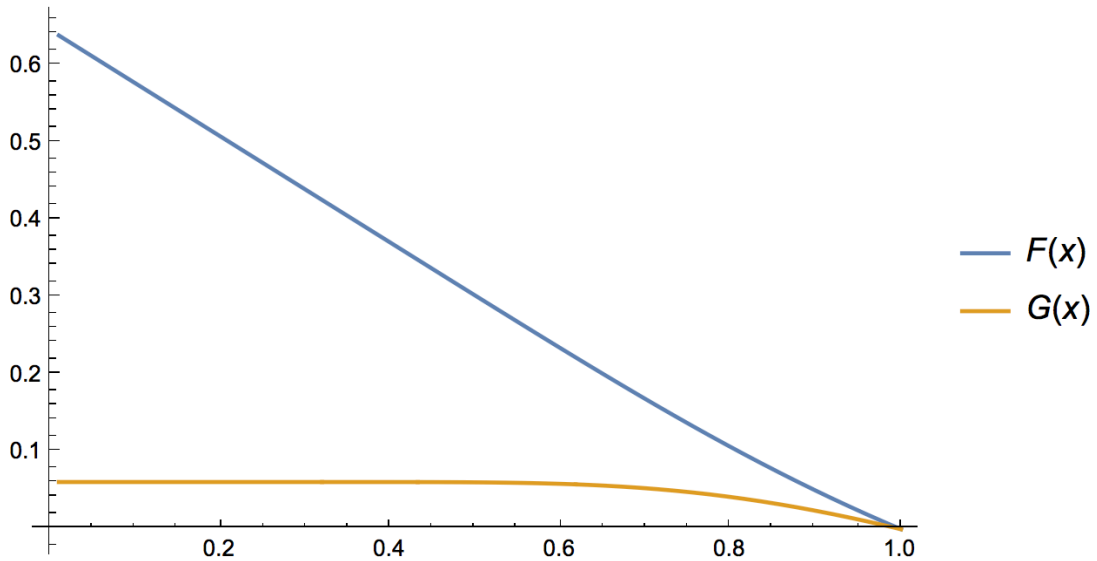


Figure 3-1 Counter-flow heat exchanger governing equations

Linearization of equation 3.10 results in the following:

$$\Theta_{h,out}(t) = \frac{\gamma-1}{\gamma-e^{-UA\frac{\gamma-1}{C_{Na}}}} \Theta_2(t) + \frac{\gamma(T_2(0)-T_{salt,in}) \left(\left(UA\frac{\gamma-1}{C_{Na}} + 1 \right) e^{-UA\frac{\gamma-1}{C_{Na}-1}} \right)}{e^{-2UA\frac{\gamma-1}{C_{Na}-2}} \gamma e^{-UA\frac{\gamma-1}{C_{Na}+\gamma^2}}} x_3(t) \quad 3-11$$

where $x_3(t) = w_3(t) - 1$ is the reduced salt flow rate.

Similarly, looking at the IHX salt outlet temperature, we have a non-linear equation,

$$T_3(t) = \frac{e^{-\frac{UA}{C_{Na}w_3(t)}(\gamma-w_3(t))}((\gamma-w_3(t))T_{salt,in}-\gamma T_2(t))+\gamma T_2(t)}{\gamma-w_3(t)e^{-\frac{UA}{C_{Na}w_3(t)}}} \quad 3-12$$

which linearizes to,

$$\Theta_3(t) = \frac{\gamma \left(e^{-\frac{UA}{C_{Na}}-1} \right)}{\gamma - e^{-\frac{UA}{C_{Na}}}} \Theta_2(t) + \frac{\gamma e^{-\frac{UA}{C_{Na}}}(T_2(0)-T_{salt,in}) \left(1 - e^{-\frac{UA}{C_{Na}}} + \left(1 - UA \frac{\gamma^2 - \gamma}{C_{Na}} \right) \right)}{e^{-2\frac{UA}{C_{Na}}-2} \gamma e^{-\frac{UA}{C_{Na}} + \gamma^2}} x_3(t) \quad 3-13$$

The temperature linearization was done around the full power point, this was an arbitrary decision to make the system as accurate as possible near the operating limits. This induces more error at low powers, but with the increased margin from thermal limits, the controller has more leeway/time to compensate for the modeling errors.

CHAPTER 3 CONTROL SYSTEM DESIGN

The control system design is an adaptation of the SISO control model of Suzuki et al.[88] The two monitored state variables used for control are the reactor power and the salt outlet temperature of the IHX. The two control inputs are control rod position and salt pump speed. Figure 3.2 shows the general plant model. The reference input vector $\mathbf{r}^T = [r_n \ 0]$ where r_n is the operator input desired power level. $G_c(s)$ is the controller transfer function and $K_c(s)$ is the controller output feedback transfer function. $G_0(s)$ is the LTI model of the reactor and heat exchanger system and $G_i(s)$ is the model of the indicated parameters used for plant control. $G_a(s)$ is the augmented plant model that contains: $G_c(s)$, $K_c(s)$, $G_0(s)$, and $G_i(s)$. $\Delta(s)$ is a multiplicative modeling error between the real-world controlled object and the augmented plant model. The entire controlled object is $G(s)$.

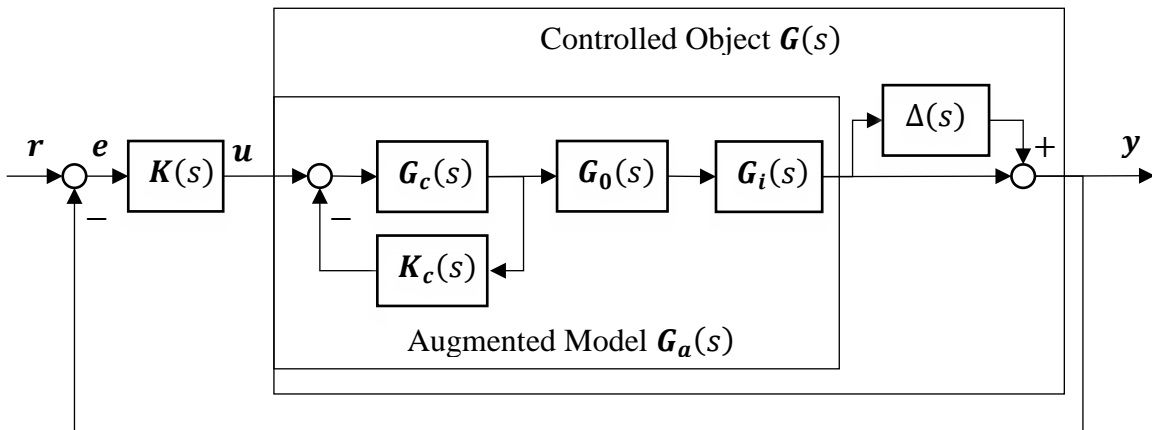


Figure 3-2 General closed loop controller model

3.1 Instrumentation and Control

The models of the CRDMs and Nuclear Instruments are taken directly from Suzuki et al.[88] The CRDM's servo motor is modeled as a simple integrator

$$G_m(s) = \frac{g_m}{s} \quad 3-14$$

where the motor's gain factor, g_m , is assumed to be 0.4 s^{-1} . The position feedback gain factor, k_f , is taken to be 2.5.

A similar model is used to approximate the salt pump motors,

$$G_p(s) = \frac{g_p}{s} \quad 3-15$$

where the salt pump motor's gain factor, g_p , is assumed to be 0.1 s^{-1} and the pump flow feedback gain factor, k_p , is 1. Combining the CRDM and pump models and feedbacks we have

$$\mathbf{G}_c(s) = \begin{bmatrix} g_m & 0 \\ 0 & g_p \end{bmatrix} \frac{1}{s} \text{ and } \mathbf{K}_c = \begin{bmatrix} k_f & 0 \\ 0 & k_p \end{bmatrix} \quad 3-16$$

The NI detector and the salt IHX outlet Resistance Temperature Detector, RTD, response transfer functions are taken to be first order lag functions. And in matrix form the instrumentation transfer function, $G_i(s)$, is:

$$\mathbf{G}_i(s) = \begin{bmatrix} \frac{k_n}{\tau_n s + 1} & 0 \\ 0 & \frac{k_d}{\tau_d s + 1} \end{bmatrix} \quad 3-17$$

where k_n and k_d are assumed to be 1. τ_n is 0.1 s. Without knowing the construction of the RTD, we can approximate its lag as $\tau_d = \frac{r_d(\rho C_P)_d}{2h_d}$ and assumed a final value of 1 s.

3.2 State Equation

Expanding the reactivity term of equation 3.6 we incorporate the feedback effects from fuel Doppler and axial expansion and coolant Doppler and related core radial expansion.

$$\rho(t) = \alpha_F \Theta_F(t) + \alpha_T \Theta_{ave}(t) + k_f x_m(t) \quad 3-18$$

where,

$$\frac{dx_m(t)}{dt} = \frac{1}{g_m k_f} (u_c(t) - x_m(t)) \quad 3-19$$

For the salt pump we have,

$$\frac{dx_p(t)}{dt} = \frac{1}{g_p k_p} (u_p(t) - x_3(t)) \quad 3-20$$

Looking at the controlled outputs, we have:

$$\frac{dx_n(t)}{dt} = \frac{1}{\tau_n} (n(t) - x_n(t)) \quad 3-21$$

$$\frac{dx_d(t)}{dt} = \frac{1}{\tau_d} (\Theta_3(t) - x_d(t)) \quad 3-22$$

for the NI and RTD respectively.

Making the appropriate variable substitutions and using the matrix form of the LTI model,

$$\frac{dx}{dt} = \mathbf{A}x + \mathbf{B}_1 \mathbf{w} + \mathbf{B}_2 \mathbf{u} \quad 3-23$$

$$\mathbf{z} = \mathbf{C}_1 x + \mathbf{D}_{11} \mathbf{w} + \mathbf{D}_{12} \mathbf{u} \quad 3-24$$

$$\mathbf{y} = \mathbf{C}_2 x + \mathbf{D}_{21} \mathbf{w} + \mathbf{D}_{22} \mathbf{u} \quad 3-25$$

we have,

$A =$

$$\begin{bmatrix} -\frac{\beta}{\Lambda} & \lambda & \frac{\alpha_F}{\Lambda} & 0 & \frac{\alpha_T}{\Lambda} & 0 & 0 & \frac{1}{k_f \Lambda} & 0 & 0 & 0 \\ \frac{\beta}{\Lambda} & -\lambda & 0 & 0 & 0 & 0 & 0 & 0 & 0 & 0 & 0 \\ \frac{Q_0}{V_F \langle \rho C_P \rangle_F} & 0 & \frac{-2h}{r_F \langle \rho C_P \rangle_F} & \frac{2h}{r_F \langle \rho C_P \rangle_F} & 0 & 0 & 0 & 0 & 0 & 0 & 0 \\ 0 & 0 & a_1 & -(a_1 + a_2) & a_2 & 0 & 0 & 0 & 0 & 0 & 0 \\ 0 & 0 & 0 & a_3 & -(a_3 + a_4) & a_4 & 0 & 0 & 0 & 0 & 0 \\ 0 & 0 & 0 & 0 & 0 & -\frac{1}{\tau_5} & \frac{a_5}{\tau_5} & 0 & 0 & 0 & \frac{a_6}{\tau_5} \\ 0 & 0 & 0 & \frac{2}{\tau_4} & -\frac{1}{\tau_4} & 0 & -\frac{1}{\tau_4} & 0 & 0 & 0 & 0 \\ 0 & 0 & 0 & 0 & 0 & 0 & 0 & -\frac{1}{g_m k_f} & 0 & 0 & 0 \\ \frac{1}{\tau_n} & 0 & 0 & 0 & 0 & 0 & 0 & 0 & -\frac{1}{\tau_n} & 0 & 0 \\ 0 & 0 & 0 & 0 & 0 & 0 & \frac{a_7}{\tau_d} & 0 & 0 & -\frac{1}{\tau_d} & \frac{a_8}{\tau_d} \\ 0 & 0 & 0 & 0 & 0 & 0 & 0 & 0 & 0 & 0 & -\frac{1}{g_p k_p} \end{bmatrix}$$

$$\mathbf{B}_1^T = [0 \ 0 \ 0 \ 0 \ 0 \ 0 \ 0 \ 0 \ 0 \ 0 \ 0 \ 0]$$

$$\mathbf{B}_2^T = \begin{bmatrix} 0 & 0 & 0 & 0 & 0 & 0 & 0 & 0 & 0 & 0 & \frac{1}{g_p k_p} \\ 0 & 0 & 0 & 0 & 0 & 0 & \frac{1}{g_m k_f} & 0 & 0 & 0 & 0 \end{bmatrix}$$

$$\mathbf{C}_1 = \begin{bmatrix} 0 & 0 & 0 & 0 & 2 & -1 & 0 & 0 & 0 & 0 & 0 \\ 0 & 0 & 0 & 0 & 0 & 0 & 0 & 1/k_f & 0 & 0 & 0 \\ 0 & 0 & 0 & 0 & 0 & 0 & 0 & 0 & 0 & 0 & 1/k_p \end{bmatrix} \quad \mathbf{D}_{11} = \begin{bmatrix} 0 \\ 0 \\ 0 \end{bmatrix} \quad \mathbf{D}_{12} = \begin{bmatrix} 0 \\ 0 \\ 0 \end{bmatrix}$$

$$\mathbf{C}_2 = \begin{bmatrix} 0 & 0 & 0 & 0 & 0 & 0 & 0 & 0 & k_n & 0 & 0 \\ 0 & 0 & 0 & 0 & 0 & 0 & 0 & 0 & 0 & k_d & 0 \end{bmatrix} \quad \mathbf{D}_{21} = \begin{bmatrix} -1 \\ 0 \end{bmatrix} \quad \mathbf{D}_{22} = \begin{bmatrix} 0 \\ 0 \end{bmatrix}$$

$$\mathbf{x}(t)^T = [n \ c \ \Theta_F \ \Theta_C \ \Theta_{ave} \ \Theta_1 \ \Theta_2 \ x_m \ x_n \ x_d \ x_3]$$

$$\mathbf{w}(t) = [r_d] \mathbf{u}(t)^T = [u_p \ u_c]$$

with the outputs of,

$$\mathbf{z}(t)^T = [\Theta_H \ z_\rho \ z_p] \quad \mathbf{y}(t)^T = [e_n \ e_t]$$

where z_ρ is the reactivity of the control rods, z_p is the measured salt pump flow rate, y_n is the indicated NI power, and y_d is the indicated salt IHX outlet temperature. The $\mathbf{z}(t)$ vector was included to show how non-control outputs are calculated for model outputs of interest. The constants of the \mathbf{A} are,

$$a = \left[\begin{array}{c} \frac{2hr_F}{(r_C^2 - r_F^2)\langle\rho C_P\rangle_C} \\ \frac{2U_{11}r_C}{(r_C^2 - r_F^2)\langle\rho C_P\rangle_C} \\ \frac{2\pi r_C L_{core} N_{pins} U_{11}}{V_{Na}\langle\rho C_P\rangle_{Na}} \\ \frac{2C_{Na}}{V_{Na}\langle\rho C_P\rangle_{Na}} \\ \frac{\gamma - 1}{\gamma - e^{-UA\frac{\gamma-1}{C_{Na}}}} \\ \frac{\gamma(T_2(0) - T_{salt,in}) \left(\left(UA\frac{\gamma-1}{C_{Na}} + 1 \right) e^{-UA\frac{\gamma-1}{C_{Na}}} - 1 \right)}{e^{-2UA\frac{\gamma-1}{C_{Na}}} - 2\gamma e^{-UA\frac{\gamma-1}{C_{Na}}} + \gamma^2} \\ \frac{\gamma \left(1 - e^{-UA\frac{\gamma-1}{C_{Na}}} \right)}{\gamma - e^{-UA\frac{\gamma-1}{C_{Na}}}} \\ \frac{\gamma e^{-UA\frac{\gamma-1}{C_{Na}}} (T_2(0) - T_{salt,in}) \left(e^{-UA\frac{\gamma-1}{C_{Na}}} + UA\frac{\gamma^2 - \gamma}{C_{Na}} - 1 \right)}{e^{-2UA\frac{\gamma-1}{C_{Na}}} - 2\gamma e^{-UA\frac{\gamma-1}{C_{Na}}} + \gamma^2} \end{array} \right]$$

Table 3.1 and 3.2 list the Design parameters used for building the control model.

Table 3-1 Core Physical and Control and Instrumentation Design Parameters

Control and Instrumentation				Core physical parameters			
g_m	0.4	s^{-1}	CRDM gain factor	Q_0	10^6	kW	Nominal Reactor Power
k_f	2.5		CRDM proportional feedback gain	V_F	0.499363	m^3	Total Heavy Metal Volume
g_p	0.1	s^{-1}	Salt pump gain factor	$\langle \rho C_P \rangle_F$	1,835.87	kJ/m^3-K	Fuel volumetric heat capacity
k_p	1		Salt pump proportional feedback gain	r_F	0.002738	m	Fuel radius
τ_n	0.1	s	NI response time delay	h	197.132	kW/m^2-K	Fuel to Clad heat transfer coefficient
k_n	1		NI gain	$\langle \rho C_P \rangle_C$	4,169.61	kJ/m^3-K	Clad volumetric heat capacity
τ_d	1	s	RTD response gain	r_C	0.00372	m	Clad radius
k_d	1		RTD gain	U_{11}	92.3814	kW/m^2-K	Clad to coolant heat transfer coefficient
				N_{pins}	49,717		Number of fuel pins
				L_{core}	1.016	m	Active core height

Table 3-2 Loop Design Parameters

PHTS Parameters				IHTS Parameters			
C_{Na}	7,195.58	kW/K		C_{salt}	4,950.81	kW/K	
T_2	772.15	K	Hot-leg temperature	T_3	765.15	K	IHX outlet temperature
T_1	633.15	K	Cold-leg temperature	$T_{salt,in}$	563.15	K	IHX inlet temperature
$\langle \rho C_P \rangle_{Na}$	1,084.71	kJ/m^3-K	Na volumetric heat capacity	UA	36,542	kW/K	IHX heat transfer coefficient
τ_4	35.722	s	Hot-leg time delay				
τ_5	48.930	s	Cold-leg time delay				
V_{Na}	1.540619	m^3	Active core coolant volume				

Table 3.3 and Table 3.4 provide the delayed neutron and reactivity feedbacks used in building the model.

Table 3-3 Core Reactivity Feedbacks at Various Times in Core Life

	Fuel Related			Coolant Related		
	Fuel Doppler	Axial Expansion	α_F	Coolant Doppler and Thermal Expansion	Radial Expansion	α_T
	pcm/K	pcm/K	pcm/K	pcm/K	pcm/K	pcm/K
BOC	-0.3401	-0.4655	-0.8056	0.7577	-0.1950	0.5627
MOC	-0.3438	-0.5818	-0.9256	0.8007	-0.1978	0.6029
EOC	-0.3467	-0.4386	-0.7853	0.8366	-0.1978	0.6388

Table 3-4 Delayed Neutron Parameters at Various Times in Core Life

Delayed Neutron Precursor Data			
	$\bar{\beta}$	λ_{eff}	Λ
	pcm	s ⁻¹	s
BOC	373.8	0.5311	2.670E-07
MOC	379.1	0.5320	2.707E-07
EOC	378.9	0.5322	2.704E-07

3.3 Design Specification

The controller has fundamental physical limits that it needs to maintain. First deal with reactivity and the others deal with operational needs. The control rods have two limits, rate and magnitude, placed on them pertaining to reactor safety. The rod withdrawal speed is limited to ensure a maximum reactivity insertion rate of 2¢/s , 7.5 pcm/s , and a rod stop limit of 20¢ , 75 pcm . [61, 90] Another constraint on control rods is to minimize control rod motion for transients. [91] Applied to an automatic control scheme, control rod mileage needs to be limited with minimal control action overshoot.

From an operational perspective, from looking at the model in Part 2, the reactor needs to have a design rate of power change of at least 4.2 \%/min . To achieve this, we

want to have a rise rate for a doubling of reactor power to be less than 5 minutes, specifying a minimum closed loop control bandwidth of 0.0067 rad/s.[92] The control rod speed and desire to minimize rod motion will put an upper limit on the bandwidth, but this needs to be evaluated during loop shaping.

The closed loop model needs to be stable, maximum real value of the closed loop model's A eigenvalues needs to be less than zero.[93] It needs to satisfy performance criteria, low sensitivity at low frequencies, and the model needs to satisfy robustness criteria, that at frequencies above cross over the closed loop transfer function and complementary sensitivity have a roll-off of 20-40 dB/decade.[88] This will ensure that the negative gain will grow faster than the positive gain from measurement noise.

3.4 Loop Shaping and H_∞ Synthesis

We followed the approach of Suzuki for loop shaping with some modifications. First is that there is a need for our controller to have good error cancelation around the cross over frequency. To do this we used a PID to shape the low frequency signal and modified it to include a lead compensation feature.

$$W_S(s) = \begin{bmatrix} \frac{12.5 (s+79.99) (s+0.01)}{s (s+120)} & 0 \\ 0 & \frac{10^5 (s^2 + 0.1s + 0.01)}{s (s+34)} \end{bmatrix} \quad 3-26$$

Because the H_∞ synthesis was done using the built in MatlabTM function of the Robust Control Systems ToolboxTM, `ncfsyn`, the complementary sensitivity shaping was done with a simple lag compensator as the built-in synthesis requires a proper transfer function to be input. Other MatlabTM synthesis approaches have even more restrictive stability criteria and do not allow poles of zero. Because our sensitivity shaping transfer function is based on an integrator, it has a zero pole, and the integrating

function is needed to reduce model error at low frequencies, we were unable to use the other synthesis functions. Matlab technical support reason for this was:

“...[W]e discussed that we do only consider systems with poles having a negative real part as stable. The systems given in the weights $[W_S(s)]$ are considered as marginally stable. One rationale for this is to see the behavior of these systems with constant inputs. For example, if you provide a step or a constant input to either of the systems, the output that comes out is a ramp signal, which goes unbounded as you increase the simulation time, which does not show a stable behavior.”

$$W_T(s) = \begin{bmatrix} \frac{0.1(s+0.02)}{s+0.01} & 0 \\ 0 & \frac{0.1(s+0.02)}{s+0.01} \end{bmatrix} \quad 3-27$$

The remaining component is the augmented plant model:

$$G_a(s) =$$

$$\begin{bmatrix} \frac{-8.239 \cdot 10^7 s^4 - 1.201 \cdot 10^{10} s^3 + 6.582 \cdot 10^{10} s^2 + 4.036 \cdot 10^{10} s + 1.078 \cdot 10^9}{s^9 + 1.4 \cdot 10^9 + 3.486 \cdot 10^{11} s^7 + 2.296 \cdot 10^{13} s^6 + 2.818 \cdot 10^{14} s^5 + 8.742 \cdot 10^{14} s^4 - 1.189 \cdot 10^{12} s - 8.07 \cdot 10^9} \\ \frac{1.498 \cdot 10^7 s^6 + 3.552 \cdot 10^9 s^5 + 2.058 \cdot 10^{11} s^4 + 9.121 \cdot 10^{11} s^3 + 4.655 \cdot 10^{11} s^2 + 20.9 s + 2.15 \cdot 10^8}{s^9 + 1.4 \cdot 10^9 s^8 + 3.499 \cdot 10^{11} s^7 + 2.327 \cdot 10^{13} s^6 + 3.024 \cdot 10^{14} s^5 + 1.126 \cdot 10^{15} s^4 + 9.311 \cdot 10^{14} s^3 + 8.749 \cdot 10^{13} s^2 + 2.609 \cdot 10^{12} + 2.62 \cdot 10^{10}} \\ \frac{2.356 \cdot 10^{11} s^2 + 1.3 \cdot 10^{11} s + 2.558 \cdot 10^9}{s^9 + 1.4 \cdot 10^9 s^8 + 3.373 \cdot 10^{11} s^7 + 2.025 \cdot 10^{13} s^6 + 1.233 \cdot 10^{14} s^5 + 1.956 \cdot 10^{14} s^4 + 1.01 \cdot 10^{14} s^3 + 8.984 \cdot 10^{12} s^2 + 2.632 \cdot 10^{11} s + 2.62 \cdot 10^9} \end{bmatrix}$$

where the first column represents from u_p , the second column is from u_c the first row is to x_n and the second row is to x_3 . The final H_∞ synthesis controller K , has 36 degrees of freedom and was generated using the Robust Controller Toolbox™ command,

$[K \sim \gamma] = \text{ncfsyn}(G_a \quad W_S \quad W_T)$. The resulting $\gamma = 2.004$ being less than 3 shows that the controller tracks the loop shaped model within acceptable bounds.

During modeling, we encountered problems with being able to obtain satisfactory gain margins with the need to have low frequency error cancellation with an integrator. Because there is a pole at zero, the shaping regulator can become unbounded with high frequency errors. This was frequently observed during model development. This unsatisfactory response for high frequency performance can also be seen by our inability to obtain negative gain margins and achieve the desired plant performance characteristics, even for a marginally stable controller that met overall design objectives, equations 3.26 and 3.27. Figure 3.3 shows the closed loop Bode diagrams for the final closed loop system. We attempted the use of improper transfer functions to force the desired high frequency gain response similar to that taken by Suzuki. This approach could not yield a controller using H_∞ synthesis.

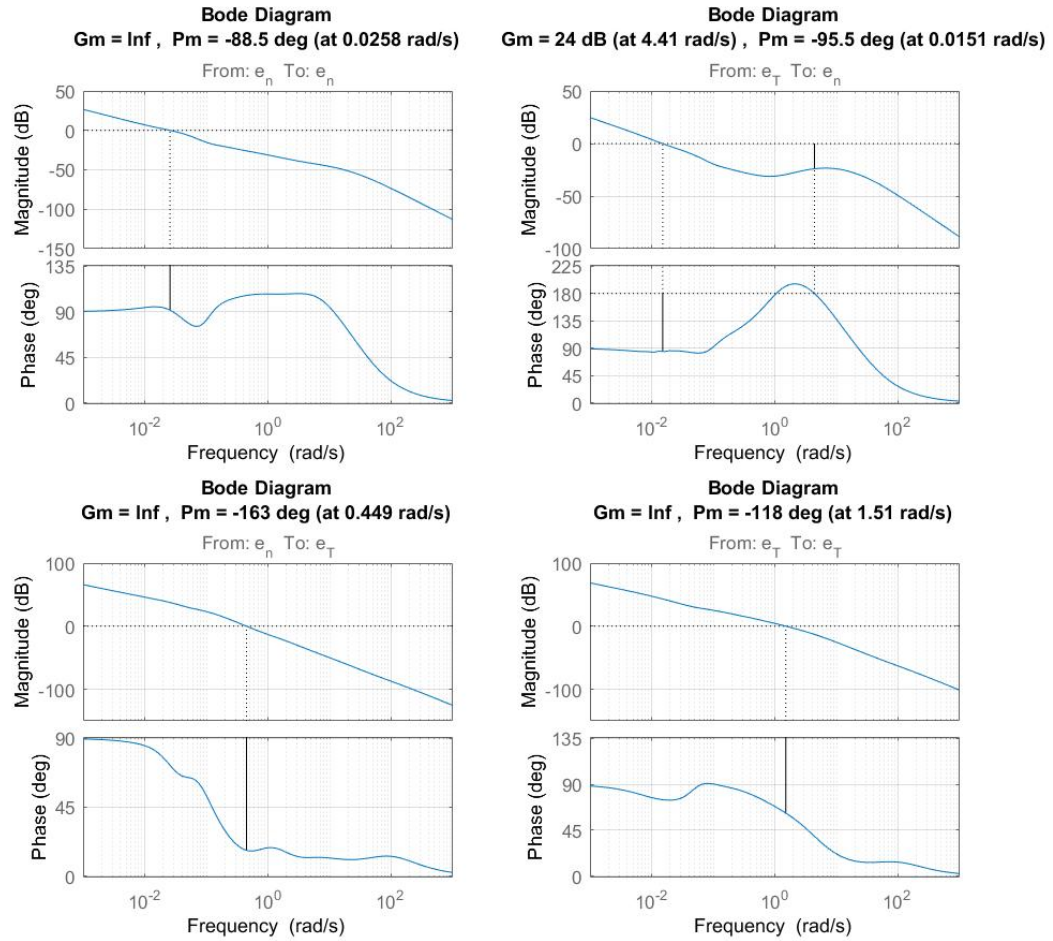


Figure 3-3 Bode diagrams for the closed loop system.

Examining the response of the plant in Figure 3.3 using sensitivity, $S = \frac{1}{1 + G_a K}$ and complementary sensitivity, $T = 1 - S$, we can see that the closed loop plant has excellent low frequency performance with complementary sensitivity near 0 dB, no resonance peak and bandwidth that results in a desired final controlled plant response, 0.0104 and 1.103 rad/s for reactor power to pump control and salt outlet temperature to external reactivity respectively.[92] The sensitivity function for reactor power to pump control has a 0dB crossover of 0.0758 rad/s, indicating that plant inputs with a frequency

less than this value will be attenuated, and others will be amplified.

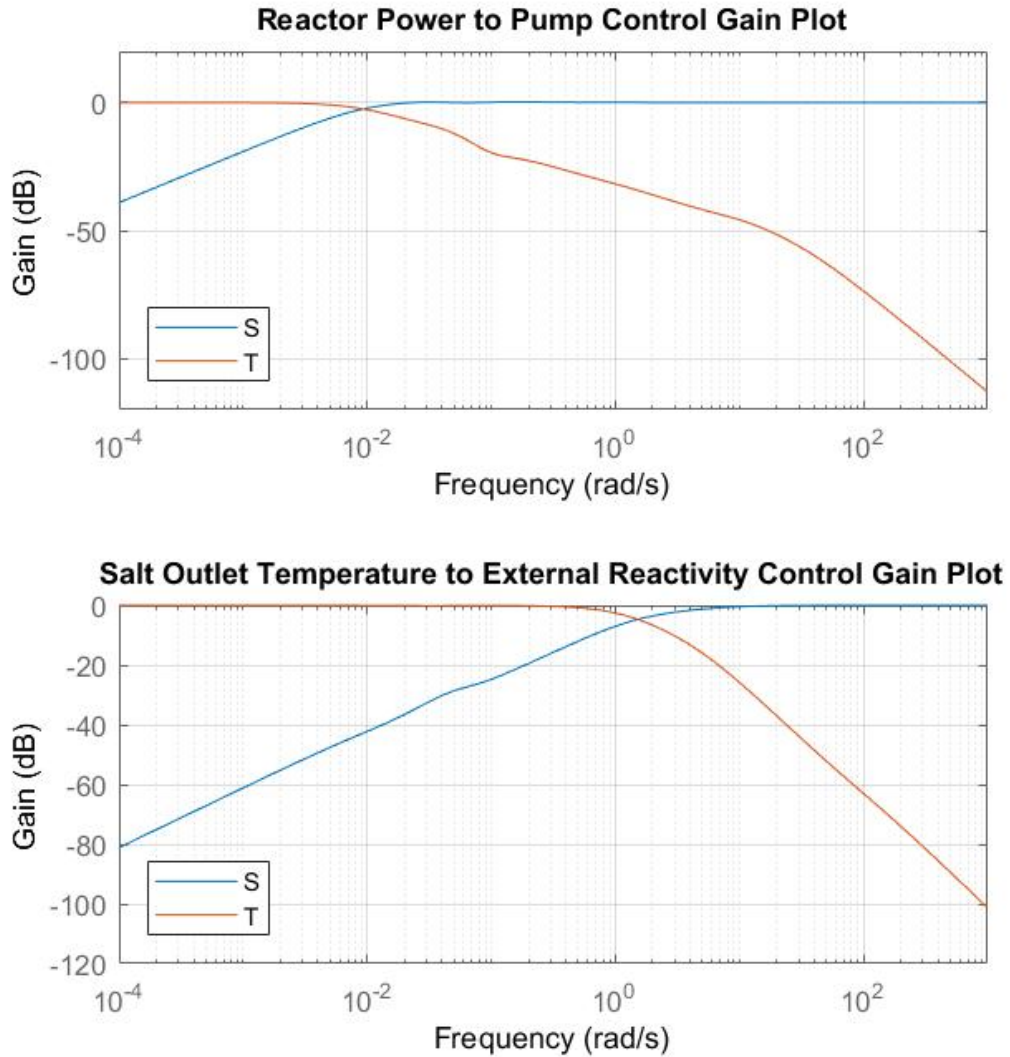


Figure 3-4 Sensitivity and complimentary sensitivity graphs.

The salt outlet temperature to external reactivity control does not have a 0dB crossover, indicating that all higher frequency noise will be attenuated to some level. The maximum sensitivity remains close to 0dB for both responses, indicating monotonic noise amplification. This can be seen better by looking at the load disturbance gain,

$G_{wd} = G_a S$, and the measurement noise gain, $G_{un} = KS$, as seen in figure 3.4.

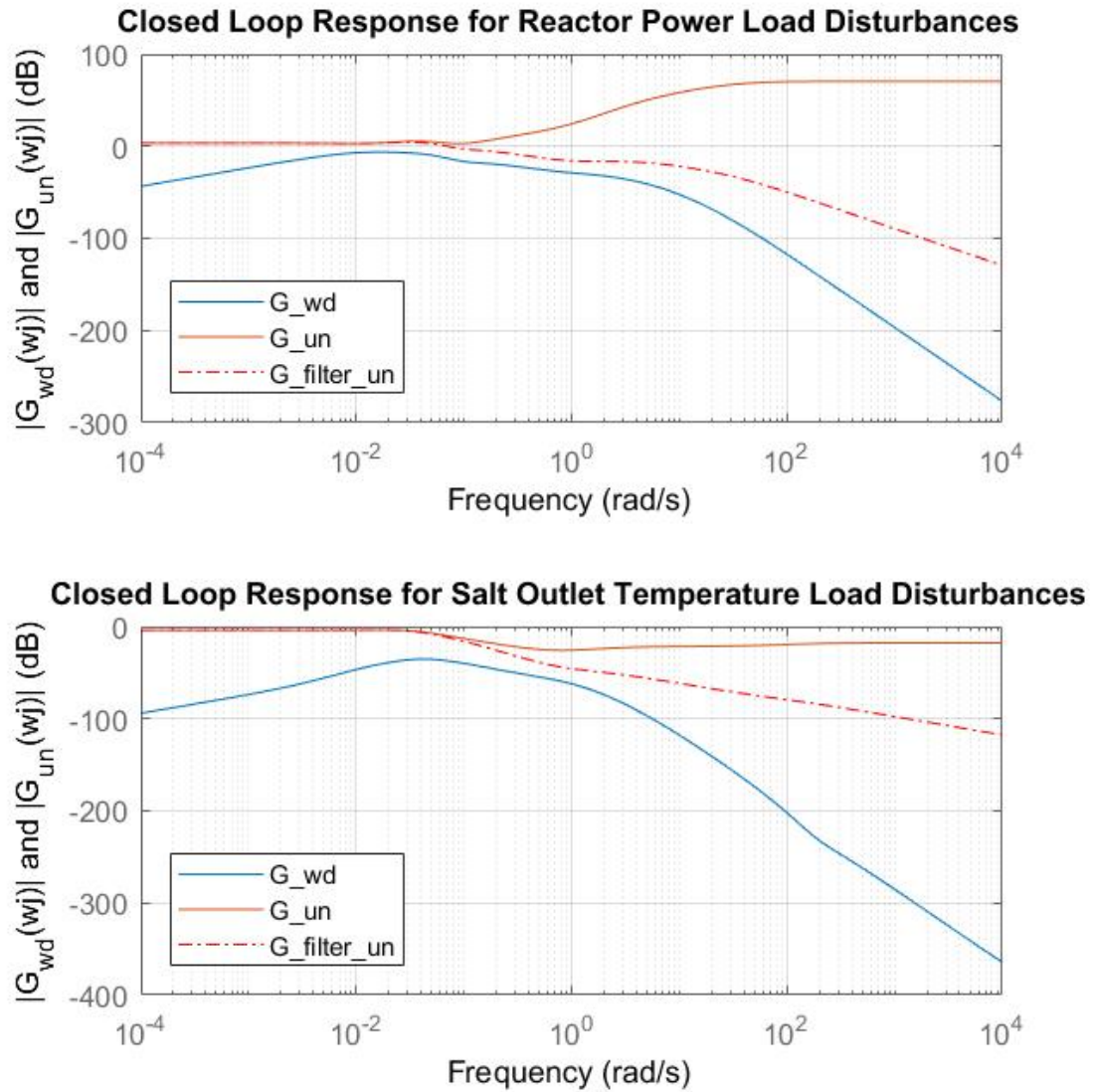


Figure 3-5 Controller disturbance and noise gains

Figure 3.5 also contains low pass filters for the measured parameters, $F_{lp,n} = 0.1^2 / (s + 0.1)^2$ and $F_{lp,3} = 0.1 / (s + 0.1)$. By including the low pass filters outside of the H_∞ synthesis of the controller, we can achieve satisfactory high frequency

performance for the plant. The final plant controller is shown in Figure 3.6 where $\mathbf{F}_{lp} = \text{diag}(F_{lp,n} \ F_{lp,3})$.

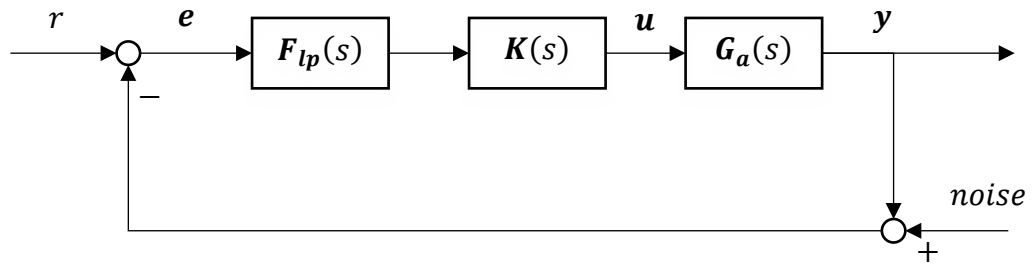


Figure 3-6 Final closed loop controller

CHAPTER 4 SIMULATION RESULTS

4.1 Open Loop Simulation without Control

To assess the uncontrolled plant model and get an estimate for the error induced through linearization of the IHX governing equations, we evaluated the open loop plant model both in steady state to steady state step changes and in transient response.

To evaluate the steady state to steady state transient response, we set the time derivative of equation 3.23 to zero and solved $\mathbf{x} = -\mathbf{A}^{-1}\mathbf{B}_2\mathbf{u}$ for the desired step response of \mathbf{u} . Table 3.5 provides the results of the step changes in reactivity and flow.

Table 3-5 Modeled Steady State to Steady State Step Response

	\mathbf{u}_c	\mathbf{u}_p	
n	0.008204	0.4115	
c	$21.62 \cdot 10^6$	$1.085 \cdot 10^9$	
θ_F	0.97	-34.07	°C
θ_C	0.85	-39.80	°C
θ_{ave}	0.67	-48.78	°C
θ_1	0.33	-107.67	°C
θ_2	1.01	10.11	°C
ρ_c	0.4	0	pcm
x_n	0.82%	41.15%	
θ_3	0.98	-30.80	°C
x_3	0%	100%	

There are some useful operational parameters that can be obtained from Table 3.5. For every 1 pcm of reactivity corresponds to a 2.44°C change in salt outlet temperature and a 2.1% change in reactor power. For a 1% change in salt flow, reactor power will change 0.41% and salt outlet temperature will change -0.31°C.

In evaluating the dynamic response, the best way to describe the response of the reactor responds to control inputs sluggishly, Figure 3.7. It is like driving a semi-tractor compared to a sports car. There is a significant thermal inertia associated with the system due to the overall sodium mass and the strong prompt negative reactivity feedbacks make for very docile plant response to reactivity perturbations. For a 0.4 pcm reactivity insertion at a rod speed of 5 pcm/s, the rise time of salt outlet and reactor power were 84 s and 26 s, respectively.

One concern that further justifies the measured indication filtering in the final controller design, is the prompt jump/drop upon initiation and termination of rod motion. The large and immediate error signal generated could cause rod chatter (inward/outward) shims to chase power that could lead to instability and reactor protective action.

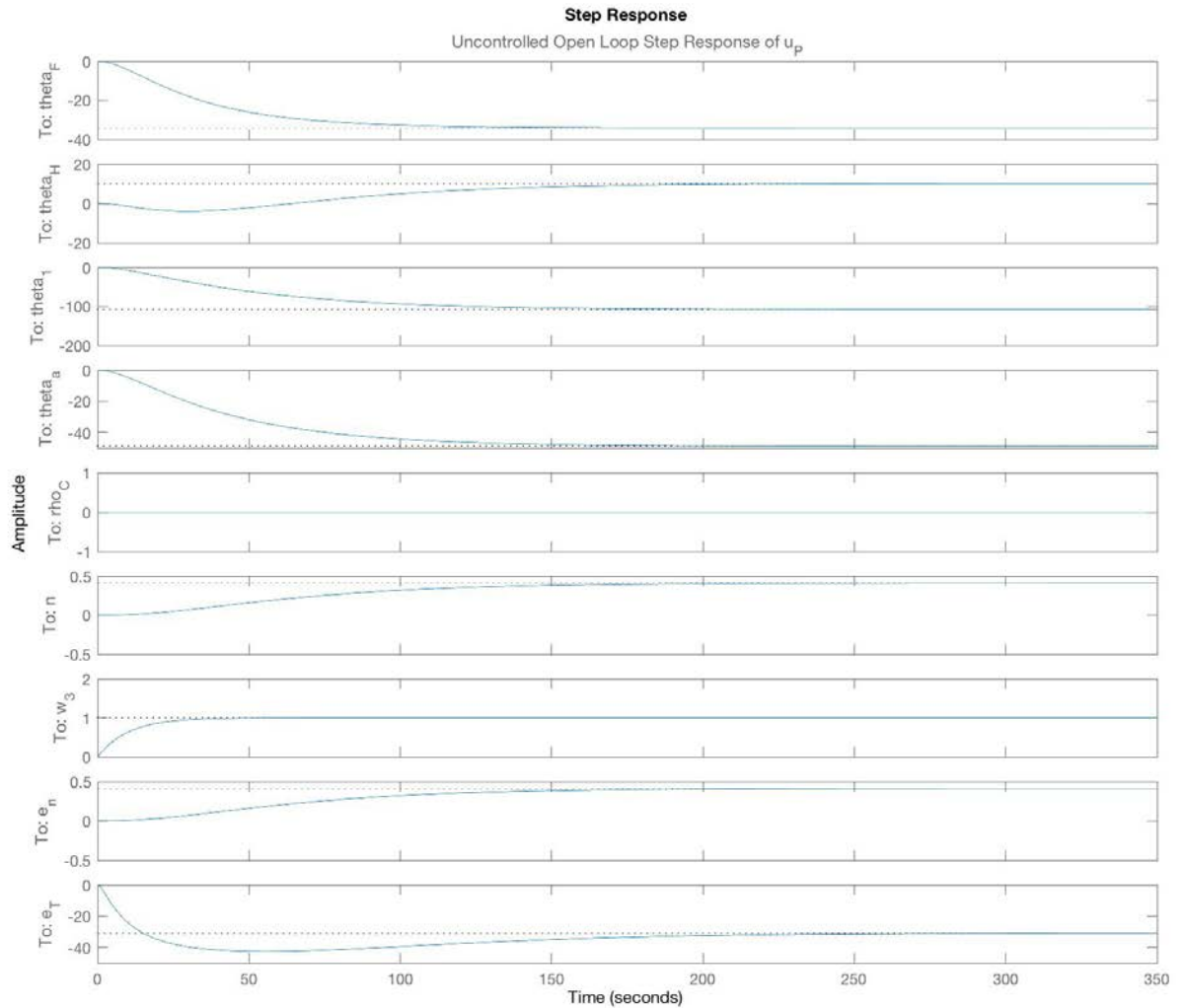


Figure 3-7 Transient response to a step change in pump flow

4.2 Closed Loop Simulation with Optimal Control

The closed loop response to a unit step function in target reactor power is shown in Figure 3.8. While this response is not physically achievable in real life, it represents going from 100% to 200% power, it is useful in showing the dynamics of the closed loop system to a more challenging transient than what is in its operational envelope (50%-100% power at 100% primary flow rate). All other transients will result in a less aggressive controller action (lower magnitude in error signal). Reactor power and salt

pump are both slightly under damped, some improvements can be had by making them critically damped, but this will increase the needed mileage from the CRDMs.

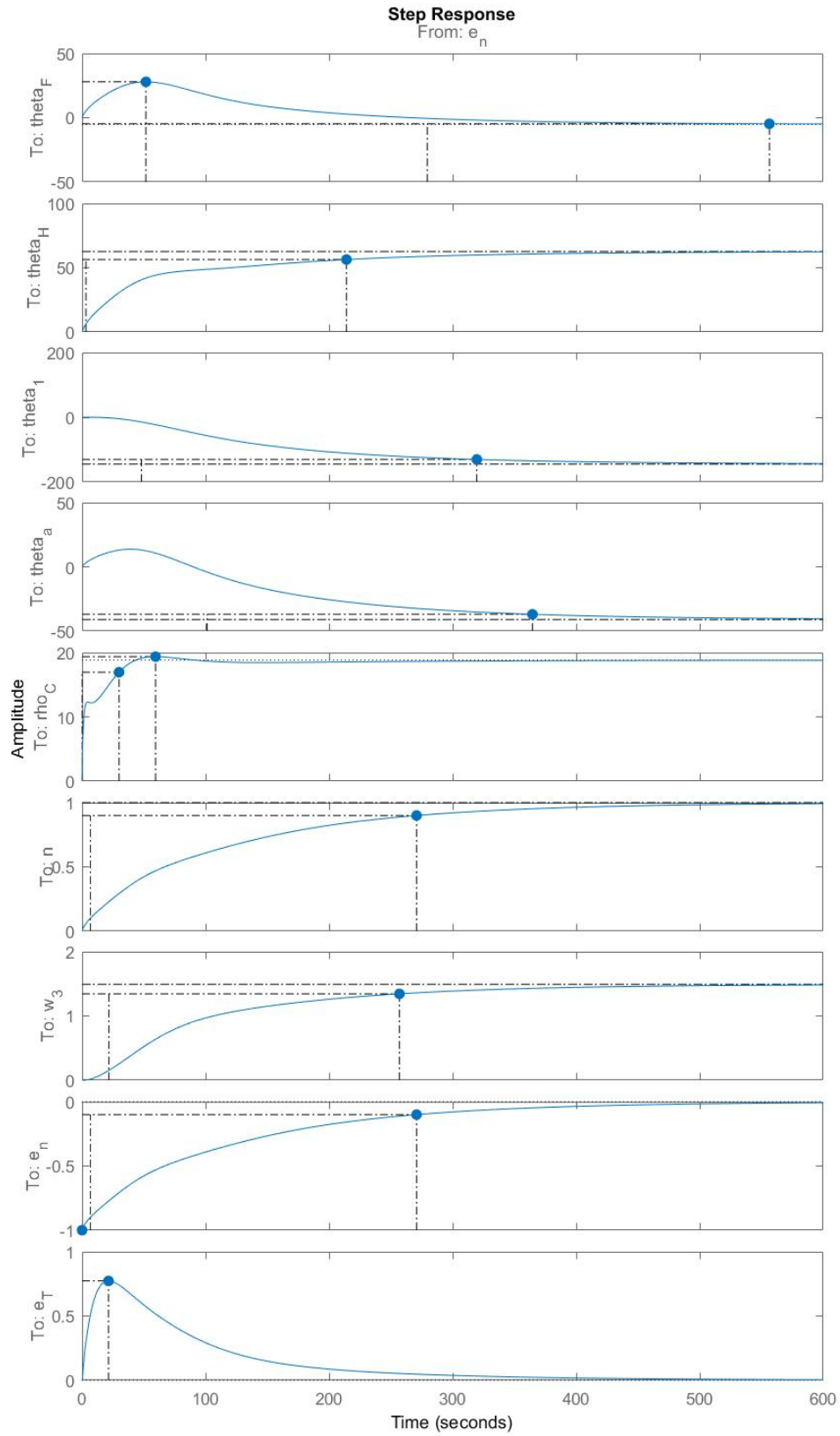


Figure 3-8 Closed loop response to step change in desired power level.

Focusing on the initial portion of external reactivity's response to the design change in target reactor power, Figure 3.9, we can see how the final controller is well within the design objectives. First, examining the plot shows that the control rods are slightly overdamped, this was done to bring the rise time for the reactor power to be less than 5 minutes, further reductions in reactor power rise time will increase the CRDM control effort, as the CRDMs initiate the transient acting to raise reactor power, while reactivity feedbacks are controlled by varying the salt flow rate. The maximum reactivity insertion rate is 5.6 pcm/s within the design limits of the CRDMS of 7.5 pcm/s. Next, the control rod traveled a maximum of 20.8 pcm, well within the rod stop limit of 75 pcm. Finally, the CRDM has an ideal mileage of 18.8 pcm and an actual mileage of 20.9 pcm, 11% above the ideal amount, which is reasonable and should be within the lifetime mileage of the CRDMs based on a reasonable anticipated number of transients, yielding acceptable maintenance and replacement criteria.

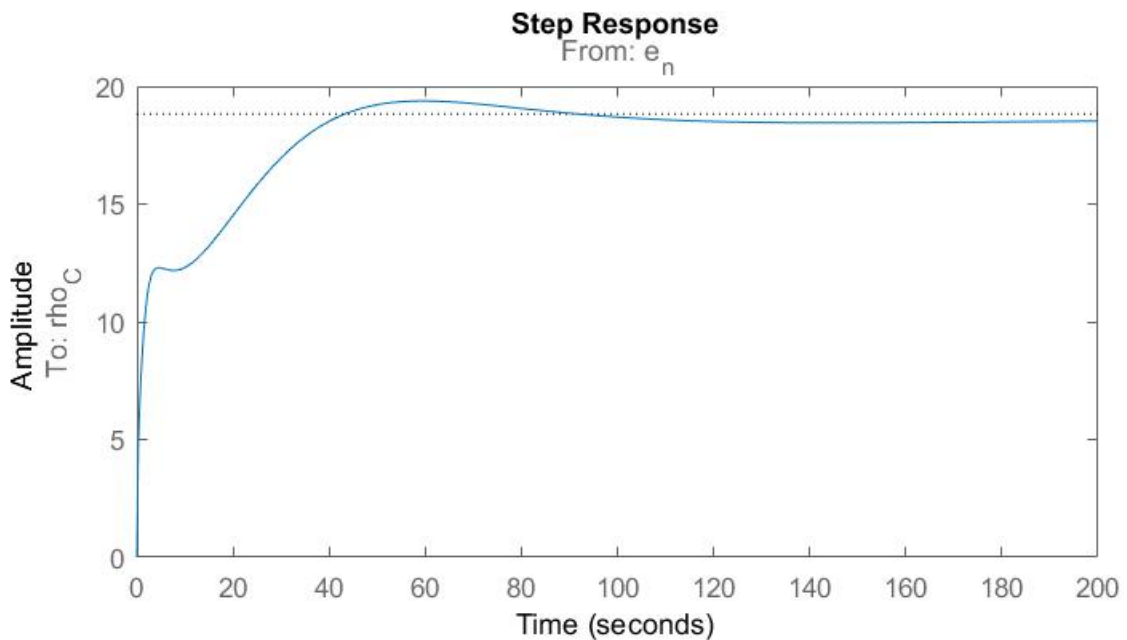


Figure 3-9 Closed loop external reactivity response to step change in desired power.

The CRDM motion is shown to be a continuous function, not step wise continuous at a fixed rod speed. With the advancement of solid state technology, there is no operational/technical reason to not have variable speed CRDMs. Because of the plant's sensitivity to high frequency noise, smoothing the CRDM reactivity insertions will improve controller response.

CHAPTER 5 CONCLUSIONS

This study shows one approach to implement a modern robust microprocessor control to a SFR to achieve desired power transients on an operationally meaningful time scale while maintaining a nearly constant salt outlet temperature to the energy storage system. This study is meant only to show the feasibility of the concept. Further consideration needs to be given to the impact of this active control scheme on passive safety responses, extending the work of Ponciroli et al. to this model. Their work showed that for conventional SFR's the active control has little impact on the passive safety ability to show protection. With the design simplification of the nTES and simplified control, 2 measured parameters and 2 related control outputs, the closed loop nTES should provide additional margin to those of a conventional SFR.

The approach of using H_∞ synthesis in designing reactor control schemes is not without precedent. Nor is the using other modern control strategies such as μ -synthesis, which handles uncertainty more explicitly than what was done with this approach. Future reactors should leverage recent developments in control theory to fully maximize their potential.

PART 4 – SAFETY EVALUATION

CHAPTER 1 INTRODUCTION

The limited safety evaluation undertaken in this part was done to evaluate the plant in off-normal situations to be able to verify that fuel and coolant temperature limitations were not exceeded during plant trips and a set of Beyond Design Basis Accidents, BDBAs which included ULOHS, ULOF, ULOF/ULOHS, and UTOP. To be able to make comparisons for the purposes of evaluating the design changes discussed in Part 2, two separate models were implemented in RELAP5-3D. The first model was for the reference design, a 1,000MW(t) S-PRISM variant. The second model was the modified version of the reference design which included the replacement of the IHX with a compact version and the addition of a TES and the proposed ACS trains.

Because of the limitations of the license available for using RELAP5-3D, we were unable to model the solar salt in the proposed IHX. Solar salt has been successfully implemented in RELAP5-3D and validated in an experimental model.[94] The issue is not a technical one, just one of having the correct binary fluid files for RELAP5-3D. Thus, sodium was used to approximate the solar salt. This approach was suitable for our needs as this work is only a conceptual study.

Chapter 2 will first provide a background of the S-PRISM including the extension of the previous model upon which this study is based and how this study differs from the former. Chapter 3 will outline the objectives of this part and how those objectives were met. Chapter 4 will provide a brief summary of the computational tools used. Chapter 5 will discuss how the computational model was implemented. Chapter 6 will discuss the

results of the transient simulations. And then, the conclusions of this study are discussed in Chapter 7.

CHAPTER 2 BACKGROUND

Because of the desire to have a low cost thermal energy storage system, the energy storage media selected was solar salt. Solar salt is a binary eutectic consisting of 60% NaNO_3 and 40% KNO_3 . It is commonly used in TES system applications especially in solar thermal. It has an operational temperature range of $\sim 600^\circ\text{C}$ to 270°C . It is commonly used as an industrial working fluid and is available in bulk at about $\sim \$750$ - $\$1,300/\text{ton}$ depending on the grade, with low chloride concentrations being preferred.[95] The salt has a thermal decomposition temperature of 630°C which may prove to be an issue during accident scenarios. The operational temperature profile fits well with SFRs, 510°C to 310°C . Of the SFR designs, aside from the already commercially deployed BN-800, GE-H S-PRISM is the next closest to commercialization and with the availability of data will serve as the reference model for this study.

S-PRISM is an extension of the DOE's IFR program that ran at INL from 1984-1994 when Congress cancelled it for political purposes three years before completion. In parallel with the development of the IFR, GE began development on the 471 MW(t) PRISM. In 1986 GE submitted a Preliminary Safety Information Document to the NRC and amended the original in response to NRC comments. The NRC responded with NUREG-1368 in 1994 concluding "that no obvious impediments to licensing the PRISM design have been identified [in the PSER][61]." GE later expanded the PRISM into an 840 MW(t) design. These two original PRISM designs were a part of the DOE's ALMR program. At the conclusion of the ALMR program GE increased the size of PRISM into the S-PRISM, 1,000MW(t) and increased core outlet temperatures 11°C . Recently, GE-H

brought back the original PRISM and the ALMR together and refers to them as Mod A, 425 MW(t), and Mod B, 840 MW(t). Both variants have the core outlet temperature reduced back to 499°C. The Mod A reactor vessel and all of its internals are rail shippable. The Mod B reactor can be transported overland and via barge, similarly to how steam generators and reactor vessels are transported to the current fleet of LWRs.[48]

Because the PRISM is based on the IFR, it is fully intended to integrate on site fuel reprocessing in a Nuclear Fuel Recycling Center. A site with multiple reactors can share and use the NFRC to produce all of the driver and blanket fuel. A key technology developed in the IFR program was pyroprocessing which electrorefines the metal fuel in a molten chloride salt bath. The uranium is removed in a dendrite form from the salt bath on a carbon electrode. The TRU are collected in a molten cadmium electrode and are never separated from each other. This improves the proliferation resistance of the metallic fuel cycle. With no pure plutonium on site extra steps which are easily identifiable would have to be added or material would have to be transported off site. Thus, inventory audits and external monitoring can assure that no fissile material can leave the site. Additionally, with extended core residence times the plutonium is considered reactor-grade and is not weaponizable.

On site fuel production allows a PRISM reactor to be loaded at construction with all of the heavy metal that it will need to operate. This can include spent fuel from LWR's that is first reduced before pyroprocessing. Thus, the PRISM only needs a supply of non-nuclear consumables to produce the fuel and operate the plant over its entire 40 to 60-year lifetime. Having all the fuel ever needed to operate the plant on hand is *the* definition of fuel security. Current LWR's can have up to a few years on hand, coal

plants have a few months, diesel generators have a few weeks, and natural gas has a few seconds.

2.1 Summary of Previous S-PRISM Study

The previous study that this one is based upon was completed in 2010.[90] It consisted of an evaluation of different fuel types and their performance under different accident scenarios. There were three fuels considered in that work: metallic, oxide, and nitride. The investigator conducted a detailed design of each core in ERANOS 2.0.

The investigator built a simple RELAP5-3D model of the S-PRISM variant. This model contained two independent IHTS, one S/G for each of the two IHX, a slight modification from the design reference S-PRISM which has only one S/G for the two IHXs.

The model contained two lumped feedback effects. First, the fuel Doppler and axial expansion reactivity feedback mechanisms were tied to the heat structures of the fuel. The physical expansion of the fuel was not explicitly modeled it was converted into a fuel temperature feedback. The complexity of directly modeling the feedbacks in a separate control system would not add any additional value to the model.

The three remaining reactivity feedback mechanisms are coolant Doppler, coolant leakage, and fuel radial expansion. The coolant feedback mechanisms are a function of coolant density and were simultaneously calculated in ERANOS. These were the only feedback mechanisms that provided positive feedback. The fuel radial expansion occurs due to the heating of the upper and lower core restraints. The detailed engineering design of the constraints weren't available. The assumed model was an upper support grid of HT9 that expanded with temperature. The lower core restraints weren't modeled. In this

scenario, the fuel would flower inserting negative reactivity. The upper restraint was not included in the RELAP model as a separate heat structure. Instead, it was lumped into the coolant temperature, assuming instantaneous heat transfer to the restraint, neglecting the time lagged capacitive effect of the mass of metal of the restraint. Table 4.1 provides a summary of the reactivity feedback effects from the previous work. RELAP models the coolant feedback in terms of coolant density not temperature. The model was run to determine the reference temperature and density for steady operations at the initiation of each event. NUREG-1368 reported reactivity feedbacks for fuel Doppler, -0.61 pcm/K, axial expansion, -0.27 pcm/K, sodium density, 0.67 pcm/K, and radial expansion, -0.69 pcm/K. The net fuel prompt feedback was -0.88 pcm and the coolant temperature feedbacks of -0.02 pcm.[61] The reactivity feedbacks used in this study are therefore conservative estimates based on the available data.

Table 4-1 Previous Study S-PRISM Reactivity Feedbacks

	Fuel Related			Coolant Related		
	Fuel Doppler	Axial Expansion	α_F	Coolant Doppler and Thermal Expansion	Radial Expansion	α_T
	pcm/K	pcm/K	pcm/K	pcm/K	pcm/K	pcm/K
BOC	-0.3401	-0.4655	-0.8056	0.7577	-0.1950	0.5627
MOC	-0.3438	-0.5818	-0.9256	0.8007	-0.1978	0.6029
EOC	-0.3467	-0.4386	-0.7853	0.8366	-0.1978	0.6388

The zero-power point kinetic reactivity RELAP was used to control the heat source term during transients. Because of the large neutron MFP relative to the core side, the neutron flux in the reactor is strongly shaped. Using a nodal kinetics model does not add any benefit in model performance as the flux spatial and time dependent portions are separable to a small error. The nodal kinetics would unnecessarily add to the

computational overhead. Table 4.2 provides a summary of the delayed neutron parameters. The conventional 6-group delayed neutron precursor model was used.

Table 4-2 Modeled S-PRISM Delayed Neutron Precursor Data.

	BOC	MOC	EOC
β_1 [pcm]	8.238	8.335	8.331
β_2 [pcm]	69.99	70.83	70.79
β_3 [pcm]	60.88	61.64	61.62
β_4 [pcm]	138.5	140.5	140.4
β_5 [pcm]	70.78	71.91	71.88
β_6 [pcm]	25.42	25.85	25.85
β_{eff} [pcm]	373.8	379.1	378.9
λ_1 [s ⁻¹]	0.01331	0.01331	0.01331
λ_2 [s ⁻¹]	0.03055	0.03056	0.03056
λ_3 [s ⁻¹]	0.1191	0.1191	0.1191
λ_4 [s ⁻¹]	0.3178	0.3178	0.3178
λ_5 [s ⁻¹]	0.9636	0.9635	0.9635
λ_6 [s ⁻¹]	3.022	3.023	3.023
Λ [s]	2.670E-7	2.707E-7	2.704E-7

During modeling the built in RELAP, ANS 1990 standard was used to approximate fission product heat generation. The GEMs were modeled with a \$1.4 worth. The GEM differential worth was assumed to be cosine, and the GEM level a function of the gridplate coolant pressure, Equations 2-4 and 2-5.

The previous work [90], did not account for changes in fuel thermophysical properties as a function of fluence or plutonium content. To compensate for this, two materials were created to represent the driver and blanket assemblies using the material composition of [90]. The BOC fuel data assumed 100% theoretical density and modeled entirely fresh assemblies. The MOC and EOC fuel assumed 75% and 85% porosity for the driver and blanket assemblies respectively. This represented the assemblies that have achieved at least 1 atomic % burnup, (2nd or 3rd cycle assemblies). This was to account

for the degraded thermal conductivity in these assemblies, since the fresh fuel was analyzed in the BOC run. The MOC and EOC assembly conductivity and volumetric heat capacity assume sodium logging in the pores. For temperatures above 1,200K, sodium was assumed to have voided the fuel pores and was not included. The thermal conductivity was taken to be 72% that of fresh fuel, which accounted for the sodium logging. The fuel correlations were taken from [96] and the sodium thermophysical data was taken from [97]. Tables 4-3 and 4-4 were used for the volumetric heat capacities and thermal conductivities, respectively, for each of the assembly types and show the comparative data from the previous study, [90].

Table 4-3 Fuel Volumetric Heat Capacity (J/m³-K)

K	Sumner[90]	BOC		MOC/EOC	
		Driver	Blanket	Driver	Blanket
293	1.838E+06	2.102E+06	1.876E+06	2.414E+06	2.232E+06
400		2.299E+06	2.023E+06	2.443E+06	2.256E+06
500	2.194E+06	2.484E+06	2.162E+06	2.697E+06	2.472E+06
600		2.676E+06	2.290E+06	3.022E+06	2.739E+06
700		2.865E+06	2.420E+06	3.398E+06	3.051E+06
800	2.733E+06	3.046E+06	2.545E+06	3.783E+06	3.372E+06
868	2.87E+06				
890		3.173E+06	2.634E+06	4.133E+06	3.665E+06
900		3.181E+06	2.640E+06	4.008E+06	3.558E+06
1000	2.342E+06	2.436E+06	2.077E+06	2.724E+06	2.462E+06
1100		2.454E+06	2.090E+06	2.706E+06	2.443E+06
1200	2.672E+06	2.563E+06	2.167E+06	2.688E+06	2.424E+06
1300		2.738E+06	2.291E+06	2.670E+06	2.002E+06
1378		2.911E+06	2.182E+06	2.656E+06	1.992E+06

Table 4-4 Fuel Thermal Conductivity (W/m-K)

K	Sumner[90]	BOC		MOC/EOC	
		Driver	Blanket	Driver	Blanket
298	6.3095	9.0031	14.7191	6.4822	10.5977
400	10.8523	10.9656	16.7321	7.8952	12.0471
500	14.2958	12.9915	18.8742	9.3539	13.5895
600	17.1094	15.1185	21.1832	10.8853	15.2519
700	19.4883	17.3465	23.6590	12.4894	17.0344
800	21.5489	19.6754	26.3016	14.1663	18.9371
900	23.3666	22.1053	29.1110	15.9158	20.9599
1000	24.9925	24.6362	32.0873	17.7381	23.1028
1100	26.4633	27.2681	35.2304	19.6330	25.3659
1200	27.8061	30.0009	38.5403	21.6007	27.7490
1300	29.0413	32.8348	42.0171	23.6411	30.2523
1400	30.1849	35.7696	45.6607	25.7541	32.8757

Because of the higher fuel temperatures in the oxide and nitride fuels compared to the metallic fuel, the unprotected transients considered had much higher PHTS coolant temperature excursions. These oxide and nitride fuels are less compatible with the temperature constraints of the solar salt. As a result, they are not considered in the present study due to increased effort to have compatibility.

2.2 Modification of S-PRISM

Because of the fidelity of the data the 1,000 MW(t) S-PRISM variant was selected for this study. The core outlet temperature used was 499°C to make more direct comparisons with the Mod A and Mod B PRISM variants. The other modifications consist of replacing the shell and tube IHXs and steam generator with compact plate-fin heat exchangers and adding a plate-fin heat exchanger in parallel with the main salt flow to/from the storage tanks for the AHX.

Compact heat exchangers are not new and have been around for several decades. They are extensively used in applications where a small form factor and high

performance are needed. The design reference S-PRISM contained a compact heat exchanger, the helical-coil steam generator. There has been recent work to qualify compact heat exchangers for nuclear applications. [

There are two main methods of fabrication for compact heat exchangers suitable to the application at hand. First is diffusion bonding, where the plates are stacked and heated at high pressure and temperature fusing the plate pack into a contiguous block. The other form of fabrication that is acceptable is welding the plates together. Each of these methods of construction are needed in the plant. First the IHX which serves as a primary vessel boundary needs to have the greatest degree of integrity, especially considering that it is part of the reactor vessel boundary. The SHX would similarly be diffusion bonded, due to the chemical incompatibility of the two coolants. The AHX is external to the reactor vessel and has a lower operational pressure and temperature requirement, thus using welding to assemble the plate pack is suitable in this application. The AHX is accessible during normal operation and can be easily inspected during outages to monitor weld performance over time.

Compact heat exchangers have the benefit of being extremely modular due to their size and how they are made. This allows for much easier scaling of heat transfer surfaces without adversely affecting the system pressure drop. It is for this reason that these types of heat exchangers are being extensively considered in the current NGNP design study for the steam generator and recuperators. [98] This design work has also been extended into RELAP and tested against empirical models to assess the method of performance, showing that they can be successfully modeled within reasonable accuracy. [98]

CHAPTER 3 OBJECTIVES AND APPROACH

The approach in assessing the design effectiveness of the modifications to PRISM was to follow a similar methodology to that in NUREG-1368 which divided the sets of transients considered into three categories:

EC-I Anticipated Operational Occurrences

EC-II Unlikely Events

EC-III Extremely Unlikely Events

The NRC used a deterministic approach to evaluate the performance of the reactor, using risk informed engineering judgement to select which deterministic events should be considered. Additionally, the design focus here extended to that in the PSID was that of accident prevention, not mitigation. To this end the objective was to prevent fuel melting in all three event classifications. EC-I and II have more restrictive temperature constraints, as they are more likely to occur and thermal excursions should be limited to prevent accelerated creep in core, vessel, and structural materials.

The fuel temperature for EC-I and EC-II events should remain below the null fuel-cladding reaction temperature of 977.6K.[99] Primary coolant temperature excursions should not exceed peak operational temperatures by 50°C for longer than 1-hour. The fuel temperature during EC-III events should not exceed 977.6K for one hour not to exceed 1,090K.[99] The ACS temperature in the operative ACS should not exceed 600°C for longer than one hour, not to exceed 630°C. Based on NUREG-1368, the EC-I and EC-II events would have negligible impact on long term reactor and core performance (4.2.6). Fuel temperatures above 977.6K correspond to a cladding

dissolution of approximately 0.9 μm roughly 0.2% of the original cladding thickness.[99] Because using high temperature structural codes was beyond the scope of this, the transient temperature limits for EC-I and EC-II seemed to be a reasonable engineering judgement.

Fuel melting temperatures for the driver fuel and blanket fuel are reported at 1227K and 1298K respectively.[99] The driver fuel is based on conservative plutonium alloying quantities. The blanket assemblies which are only a binary uranium zirconium eutectic have a higher melting temperature than the ternary alloy of the driver fuel.[99]

3.1 Transients to be Evaluated

The approach taken here to select the bounding events mirrors those of NUREG 1368. We did not make a rigorous quantification of the probabilities associated with the events and relied on good engineering judgement informed by available probabilities.

The following assumptions were used to select the bounding events.

- *Select worst case plant states (specified by system, pressure, temperature, flowrate, etc.) as initial conditions for the challenges to the safety functions.*
- *Assume non-safety grade equipment fails (either as an initiator or in response to the initiating event in a way that exacerbates the accident to the maximum degree physically possible, unless a lesser degree can be justified. This will account for any uncertainties caused by using commercial-grade procurement and construction, and the lesser operational surveillance associated with the non-safety grade designation.*

- *Assume failure of unique safety-grade equipment for a period of time (bounds uncertainties in failure probabilities of safety-grade equipment).*
- *Allow a reasonable time (consistent with emergency planning provisions to recover safety-grade equipment where no plant damage has occurred) anticipated transient without SCRAM, station blackout, loss of all cooling.*
- *Assume multiple human errors or other initiating events consistent with events that have actually occurred.*
- *Assure at least an equivalent challenge to that applied to LWRs.*

For simplicity, the bounding events of NUREG 1368 that can be tested on the reference S-PRISM model will be tested. The process of determining the appropriate bounds for the modified design will use the above outline. Table 4.3 and Table 4.4 contains the applicable bounding events and their specifications for the reference model and are taken directly from NUREG 1368. Of these, only BE-7, flow blockage, cannot be tested. Neither will BE-8 be considered due to a lack of public data.

Table 4-5 Bounding Event Description

	Description
1	<p><u>Unprotected transient overpower (UTOP) events.</u> Assume that the worst-case control rod withdrawal event occurs. Assume that all control rods remain full out (at the mechanical stops) for 12 hours and then the reactor is scrammed. Analyze this event for two cases on one module:</p> <ul style="list-style-type: none"> • A All Forced Cooling remains functional. • B All Cooling except the RVACS is lost at the time the control rods are withdrawn.
2	<p><u>Station blackout.</u> Assume that SCRAM occurs and natural circulation cooling is the only available cooling for all modules on the site. Assume 24-hrs pass before AC power is restored.</p>
3	<p><u>Loss-of-heat-sink events.</u> From full-power conditions, assume that all cooling via the normal cooling system and the auxiliary air cooling systems is lost (loss of the intermediate loop). A SCRAM is assumed to occur as soon as the reactor protection system detects off-normal conditions. Analyze the event for two cases:</p> <ul style="list-style-type: none"> • A All airflow pathways in RVACS are assumed to be fully blocked for 12-hours. Assume sabotage on one module and analyze until the peak temperatures have passed. • B Assume a 75-percent blockage of the RVACS airflow pathways for an indefinite period of time. Assume an earthquake that affects all modules and analyze until the peak temperatures or 12 hours have passed.
4	<p><u>Unprotected loss-of-flow (ULOF) events.</u> Assume an unscramed ULOF event on one module and analyze this event for two cases:</p> <ul style="list-style-type: none"> • A Assume that the flow through one pump stops suddenly and the others continue to operate normally. Analyze the event until new equilibrium power and flow rates have been established. • B Assume that the pumps are tripped and begin to coastdown. For this case, one of the pumps does not coastdown and it ceases pumping instantaneously. Analyze for the first 10-minutes of the event.
5	<p><u>Steam generator tube rupture event.</u> Determine a justifiable number and the sequence of steam generator tube ruptures and analyze assuming failure to isolate or to dump water from the steam generator for 12 hours. Evaluate this event without forced cooling (one module).</p>
6	<p><u>Large sodium (Na) leaks (single module).</u> Assume leaks in the intermediate heat transport system piping. Determine the size of the leak in accordance with the criteria for moderate-energy fluid system piping. Evaluate for sodium fires and leaks from the reactor vessel into the guard (containment) vessel.</p>
7	<p><u>Flow blockage.</u> Assume blockage of flow to or from one fuel assembly.</p>
8	<p><u>External events.</u> Evaluate external events that exceed those traditional analyzed as design basis events in a manner consistent with their application to current-generation light water reactors.</p>

Table 4-6 Bounding Event Summary

	Description	Probability range estimate
BE-1	Assumed worst case failure of non-safety-grade control system (due to fire or other mechanism). Results in inadvertent withdrawal of all control rod, combined with failure to SCRAM	<ul style="list-style-type: none"> • Fire or control system failure, 10^{-1}-10^{-4}/yr • Failure to SCRAM, 10^{-5}-10^{-7}/yr • Modules on site 10 Rang or prob. = 10^{-5}-10^{-7}/yr
BE-2	Two- to sixteen-hour station blackout is assumed for light water reactors (LWRs). Additional time added to compensate for lack of design detail.	<ul style="list-style-type: none"> • 2-16 hr station blackout, 10^{-5}/yr for LWRs • Additional 20-hr loss, 10^{-2}-10^{-3}/yr • Modules on site 10 Rang or prob. = $< 10^{-7}$-10^{-8}/yr
BE-3	Severe external event could cause loss of offsite power and temporary loss of reactor vessel air cooling system (RVACS). Auxiliary cooling system is non-safety-grade.	<ul style="list-style-type: none"> • External event causes loss of offsite power and blocks RVACS, 10^{-7}/yr • Modules on site 10 Rang or prob. = $< 10^{-6}$/yr
BE-4	Loss of one synchronous machine is an anticipated event combined with anticipated transient without SCRAM (ATWS).	<ul style="list-style-type: none"> • Instantaneous loss of flow through one primary pump, 10^{-2}/yr • Failure to SCRAM, 10^{-5}-10^{-7}/yr • Modules on site 10 Rang or prob. = 10^{-6}-10^{-7}/yr
BE-5	Steam generator (SG) and its water dump and isolation system are non-safety grade. Experience with SG tubes indicates multiple failures have occurred. Exact number to be determined later but should be at least 40 based on prototype fast reactor (PFR) experience.	Multiple SG Tube ruptures have occurred in the past. Such ruptures would leave plant on RVACS cooling only.
BE-6	Consistent with Clinch River Breeder Reactor (CRBR).[leak from reactor vessel or IHTS]	<ul style="list-style-type: none"> • IHTS or reactor vessel leak, 10^{-6}-10^{-7}/yr (per CRBR PRA) • Modules on site 10 Rang or prob. = 10^{-5}-10^{-6}/yr
BE-7	Fabrication error results in blocked assembly being inserted into core.	Fabrication errors have occurred in the past. Experience shows fabrication and loading errors occur.
BE-8	Severe external event analysis	Under development for ALWR's; will be developed for PRISM

3.2 Baseline Events

The design basis event for the PRISM was a reactor SCRAM from full power with maximum power history and only RVACS available. NUREG-1368 reported that this event resulted in a peak PHTS sodium temperature of 607°C with 95% certainty of being less than 646°C with system equalization occurring in 30-hours. This event will test the model of the hydrodynamic volume, decay heat, and the RVACS. All of which are critical to this study.

The UTOP for a \$0.30 reactivity insertion, BE-1, has a peak fuel temperature of 1251K and a peak coolant temperature of 656°C.[99] Based on the equilibrium of 130% power this is BE-1A where all forced cooling remains functional. These temperatures will be checked for the reference model. Because the reference model is 11°C cooler than the one reporting these temperatures, the comparison will be appropriately compensated for the temperature difference.

Of the 8 bounding events, 4 challenged the containment boundary, BE-1 (UTOP), BE-3 (protected LOHS for 36-hours), BE-4 (ULOF), and BE-7 (single assembly flow blockage).(NUREG) BE-7 will not be considered in this study, thus the comparison between the reference model and the modified S-PRISM will use the first three for the comparison.

3.3 Modified Design Basis Event

The design basis event for the purpose of the modified design will remain unchanged, Reactor SCRAM from full power and worst-case power history with loss of ACS. This event will be simulated by initiating a reactor trip with a failure of one ACS

check valve. The failure of an AHX discharge check valve has an estimated failure rate of 10^{-2} - 10^{-3} /yr-valve for significant reverse flow failure but not affecting forward flow. Reverse flow leakage is considered an operational issue. The main concern is with a jamming of the check valve in the closed position. This is estimated to occur at a rate of 10^{-2} /yr provided that the check valve has failed. Assuming 10 reactors on the site and estimating a SCRAM occurrence at 10^{-1} /reactor yr. the resulting probability is 10^{-4} - 10^{-5} /yr. Failure of both check valves or a failure of a single channel to actuate pushes the probability of a reactor SCRAM with loss of both ACS trains to an EC-III event and is not anticipated to be worse than the DBE for the original PRISM.

The check valve used in this application will have very few duty cycles, forced shut for 18-month operations then in forward flow for natural circulation for 1-month refueling outages. This will reduce wear on the stem and spring. The check valve failure probability was for ECCS accumulator swing check valves, where back leakage can cause pressure equalization with the primary system and cause early ECCS discharge in a LOCA.[84] Here seat leakage only affects system efficiency. Only valve failure to open affects safety and is a much less probable event. A failure of the opening assist torsional spring, does not cause a valve failure. It closes the valve about 0.5° .

3.4 Modified Bounding Events

BE-1

The BE-1A will remain unchanged and will serve as a direct comparison between the published data and the reference plant. The component that this will validate is the compact IHX. Because the NTU were set to have an equivalent TTD to the reference

model and natural circulation is not entered, there should be little to no difference between this and the reference plant.

BE-1B will require modification. The failure of both ACS trains to actuate would push this into EC-III, due to the posterior probability being $<10^{-9}$. To keep this in EC-II only one ACS train will fail to actuate. For a failure of both ACS trains, the plant response would be identical to the reference design.

BE-2

This bounding event will have no modification. It is expected to have much lower temperatures than the reference case due to the loss of neither ACS train.

BE-3

This bounding event will have an indefinite loss of the RVACS. The inclusion of the loss of either train of the ACS pushes this event into EC-III. As such it will be evaluated for a loss of RVACS with a single operational ACS train.

BE-4

The 'A' bounding event will have no modification. The 'B' bounding event will include a failure of one ACS train of ACS to actuate. While this is an EC-III event it is a partial loss of heatsink coupled with the ULOF. It is assumed that the non-safety grade salt tanks are unavailable.

BE-5

This bounding event is modified by simulating a double end break on the salt inlet piping without a protective action. The lack of a protective action is due to operator error failing to recognize the event. While forward flow through the ACS is assured, operator action is required to manually trip the plant, opening the AHX dampers. This is a similar

event to BE-3. Because the AHX remove much more heat than the RVACS. It is expected that this event will provide a more severe temperature excursion. Operators will trip the plant at 12-hours into the event.

BE-6

There will be no modification to this bounding event. It will not be analyzed here because the design of PRISM prevents uncovering the IHX in this bounding event. BE-5 is the comparable version of this BE-6 but because of the break being salt the risk for a sodium fire is eliminated, and becomes a high temperature fluid spill which poses burn risks to personnel and equipment. The difficulty of modeling the spread of the salt and the risks associated with it is beyond the scope the present work and will have no further consideration, but requires resolution if this concept is pursued further.

BE-7

This bounding event will remain unchanged and is beyond the capabilities to model in RELAP.

BE-8

The faulted modes of the reference design where there is a loss of the ACS and instances where there is a temporary loss of all DHR are beyond design basis events. The previous work in modeling them shows adequate margin to fuel damage, or benign fuel melting due to the lack sodium boiling allowing the melted fuel to re-solidify and be transported out of the core. Additionally, the non-safety grade salt piping out of the safety boundary can be used to provide DHR in the event of the simultaneous loss of all three safety DHR paths. Consideration for such events, e.g. aircraft impact or kinetic weapons, removing RVACS and both ACS trains needs to be done on a probabilistic basis. Here

operator action and credit for other non-safety paths for DHR can be considered. As these events duplicate the reference plant's BE-3A, the modified plant will have better performance in these situations than the reference plant as the likelihood of damaging the installed piping and cold salt tank/pumps, located several hundred meters away is greatly reduced.

Where this bounding event needs consideration has been done in the modified BE-4B and BE-6. These bounding events show how a complete physical separation of the reactor from the cold tanks is entirely benign. These events do not include a loss of off-site (outside the nuclear island) power. The BE-8 considered here will be these two bounding events compounded by a SBO and ATWS. The purpose of doing this is to provide technical justification for the NRC to not regulate structures outside of the nuclear island, and reactor control station. The unprotected step increase of salt pump flow to 200% of rated flow, which is 110% of design flow, will also be simulated to show how complete control system failure has a benign impact on the plant with adequate margins to fuel failure outlined above. These transients are considered EC-II because no credit is taken for PRA on the affected components.

CHAPTER 4 COMPUTATIONAL TOOLS

The primary tool used for evaluating the safety performance of the reference and modified S-PRISM was RELAP5-3D. This code was originally designed to model reactor accidents in LWRs. It includes a fully integrated multidimensional thermal-hydraulics and kinetics models making it suitable for modeling reactor systems in transient events where reactivity feedback mechanisms are controlled by various thermodynamic states in the plant. RELAP has been extensively modified to allow modeling of advanced reactors including various liquid metal and molten salt cooled reactors, with built in thermodynamic models for these various working fluids. For a more comprehensive review of the software the reader is recommended to the previous work of which this current work is an extension.

RELAP5-3D is a command line code with a highly-structured set of inputs. It can be difficult and time consuming to generate the input decks and parse the generated outputs. To aid in this process, SNAP, Symbolic Nuclear Analysis Package, was used to generate the model files, control restart files and parse the output data. SNAP includes direct interfaces with Matlab™ to allow direct access from inside Matlab™ to plot data generated from inside RELAP, simplifying generating final output data and evaluating transients. SNAP was developed by the NRC to aid in nuclear analysis and is very powerful tool in this regard. The Job Stream programming tool in SNAP was very useful in creating and running the different scenarios. It allows creation of a remote server which can be accessed remotely for file processing. It also allows for problem parallelization as multiple cases can be run simultaneously or in a planned sequence.

In generating the inputs decks for RELAP there was significant difficulty in creating the gas pressurizers which are used extensively in SFRs for plant pressure control. RELAP has difficulty calculating the various parameters in two phase systems where one fluid is a liquid with a low vapor pressure and the other is a non-condensable gas. To be able to generate the needed parameters for steady state conditions, the gas pressurizers were replaced with time dependent volumes containing the incompressible working fluid with temperatures and pressures near where the final operating point would be to aid in model convergence.

The Steady State option of RELAP was not acceptable in this application as it led to significant model instability and increased real-world time in developing the solutions. Future users are not recommended to use this feature. Additionally, careful review of the code manual is recommended for the general input constraints especially on time steps and how those steps are advanced. The maximum time step is limited to the Courant Limit that is computed at each time step. It is recommended to run the problem to get a sense for the limiting time step Courant limit and set the maximum time step below that to ensure that the code advances smoothly with minimal computation time. Different problems require additional features. For example, the implementation of the helical steam generator needed a water packing model designed, option 12 of card 1, originally for the Hanford N-reactor. Without this option specified the outlet temperature and pressure provided non-physical results and indicated an unstable system.

CHAPTER 5 COMPUTATIONAL MODEL

The computational model, while based on the previous study, is a significant departure from it. Because the first study's focus was on designing and testing the suitability of a new fuel. The bulk of the model fidelity was spent on that. This study's focus is on the thermal-hydraulic aspects of comparing two separate modeled plants. The nuclear data: reactivity feedbacks, delayed neutron precursor information, and decay heat were taken directly from the previous study without modification.

5.1 Baseline S-PRISM

Piping sizing information was extracted from several sources, mainly by taking measurements off of published drawings to estimate the relative sizing. In some cases, CAD models were built to determine volume fractions of the discretized three-dimensional structures in RELAP. This was done specifically to calculate the volume around the reactor vessel lower elliptical head up to the tops of the lower outer core support baffles. Where needed thermal-hydraulic models were built in EES with the appropriate data brought into modify the structures in RELAP.

As stated previously, the model is based on the 1,000 MW(t) S-PRISM because of the publicly available reference material was much more plentiful and with enough fidelity to be able to put together a somewhat reasonable approximation to the more detailed proprietary design work done by GE-H.

The greatest modeling effort was on the heat transfer surfaces and getting the relative elevations of the various components as close as possible to the actual design. Because the structure of the PRISM module is mostly open the natural circulation

pressure losses are concentrated in three areas: the core, the IHX and the internal piping which included the RCPs.

5.1.1 Nuclear Fuel

There were three main components considered as a part of this study: driver fuel, blanket fuel and the GEMs. The driver fuel was split into two groups of assemblies, average driver fuel and hot driver fuel each containing 114 and 25 assemblies respectively. The blanket fuel was divided into three groups, average internal blanket, hot internal blanket, and the radial blanket each of 37, 12, and 48 assemblies respectively.[90] No other core structure had a hydrodynamic structure. The control rods, GEMs, and reflectors were not included in this model.

All of the heat generated from fission, including gamma and neutron radiation was assumed to be generated entirely within the fuel assemblies. This will lead to slightly hotter assemblies as the heat from the gamma and neutron radiation that is normally generated in the control rods, reflectors, sodium outside of the assembly ducts, and in the shielding and transported by the core bypass flow is now entirely in the main core flow. To obtain a reasonable hydrodynamic model for the core pressure drop, the core bypass flow rate was assumed to be 1.5%. This further elevated fuel temperatures. While this approach is not a good physical model it is a conservative model with higher fuel temperatures than what would be in the production core.

The pressure drop across the metal core is reported at 430 kPa.[100] This was assumed to neglect the 64.5 kPa pressure form the elevation change over the 4.07035 m pin height. Using the core thermal hydraulic model from the previous study, the observed pressure drop using RELAP rod bundle estimates was a fairly uniform 220 kPa across

each assembly at full flow. This needed modification. To better estimate the pressure drop and needed assembly orificing the following model was used for the Darcy friction factor:

$$\lambda_p = A + BRe^{-C} \quad 4-1$$

where,

$$A = 0; B = 0.210 \left\{ 1 + \frac{124}{(h/d)^{1.65}} [1.78 + 1.485(s/d - 1)] (s/d - 1) \right\}; C = 0.25$$

$$1.0 \leq s/d \leq 1.5; 10^4 \leq Re \leq 2 \cdot 10^5; 8.0 \leq h/d \leq 50$$

This model is applicable to $\pm 15\%$ over the above range for triangular pitch pins.

To provide a starting point, minimum assembly flows were calculated to maintain assembly coolant outlet temperatures below 583°C . To estimate the needed orificing, the assembly outlet temperatures were set to be that assuming adiabatic mixing of the core flow with the 1.5% core bypass with bypass temperature remaining constant at the core inlet temperature of 371°C . The mixed outlet temperature was set at the hot-leg temperature of 499°C . This resulted in an assembly outlet temperature of 506.4°C . Table 4.5 lists the results of the modeling including the needed orificing to reach the actual 430kPa pressure drop in the metallic fueled S-PRISM. There was also a calculation to determine the core bypass orificing. Because of the limitations in how the modeling is implemented the pin and orificing pressure drops were considered to include all of the pressure drops across the assembly including the pressure drop through the nozzles below the grid plate, lower and upper shielding, and the assembly handling structures.

Table 4-7 Reference S-PRISM Core Hydrodynamic Data

Group	# Assy	BOC Power MW	Min Flow kg/s	Flow kg/s	Assy Flow Area m ²	ΔP kPa	Re	Orifice D _H m	Orifice Area m ²
Ave DF	114	607.61	2,146	3,257	0.8511	39.83	158,675	0.04786	0.205
Hot DF	24	159.07	561.9	852.6	0.1792	58.33	197,317	0.05396	0.05489
Ave IB	37	119.64	422.6	641.3	0.1801	24.56	191,897	0.03694	0.03965
Hot IB	12	42.01	148.4	225.2	0.05841	28.22	207,761	0.03852	0.01398
RB Bypass	48	71.67	253.2	384.1	0.2336	6.353	88,611	0.02483	0.02324

The pin hydraulic model of Equation 4.1 was added into RELAP with the following parameters. RELAP has the capability of modeling hydraulic losses across the entire flow range. To do this Equation 4.2 was used to model the laminar hydraulic losses.

$$\lambda_p = \frac{64}{Re\Phi_S} \quad 4-2$$

where the shape factor $\Phi_S = \frac{1}{0.407+2.0\sqrt{s/d-1}\left(1+\frac{17.0(s/d-1)}{h/d}\right)}$. Table 4.6 contains the

parameters included in the fuel assembly hydrodynamic structures and Table 4.7 contains the fuel assembly parameters.

Table 4-8 Fuel Assembly RELAP Darcy Friction Factor Correlations

	A	B	C	Φ_S
Driver Fuel	0	0.253840	0.25	0.9898
Blanket Fuel	0	0.246331	0.25	0.7218

Table 4-9 Fuel Assembly Physical Parameters

[mm]	Driver Fuel	Blanket Fuel
Assembly Pitch	161.417	161.417
Duct Gap	4.318	4.318
Duct Wall Thickness	3.937	3.937
Pin Count	217	127
Pin OD	7.4422	12.0142
Pin Cladding Thickness	0.5588	0.5588
Fuel OD	5.47624	10.0457
Spacer Wire Diameter	1.4224	0.9398
Spacer Pitch	203.2	203.2

The fuel assembly hydrodynamic volume length was set at 4.07035 m. It was discretized into three separate areas: lower plenum, active core, and upper plenum. The active core did not contain any axial blankets and was 1.016 m in length and divided into 8 separate volumes. The lower plenum was 1.00744 m and broken up into 4 equal hydrodynamic volumes. The upper plenum was 2.04691 m and broken up into 4 equal hydrodynamic volumes. Each assembly was connected to the grid plate volume (102) and the grid plate upper elevation was adjusted 0.05182 m lower to accommodate the pin grid overlap. This placed the core mid-plane at an elevation of -15.9903 m below grade. The IHX mid-plane was -8.7161, leaving an elevation difference of 7.27442 m to drive natural circulation flow.

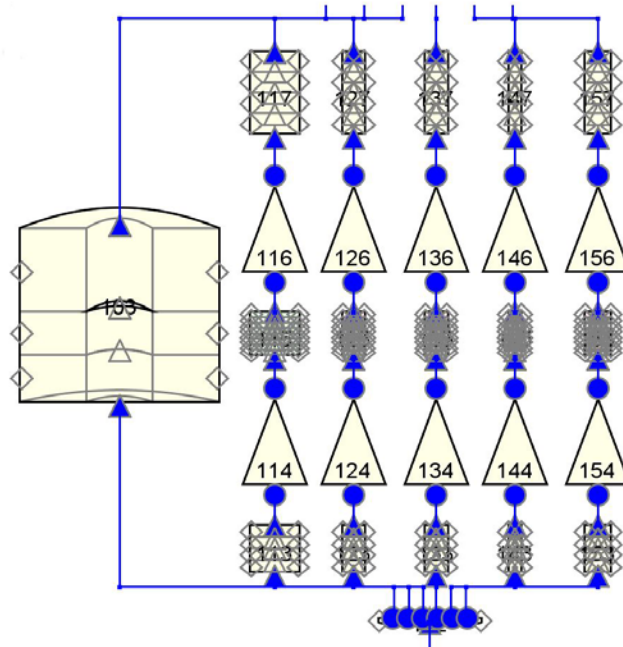


Figure 4-1 Core RELAP hydrodynamic structures

Figure 4.1 shows the hydrodynamic volume layout for the core portion of the PHTS, the darker red volumes have associated heat structures. The junctions between the fuel assembly lower plenums (113, 123, 133, 143, 153) and the grid plate branch were where the fuel orifices were placed. The orifices for the core bypass flow were modeled as the grid plate branch (102) connecting to the radial sodium shield pool (103) and the upper discharge plenum branch (104) connecting to the radial sodium shield pool.

The active fuel heat structures were divided into 9 radial nodes, 6 for the fuel, 1 for the gap and 2 for the clad. There were no other heat structures associated with the fuel pins. No special correlations were used to model the fuel and the rod bundle with crossflow option was used to estimate the heat transfer coefficient. This was checked against the following model:

$$Nu = Nu_l + f(\varepsilon_6, S/d) Pe^{\varphi(S/d)}, \quad 4-3$$

$$1 \leq S/d \leq 2; 0.1 \leq \varepsilon_6 \leq \infty; 1 \leq Pe \leq 4000$$

The Nu_l is the laminar flow Nusselt number, Equation 4.4, ε_6 is a thermal modeling parameter calculated by main harmonics, $k = 6$, in Equation 4.5; and f and φ are given by Equations 4.6 and 4.7 respectively.

$$Nu_l = \left[7.55 \frac{S}{d} - \frac{63}{(S/d)^{17} S/d (S/d^{-0.81})} \right] \left[1 - \frac{3.6 S/d}{(S/d)^{20} (1 + 2.5 \varepsilon_6^{0.86}) + 3.2} \right] \quad 4-4$$

$$\varepsilon_k = \frac{\lambda_w \frac{1+x_1 + \left(\sigma + \frac{x_1+x_0}{x_1-x_0}\right)(1-x_1) - m \left[1+x_1 + \left(\sigma + \frac{x_1+x_0}{x_1-x_0}\right)(1-x_1) \right]}{\lambda_f \frac{1-x_1 + \left(\sigma + \frac{x_1+x_0}{x_1-x_0}\right)(1+x_1) + m \left[1-x_1 + \left(\sigma + \frac{x_1+x_0}{x_1-x_0}\right)(1+x_1) \right]}}{\lambda_f} \quad 4-5$$

$$f = \frac{0.041}{(S/d)^2} \left(1 - \frac{1}{\frac{(S/d)^{30} - 1}{6} + \sqrt{1.24 \varepsilon_6 + 1.15}} \right) \quad 4-6$$

$$\varphi = 0.56 + 0.19 \frac{S}{d} - 0.1 \left(\frac{S}{d} \right)^{-80} \quad 4-7$$

where $x_0 = \left(R_0/R_2 \right)^{2k}$; $x_1 = \left(R_1/R_2 \right)^{2k}$; $m = \frac{\lambda_w - \lambda_0}{\lambda_w + \lambda_0}$; $\sigma = k \frac{\lambda_w R_1 - R_0}{\lambda_1 R_1}$; R_0 is the fuel radius, R_1 is the inner clad radius, R_2 is the clad outer radius, $k = 6$ indicates that this correlation uses the harmonics of a central coolant channel and not an edge channel, $k = 1$, λ_0 is the fuel thermal conductivity, λ_1 is the gap thermal conductivity, λ_w is the clad thermal conductivity, and λ_f is the coolant thermal conductivity.

Because the proper correlation could not be used to account for the special core geometry, the heated hydraulic diameter was adjusted to more closely approximate the predicted heat transfer coefficients. This was done during BE-1B where there were significant changes in fuel temperatures and core flow rates. Data was taken at each axial position for each assembly at all three core ages in 0.1 second increments. This was done several times to reduce the model error from an initial average error of >25% to -2.5% for the driver fuel and 7.24% for the blanket fuel. The corresponding heated hydraulic

diameter was 7.248 mm and 18.995 mm for the driver and blanket fuel assemblies respectively.

The edge and corner pins heat Nusselt numbers were evaluated using the empirical relationship of Equation 4.8 and Table 4.8:

$$Nu = a + bPe^n \quad 4-8$$

Table 4-10 Edge and Corner Fuel Assembly Pin Heat Transfer Correlations

Type of pins	a	b	n
Edge	$4.69 \frac{s}{d} - 4.131$	$0.577 \frac{s}{d} - 0.566$	$3.53 \left(\frac{s}{d}\right)^2 - 8.71 \frac{s}{d} + 5.97$
Corner	$7.13 \frac{s}{d} - 6.972$	$0.331 \frac{s}{d} - 0.342$	$5.27 \left(\frac{s}{d}\right)^2 - 13.12 \frac{s}{d} + 8.83$

Under normal conditions at full power operations Table 4.9 provides a comparison between the Nusselt numbers for each of the pins including the maximum temperature non-uniformity, ΔT_{max} . The pin location plays a significant role in the peak temperatures of the fuel and needs to be considered for the fuel temperature limits. Because RELAP is not capable of inputting these relationships, an external routine was developed. Because the edge and corner pins are a minority of the overall pins in the core, they were neglected in considering their reactivity feedback effects. To compensate for the error in the fuel reactivity feedbacks, the reactivity weighting was split between the average driver fuel and the average inner blanket. This was done because RELAP underestimated the driver fuel convective heat transport and over-estimated the blanket fuel.

Table 4-11 Comparison of Various Fuel Pin Nusselt Numbers

	Nu_{RELAP}	Nu_{center}	Nu_{edge}	Nu_{corner}	ΔT_{max} [K]
Ave DF	14.91	34.92	8.222	6.353	0.1091
Hot DF	16.67	35.9	9.173	7.124	-0.01734
Ave IB	20.06	15.99	6.959	4.561	0.09587
Hot IB	20.17	16.24	7.296	4.817	0.05079
RB	19.08	14.19	4.487	2.772	0.3894

5.1.2 Containment Vessel and RVACS

The RVACS design was based on the data provided in [101] and [61]. NUREG-1368 reported RVACS heat transport between 700-900 kW(t) during normal operations and reaching a peak of 2.5MW(t) in accident scenarios. Assuming the DHR is proportional to the surface area, the PRISM analyzed in NUREG-1368 has a reactor vessel surface area of ~304 m² along the cylinder wall. The modeled PRISM has a cylindrical surface area of 496 m². The increased surface area corresponds to a DHR capability of 1.1 to 1.5 MW(t) under normal conditions, rising to ~3.5 MW(t) at elevated temperatures. Taking the reactor vessel dimensional data from both references, the normal operating condition RVACS losses should be ~1.4MW(t) for the S-PRISM. Because radiative heat transport represents 97% of the heat loss from the reactor vessel,[102] a radiative heat transfer model was assumed.

The reactor vessel liner, sodium gap, and reactor vessel were explicitly modeled in RELAP. A test model was built that had the primary plant internals removed and was an isothermal pool at 640K. This was coupled with a heat flux boundary condition at the surface of the reactor vessel. The boundary condition was controlled by T_0 , the temperature of the UHS, 313.15K, and the surface temperature of the reactor vessel, T_w . It is given by Equation 4-9.

$$q'' = 2.078 \cdot 10^{-8} [W/m^2K^4] (T_w^4 - T_o^4) \quad 4-9$$

This was then tested with the full model under steady state conditions with, non-uniform wall temperatures. The resulting heat loss was 1.375 MW(t), and was considered acceptable for modeling the scenarios. It was only during BE-3 that the heat flux from RVACS appreciably changed, every other accident scenario had very little fluctuation from steady state conditions.

5.1.3 *PHTS Flow Path*

The PHTS was modeled predominantly with multi-dimensional structures in RELAP. The RCP downcomer piping was assumed to be 20" NPS Schedule 10S. Figure 4.3 shows the modeled flow path for the modified version, the only differences are with the IHX and its downcomer piping. Elevation data for the PHTS was taken from [91]. All elbows and area changes were explicitly modeled using the information from [103]. All elbows were assumed to be long radius to minimize pressure drop.

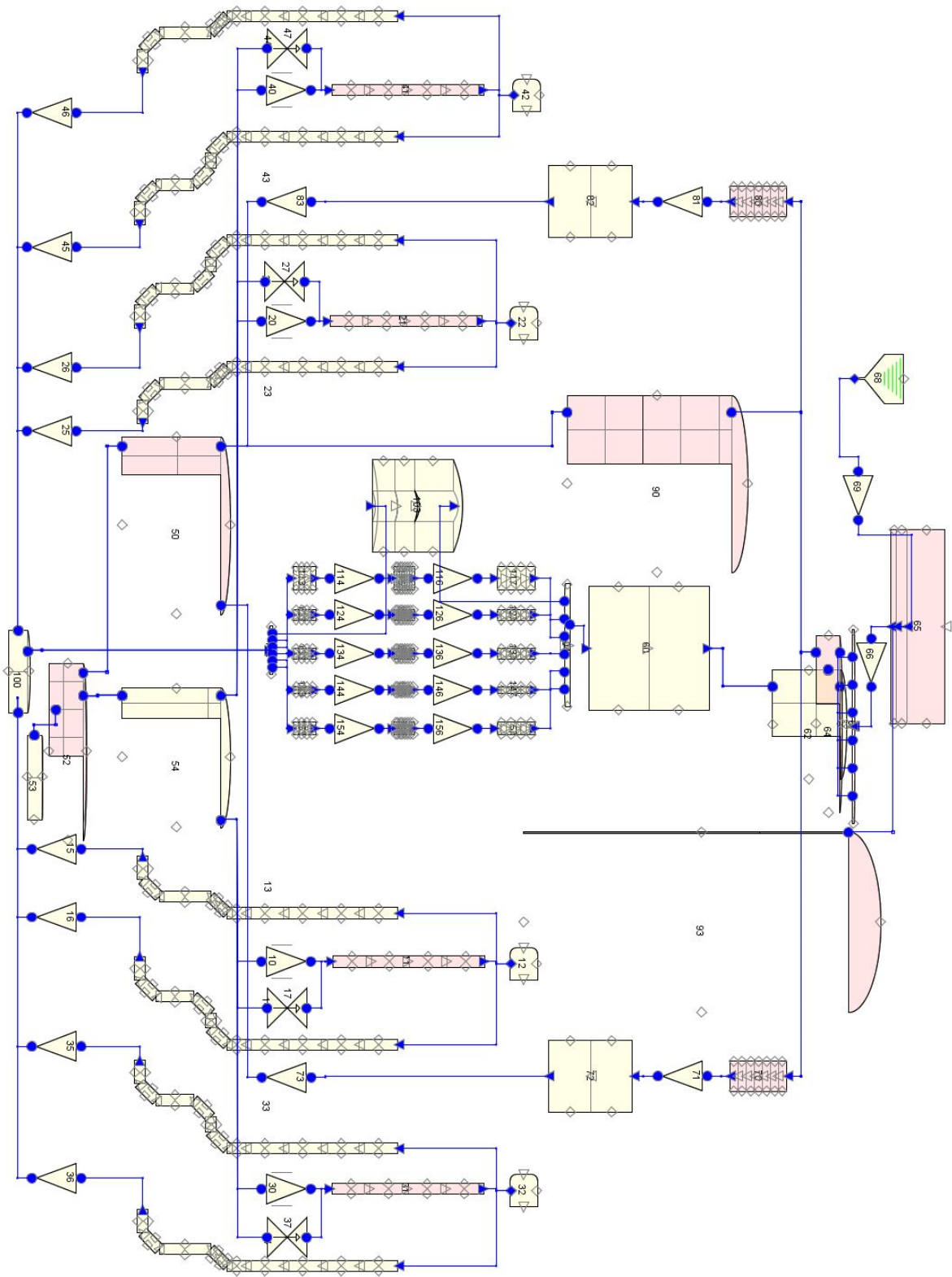


Figure 4-2 nTES primary heat transport system

The piping configuration followed published data as closely as possible. The RCPs have a 42% thermodynamic efficiency.[104] The remaining thermal energy from pumping was added into the primary system using a source term that was proportional to flow. The RCP outer surface was approximated as being adiabatic. This is not entirely accurate as there is a layer of insulation and some heat transfer occurs with the coolant between the hot pool and cold pool divider plates. The energy transfer mechanism was done because the reactor coolant pumps are self-cooled and all of the heat is transferred to the coolant.[104] The RCP stators are in two parts. There are an inner stator and an outer stator. There is an annulus that is formed between the two stators and a central pipe.[104] The central pipe was assumed to have a radius of 0.077m and the outer annulus had a gap of 0.077 m.[104] Using the flow area from [104], the inner stator's outer wall was 0.453 m, and the outer stator's wall was 0.906 m. This is consistent with the dimensions in [104] For simplicity, the stator heat structures were lumped into the outer stator with all of the flow in the RCP inside of it. A more accurate model would be to explicitly model the two stators as separate heat structures and to use three hydrodynamic structures: the central channel, the annulus, and the shroud pool. This would allow development of accurate temperature profiles within both stators with little additional modeling effort. The as modeled stator heat structures are 0.375 m thick SS 304. This is not the same as the actual composite copper, black iron, and insulation.[104] A more accurate approach would develop a composite heat capacity and thermal conductivity for the stator assemblies.

Because of the additional PHTS pressure drop, the radial dimensions of the 160m³/min pump were taken as given. Each RCP was extended another 3.296 m past the

original design's 4.4 m length to allow greater pumping power and fit within the drawing takeoffs for the pump length.

The RCP hydrodynamic volume did not do any actual pumping, even though RELAP does allow for EM pumps. The engineering data needed to use the built-in pump model was not available. Instead, a time dependent junction was used to model the pump flow for each of the 4 RCPs. During transients that required the pumps to trip, the EM pump coastdown curve from NUREG-1368 was used, Figure 4.3. The RCPs take their suction from the radial shielding outside of the core riser region. This allows them to draw coolant from low in the cold pool.

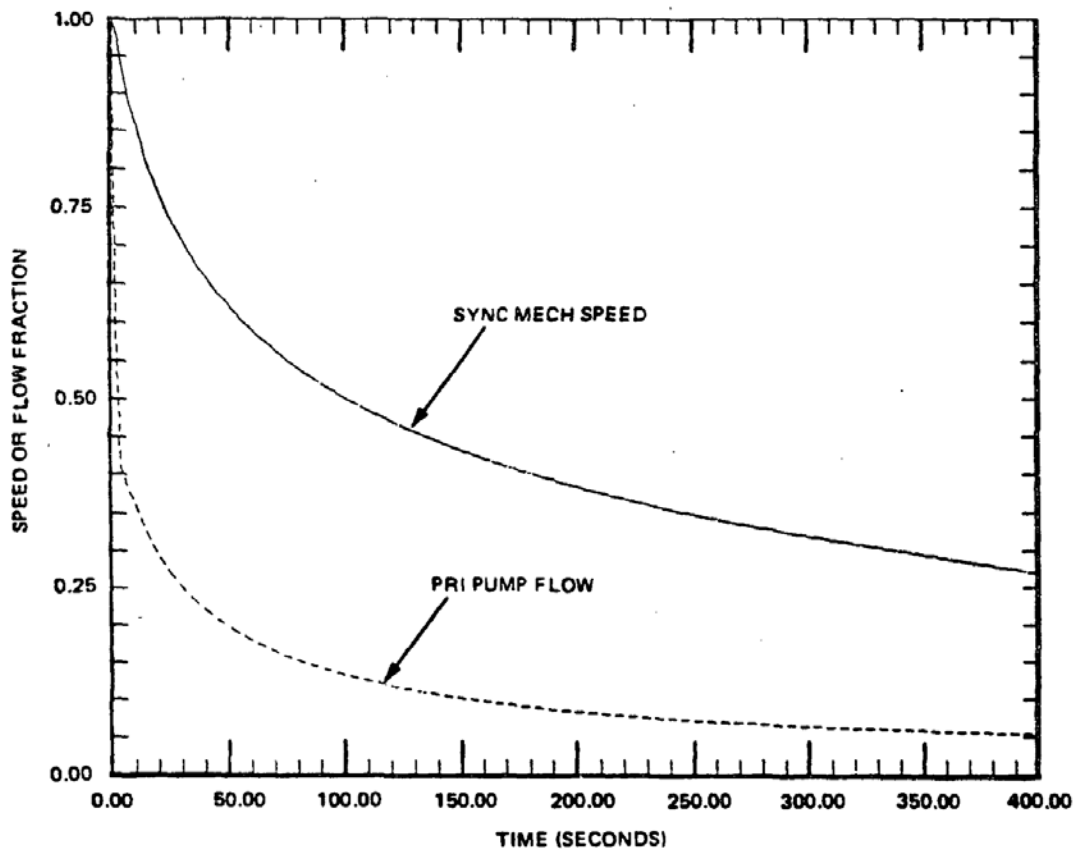


Figure 4-3 EM pump coastdown curve(NUREG)

Because the RCPs' are supported from the reactor vessel closure head,[48] their expansion joint with the pump suction is not fully sealed. The design leakage is very important through the shroud pool as it represents a significant surface area of the reactor vessel and thus is critical for DHR providing approximately 252 m² of surface area to RVACS. There are two sources of leakage for this important area to have adequate flow. The first is through the aforementioned RCP lower expansion joints, the other is through the IHX expansion joints, the IHXs are hung similarly to the RCPs.[48] The upper horizontal baffle has gaps in it for the reactor coolant pumps and the IHXs. For simplicity, the bypass flow path was from the RCP penetrations to the lower IHX expansion joints. The leakage path to the RCP suction was attempted, but was not used due to modeling anomalies when non-condensable gases were used as the cover gas for the top of the primary pool for pressure control. The other system bypass is the core bypass and was discussed previously.

The surface of the primary pool was set at a pressure slightly above atmospheric, 34.5 kPa gage, (5 psig). Helium was used as the cover gas.[102] During establishing steady state, helium was replaced with a time dependent sodium volume at the interface level, at hot-leg temperature, and the desired system pressure, structures **68** and **69** for the volume and junction respectively.

5.1.4 IHTS Flow Path

The each IHX consisted of 5,700 tubes [90] with a surface area modification to achieve the designed log mean temperature difference. The heat exchanger consists of a lower inlet branch that provides flow to inside of the IHX tubes. Flow then leaves the tubes and goes into an outlet branch attached to the IHX secondary outlet annulus.

Primary flow begins with cross flow across the tubes in the hot pool, flow then flows down around the outside of the tubes, but inside the IHX assembly. Flow then exits and goes into a short pipe into the cold pool. Figure 4.5 shows the reference implementation in RELAP.

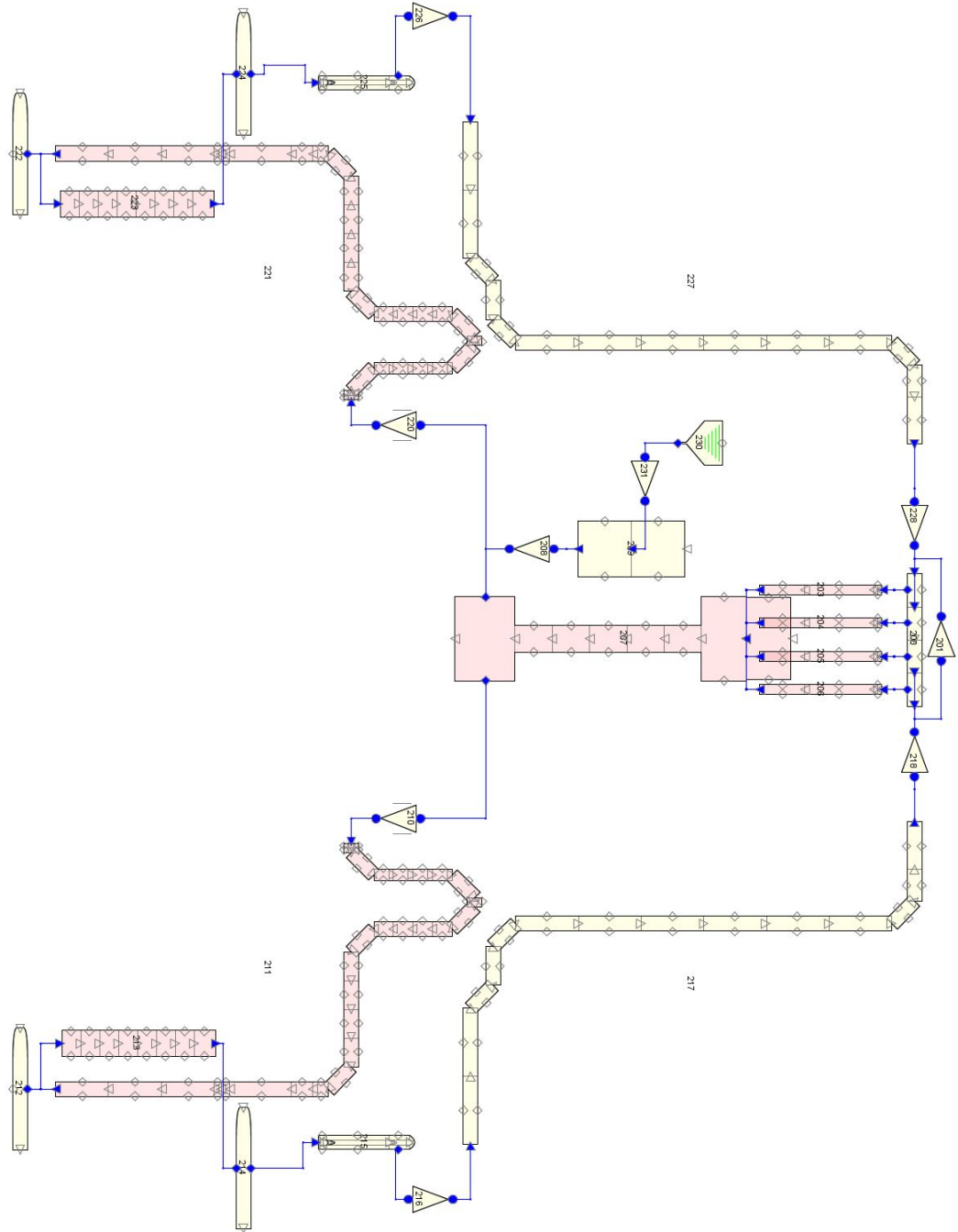


Figure 4-4 Reference S-PRISM IHTS

The sodium inlet to the steam generator is a torus located immediately above the steam generator with 4 separate downcomer pipes. There is a small pool in the top of the steam generator with very few tubes. The sodium flow diffusers were not modeled, and

were just left as abrupt pipe endings. Sodium flow is then downward in an annulus around outside of the steam helix tubes. Sodium then leaves through two pipes at the sides of the steam generator and then moves upward through the secondary EM pumps which are modeled in a similar fashion to the primary EM pumps. Flow then changes direction and goes back down to the grade level and into the IHX lower inlet plenum.

The containment isolation valves were not modeled, explicitly. By setting the time dependent junctions for the IHTS pumps to 0 flow that will secure all IHTS flow.

5.1.5 Steam Generating System

The S-PRISM steam generator plays an important function in DHR as the outer shell provides the heat transfer surface to the ACS. Figure 4.4 shows the S-PRISM S/G configuration. The tube sheet was taken to contain 617 tubes with a helix height of 10.49 m. The unknown was the pitch to diameter ratio of the tube sheet. The P/D determines how closely the tubes are packed which in turn determines how many times the tubes are wrapped around the annulus, and thus the overall length of the tube-sheet. The approach taken in estimating these dimensions was taken from [68] where helical steam generators were modeled for NGENP. The estimated P/D was 1.3787 and resulted in a total tube sheet length of 153.26 m. The sodium and water/steam inlet and exit conditions were taken from [48]. A more rigorous approach would be to develop an empirical model of the heat transfer surfaces using the models in [86] but this was not necessary. When the steam generator model was applied to RELAP it resulted in the correct steam conditions for the given sodium flow rate.

To maintain stability in the computation, the Hanford N reactor, developmental model option 12 was used. Without this and options 8 (void fraction change timestep

control), 10 (pressure change timestep control), and 13 (vertical stratification), the thermodynamic state within the SG was unstable and lead to frequent program crashes. These options also helped with dealing with the non-condensable gases within the accumulator portions of the system.

The external flow of the sodium was modeled by determining the free flow area of the sodium and its hydraulic diameter. Because of the shallow pitch of the tubes, they can be approximated as a pure cross flow heat exchanger from the sodium reference frame with little loss of accuracy. This approximation was used to estimate the hydraulic diameter.

To allow “plant startup” a simple PI controller was developed to regulate the steam temperature and feed water flow. For simplicity of design, the steam pressure was held constant as it was assumed to be regulated by the turbine throttles, outside of the steam generator control boundary. This was approximated by having a time dependent volume at the appropriate pressure to act as the steam dump. A combined error term which included steam outlet temperature program error and steam flow rate to sodium temperature difference was used. The combined error then controlled the feedwater flow. More complicated controllers can be implemented [105-107]. Additionally, by including the controllers from [105] into RELAP, one can assess the impact of the controller on any of the anticipated transients. This was not done in this study as the focus was not on designing a plant control scheme for the conventional S-PRISM, but designing a modified version. An interested person could take the model developed here and implement and test such a controller.

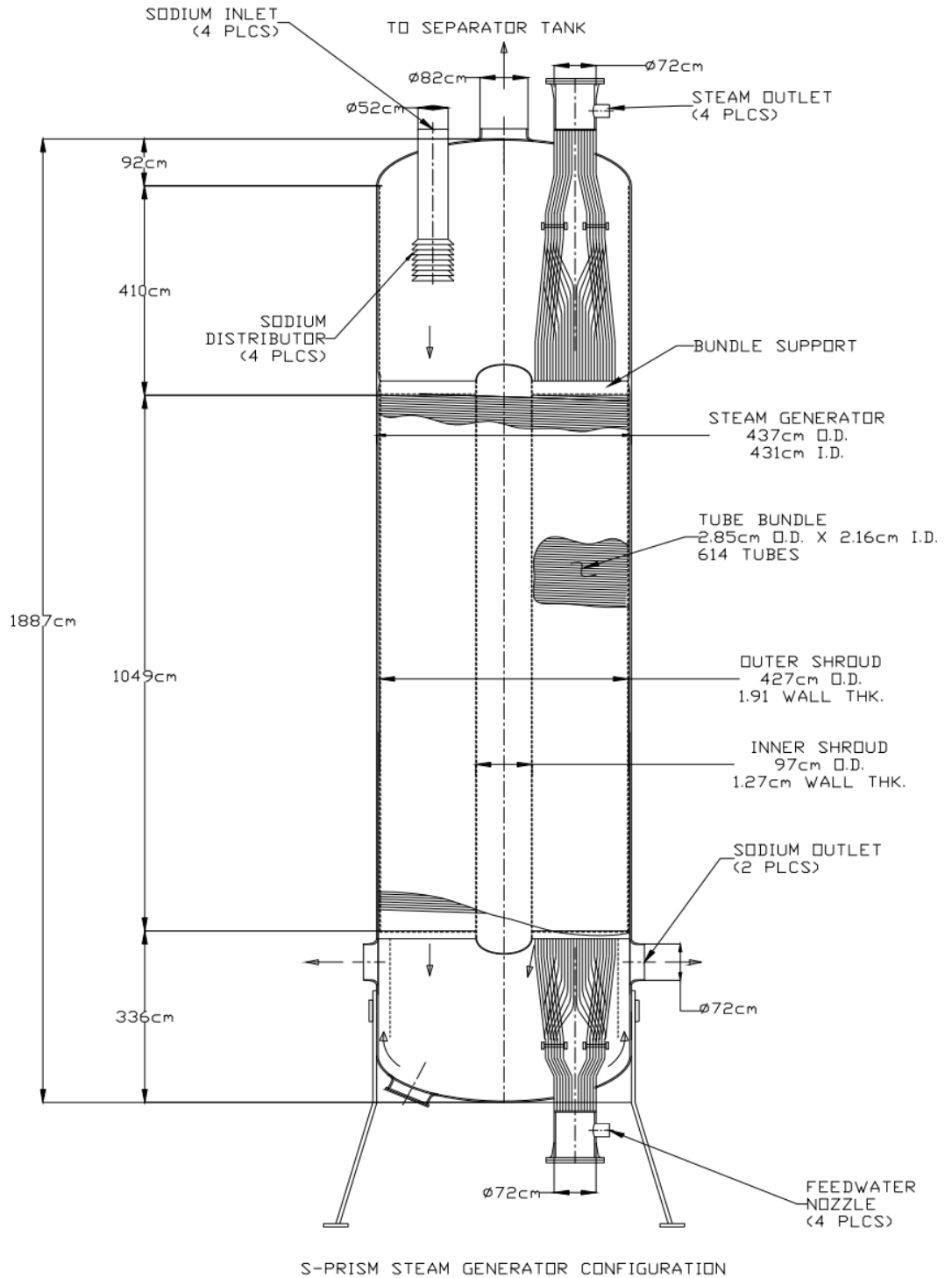


Figure 4-5 S-PRISM steam generator configuration [108]

5.1.6 ACS

The ACS is a very simple system. It consists of an insulated shroud around the outside of the steam generator shell. This system and the IHTS are not considered part of the containment boundary. Their purpose is to limit transients for the purpose of protecting equipment for long term use. The ACS, unlike RVACS, is normally offline with a set of inlet and outlet baffles. These baffles open on a loss of power and can be manually operated. There is also a fan in the system that is used for plant cooldown during refueling operations.[48] Because the ACS performs a safety function it was included. Because of the lack of available data, it was unable to be benchmarked, and comparisons needed to be made without it in service. The two factors that need to be tuned are the ACS surface area and the annulus gap. With appropriate data, the ACS can be sized to provide the necessary DHR capability.

5.2 Modified S-PRISM

The modified plant consists generally of a compact FPHXs for the IHTS and a redesigned safety-grade ACS. The basis of these systems was discussed in Part 2. This part will focus on how the designs were implemented in RELAP.

The piping system modification for the IHTS is shown in Figure 4.7. The ICP are no longer on the rising portion of the leg of **211**. They are shifted to the lowering (right hand side). The accumulator for the loop is **231**, and is at the point of lowest pressure in the system. It is an annular accumulator with the enclosing pipe being a 50" NPS Schedule 40S. Because of how the ICP is simulated with a time dependent junction **210**, the accumulator entry point is at the suction of the pump, not where it would be actually located in the third segment of **211**. The trip valve **234**, allows simulation of natural

circulation in the IHTS and opens once ICP flow has decayed to that consistent with natural circulation. This was done because time dependent junctions with a flow set at zero act like closed valves in RELAP. The time dependent volume **233** is used to initialize the problem and was removed once steady state conditions were established. At that time, the accumulator **231** was changed from being solid to being half helium half sodium, with the helium at a pressure resulting in 136 kPa absolute in the uppermost part of **211**.

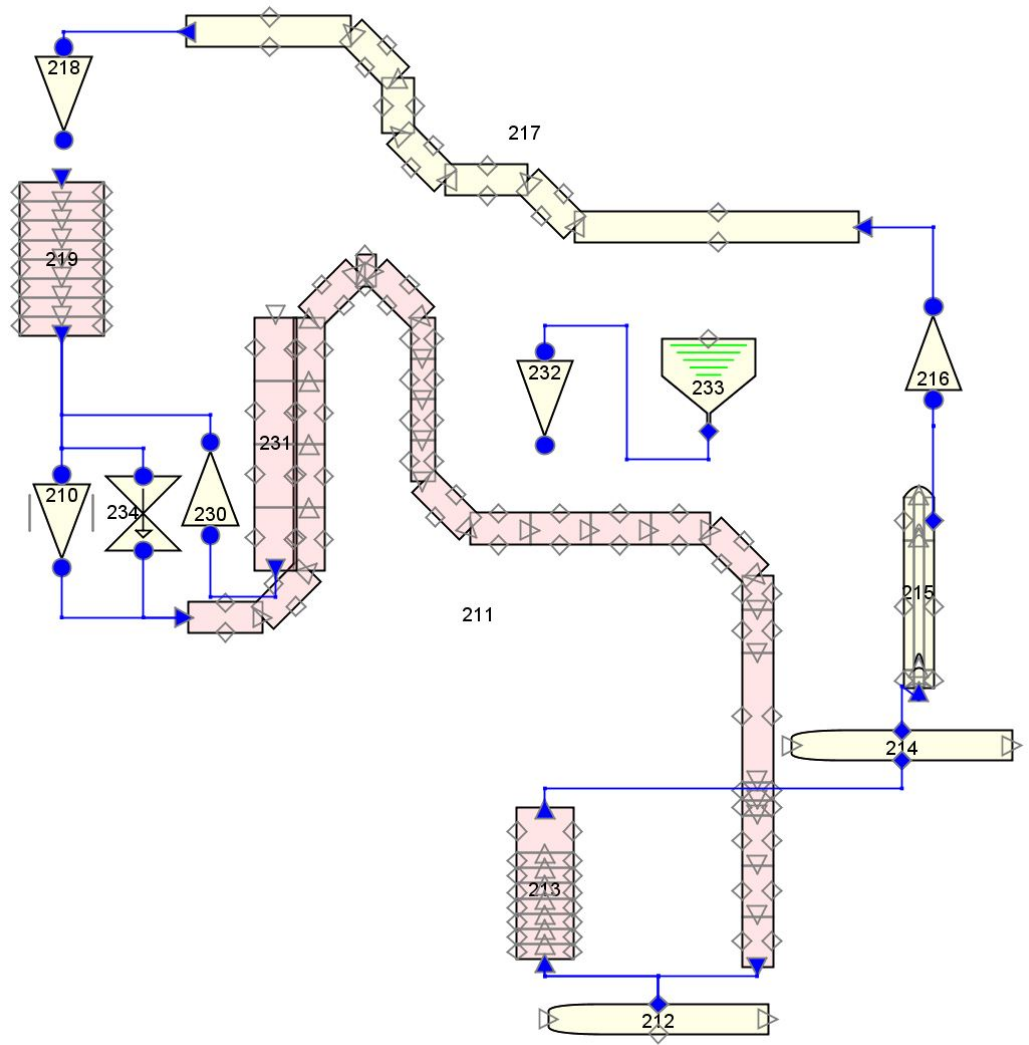


Figure 4-6 'A' Train IHTS for nTES S-PRISM

The Salt Heat Transport System, SHTS, is in Figure 4.8. The salt isolation valves, **310**, **316**, **320**, and **316** are 30" NPS motor operated gate valves with a stroke time of 3 seconds in the closed direction. The ACS heat exchangers are 331 and 341 and their associated butterfly check valves are **333** and **343**. The tee's for the ACS portion of the piping, **330**, **334**, **340**, **344** are angled tees with the branch coming from the vertical pipe at a 45° angle as shown. This is to minimize the natural circulation head loss in the system. These piping sections also include a 45° elbow to return the piping back to horizontal. To minimize the number of volumes all of the remaining ACS piping was put into **332** and **342**. The ACS piping is the same size as the remainder of the SHTS piping, 30" NPS Schedule 40S and similarly uses long radius fittings to minimize pressure loss.

Similar to the IHTS the ACS accumulators, **317** and **327**, are annular, but are 65" NPS Schedule 40S. They encircle the cold downcomer piping **311** and **321**, and are sized to allow the transition from forced circulation (high pressure side of the system) to natural circulation (low pressure side of the system). Their connections to the cold downcomer piping, **318** and **328**, are located as they would be in the actual plant locations. The SHX's are components **319** and **329** and are discussed in more detail in section 5.2.1. The SHTS check valves, **303** and **306**, are 42" NPS swing check valves. Their function is to prevent system backflow during pipe breaks outside of the piping volume shown in Figure 4.8.

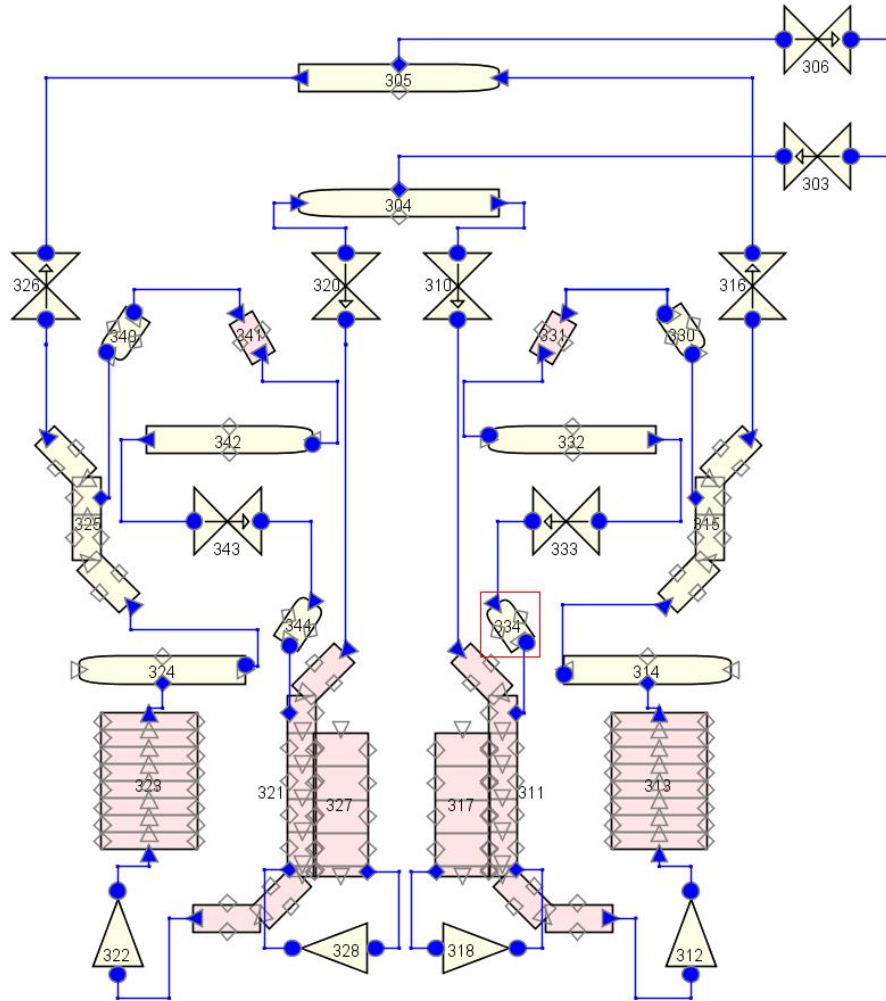


Figure 4-7 nTES Salt Heat Transport System

5.2.1 IHX

The IHX is a counter flow compact heat exchanger with a $\beta=1,538 \text{ m}^2/\text{m}^3$, (ratio of heat transfer surface area to total volume. The channel flow data using Equations 4.1 and 4.2 is in Table 4.10.

Table 4-12 IHX RELAP Darcy Friction Factor Correlations

	A	B	C	Φ_S
Sodium	0	4.32	0.425	0.7095
Salt	0	4.32	0.425	0.7095

The turbulent friction factor data was taken from Hesselgreaves[86] (eqn 5.43, 5.44 and 5.49) and the shape factor was determined from Shah and London [109] using tabulated data of the pitch/span for triangular ducts and sine ducts. The both PHTS and IHTS channels uses a sine duct Kayes and London *wavy plate-fin surface 17.8-3/8W*. [85]

The pressure drop across the primary side was 371 kPa with a Reynolds number of 14,890. The secondary side had a pressure drop of 268 kPa for a Reynolds number of 12,237. Each IHX was sized to remove half of the nominal core power plus the heat from (2) RCPs minus half of the nominal RVACS DHR at full power. The net IHX power was 520 MW(t). Stainless Steel 304 was used as the heat exchanger material.

Table 4-13 IHX RELAP Hydrodynamic and Heat Structure Data

	Primary	Secondary
Flow Area, m ²	3.489	0.8306
Hydraulic Diameter, m	0.002123	0.000805
Flow Length, m	2.982	2.982
Heat Transfer Area, m ²	19,601	238.5
Heated Diameter	0.002123	1.6·10 ⁻⁵
Pitch, m	0.001427	0.000547
Span, m	0.01049	0.00254

5.2.1 SHX

The SHX is a counter flow compact heat exchanger with a $\beta=1,373 \text{ m}^2/\text{m}^3$, (ratio of heat transfer surface area to total volume. The channel flow data using Equation 4.1 and 4.2 is in Table 4.12.

Table 4-14 SHX RELAP Darcy Friction Factor Correlations

	A	B	C	Φ_s
Sodium	0	0.17	0.2	4.9456
Salt	0	4.32	0.425	0.7095

The inability to have the salt thermo-physical data is a significant problem. The difficulty is introduced that the density, viscosity, and thermal conductivity of the two fluids are not matched. Sodium has a much higher thermal conductivity but lower density and viscosity, while the salt has a lower thermal conductivity and higher density and viscosity.

Two independent modifications needed to be made to the salt side of the heat exchanger. The secondary sodium flow rate needed to be above that of the salt, due to the difference in heat capacities of the two fluids. The salt flow for a heat exchanger was 1,594 kg/s and the corresponding sodium flow would be 1,889 kg/s. This resulted in a heat exchanger pressure drop of 473.6 kPa, which will result in reduced natural circulation performance, which is acceptable as it adds a measure of conservatism. The salt side of the IHX has a UA=63,688 kW/K. To keep this constant the resulting heat transfer coefficient for the sodium on the salt side was 267.1 kW/m²-K requiring a surface area of 238.5m². The sodium side of the heat exchanger UA was 4.194·10⁶ kW/K. These initial values were used to initialize the model. After steady state calculation, the surface area of each side was adjusted to give the desired UA. The wall thickness is 0.001 m and P91 was used as the heat exchanger material.

Table 4-15 SHX RELAP Hydrodynamic and Heat Structure Data

	Primary	Secondary
Flow Area, m ²	3.489	0.8306
Hydraulic Diameter, m	0.002123	0.000805
Flow Length, m	2.982	2.982
Heat Transfer Area, m ²	19,601	238.5
Heated Diameter	0.002123	1.6·10 ⁻⁵
Pitch, m	0.001427	0.000547
Span, m	0.01049	0.00254

5.2.3 AHX

Like the SHX the AHX will require modification from the original salt design to approximate the salt characteristics when using sodium as the working fluid. For simplicity, the ducts, surface straight fin shape 2.0, which are trapezoidal were approximated as being square. The Shah and London [109] correlation was used to determine the shape factor. The turbulent parameters were taken from Hesselgreaves[86] (5.41)

Table 4-16 AHX RELAP Darcy Friction Factor Correlations

	A	B	C	Φ_s
Sodium	0	0.771836	0.356542	0.9218
Salt	0	0.771836	0.356542	0.9218

A similar flow increase of the sodium as a replacement working fluid was needed, original salt flow was 217.7 kg/s the replacement sodium was 260.6 kg/s. A similar approach in adjusting the heat transfer surface to obtain the desired UA was implemented. The desired air and salt side UAs are 5.76 kW/K and 158.3 kW/K respectively. The heat exchangers were configured to be as they would in the actual plant with a folded core design. Each of the 4 heat exchanger modules are 1.25 m x 1.25 m x 0.2m, resulting in an approximate footprint of 3.3 m 1.25 m x 1.08 m allowing for a simpler placement above the SHX. To limit computational overhead, the number of hydrodynamic volumes and heat structures were limited. To do this the AHX was approximated as one, long heat exchanger, each of the (4) modules stacked end on end. The salt and air flow lengths were unaffected, just the respective flow areas. The AHX material was modeled as P91.

Table 4-17 AHX RELAP Hydrodynamic and Heat Structure Data

	Secondary	Air
Flow Area, m ²	0.3391	6.158
Hydraulic Diameter, m	0.01445	0.01445
Flow Length, m	1.25	0.2
Heat Transfer Area, m ²	2.283	148
Heated Diameter	2.23·10 ⁻⁴	0.01445
Pitch, m	0.0127	0.0127
Span, m	0.01905	0.01905

5.2.4 ACS Piping

Figure 4-8 shows the nodalization of the ACS system in RELAP. The AHX piping was taken to be the same as the main salt header piping, which was the same as the reference model IHTS system piping.

The AHX butterfly check valves (**333** and **343**) were modeled in RELAP using the same approach as Rao [83], however instead of directly inputting the check valve, the check valve was modeled using a time dependent junction where the equations from Rao, were solved to provide junction flow as a function of the differential pressure across it.

The check valve is modeled as a second order differential equation of the form:

$$\frac{d^2\theta(t)}{dt^2} = \sum_i \frac{T_i(t)}{I} \quad 4-10$$

$$\frac{d\theta(t)}{dt} = \int_{t_0}^t d\tau \frac{d^2\theta(\tau)}{d\tau^2} \quad 4-11$$

$$\theta(t) = \int_{t_0}^t d\tau \frac{d\theta(\tau)}{d\tau} \quad 4-12$$

where $\theta(t)$ is the angle of the check valve in degrees, where 0° is vertical and closed and 90° is horizontal and full open. $T_i(t)$ are the torques associated with the valve, see Part 2, and I is the valve disc's moment of inertia. Equations 4.10 and 4.11 were modeled in RELAP using the standard Integral function. The integral controller representing $\theta(t)$ was limited to 0° to 90°. With an actual valve design, these limits can be set accordingly.

Each check valve was modeled as being a servo control valve with its own controller. The respective valve's controller was its angle. The valve area as a function of valve angle, Equation 4.12, was tabulated for use in the servo control valve.

$$0.62\varepsilon_T + 0.38\varepsilon_T^3 = \frac{1}{1+\sqrt{a+b\theta+c\theta^2+d\theta^2}} \quad 4-13$$

The terms a , b , c , and d are experimentally determined constants with the values 26.184, 0.091, -0.014, and $1.11 \cdot 10^{-4}$ respectively.[83] ε_T is the ratio of the valve's flow area to upstream pipe area.

CHAPTER 6 TRANSIENT SIMULATIONS

6.1 Comparison to Published Data

6.1.2 Baseline Event 1 – SCRAM with loss of ACS

This event is taken directly from NUREG-1368. Because NUREG-1368 did not consider the ACS as part of the safety boundary, and was considered as part of the safety boundary here, two different versions of this accident scenario were run. The first option included the thermal mass of the IHTS and the ACS, but without any heat removal capability from the AHX's. The second version consisted of a reactor plant trip with IHTS pump coast down occurring within 2 seconds.[61]

Figure 4.9 shows the comparison between NUREG-1368 with RVACS performing nominally (a) and the modified S-PRISM showing the loss of both ACS channels with IHTS and ACS hydraulic volumes remaining intact (Nominal) and the direct comparison to NUREG-1368 where the ICP's coasted down in 2 seconds and the IHTS and SHTS removed from the model. The transient initiation temperatures differ by approximately 84°C. This is due to the RELAP model taking into account the entire thermal mass of the primary system. The cold leg volume is approximately twice the size of the hot leg volume. Another factor may be that the mass of the modeled PHTS may be too large and not accurately take into account the volume of coolant displaced by the reactor vessel internals. For lack of better information, the remainder of the analysis will be considered accurate.

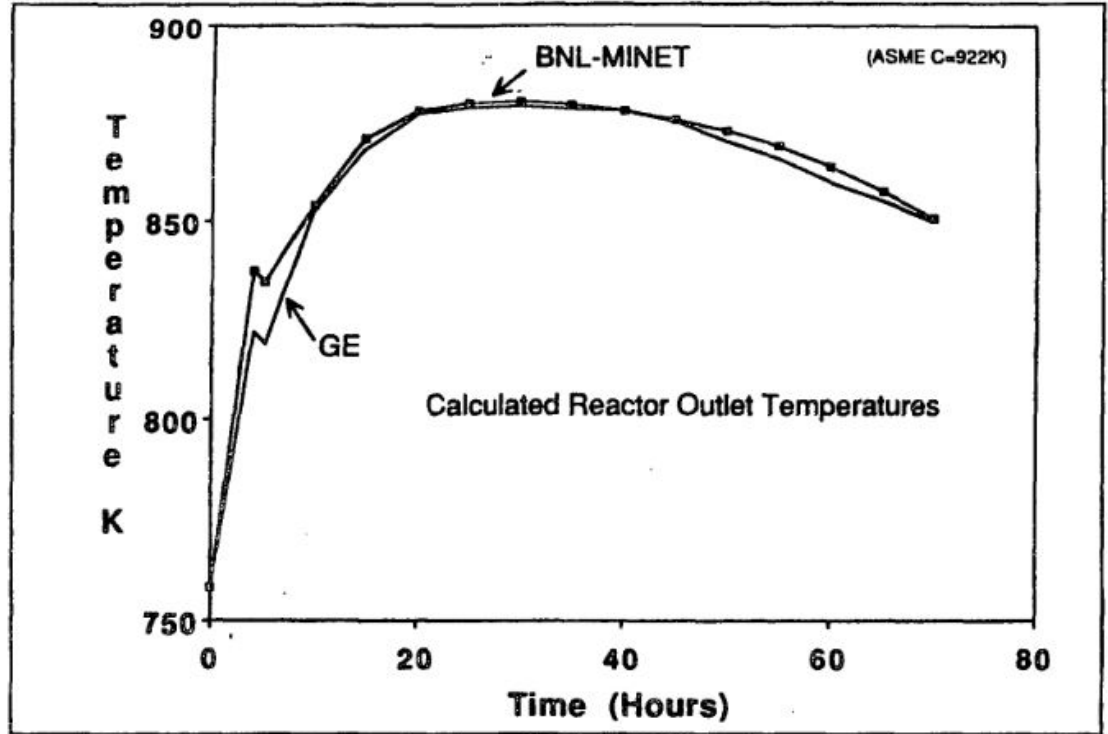


Figure 15.1 PRISM LOHS with RVACS performing normally

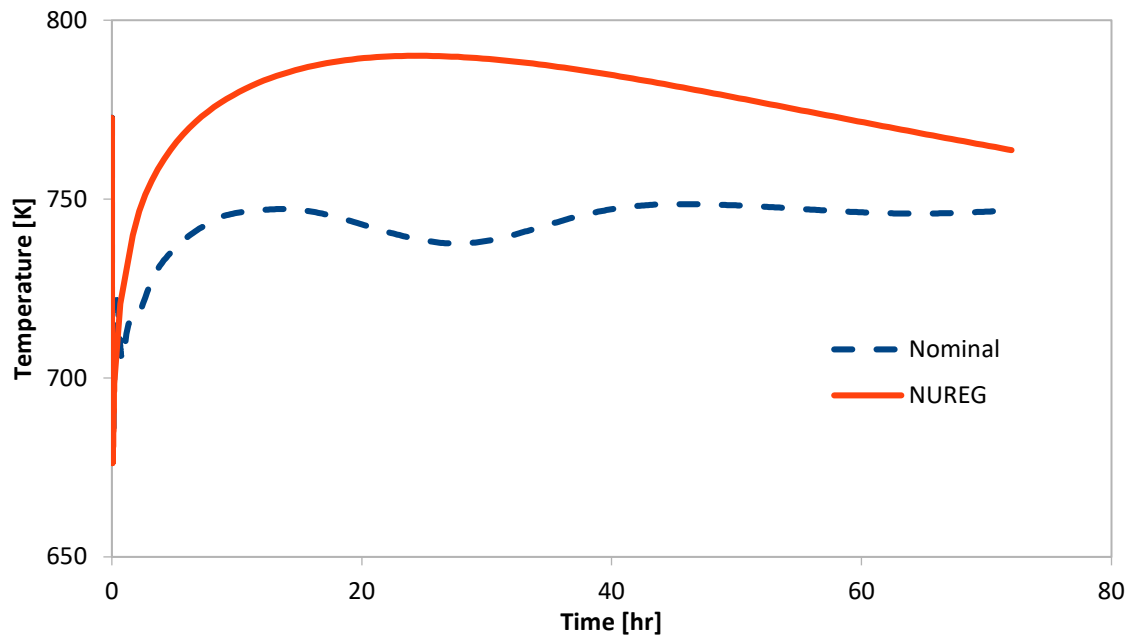


Figure 4-8 Comparison of NUREG-1368 to the modeled plant. Figure (a) is from NUREG-1368. Figure (b) is the model in two different scenarios, the one labeled NUREG is for a direct comparison to (a) the nominal assumes an intact safety boundary.

6.1.3 *Baseline Event 2 – UTOP with \$0.3 Reactivity Insertion*

This baseline event is a \$0.30 reactivity insertion with a failure to SCRAM and no plant trip. This event provides a comparison of the reactivity feedbacks associated with the S-PRISM core used in this study and the one published by [99].

The simulation was run in several different configurations. First, it was tested using the fuel as specified by [90] under BOC conditions. Then the fuel thermophysical properties were set to those derived from [96] while using the different fuel kinetic data from [90].

Table 4-18 Summary of UTOP Temperatures[99]

Table 4-18 provides the summary of the UTOP for the reference S-PRISM at various reactivity insertions.[99]

Magnitude (cents)	Peak Fuel Temp (K)	Peak Coolant Temp (K)
30	1250.9	929.3
40	1325.4	975.4
50	1412.6	1031.5
60	1507.0	1094.8

The power transient of the modeled reactor did not match that of the reference reactor using the thermophysical and kinetic data of [90]. The reference core had a peak power of 180% and a final steady state power of 130%. Similarly, the reactor described in NUREG-1368 undergoing a 40¢ reactivity insertion reached peak power at 172% with final power stabilizing at 120%. Peak fuel, cladding and coolant temperatures occurred approximately 31 seconds into the transient (near the end of rod motion) and were 1,292 K, 979 K, and 951 K respectively.[61] The reactivity feedbacks associated with the NUREG PRISM are on the same order as the reference S-PRISM, but of a slightly larger magnitude. The modeled reactor of [90] had a peak power of 284% and a steady state power of 267%.

This suggests a significant difference in the doppler and density reactivity feedbacks. To estimate this divergence, a linear temperature feedback coefficient was

assumed. The reference plant had a steady state to steady state transition of 510 °C to 803°C. Assuming a constant core inlet temperature of 371.1 °C, the reference reactor had an average coolant temperature change of 73.1 °C for a 30¢ reactivity insertion. The modeled reactor had an average coolant temperature change of 185.5°C for a similar reactivity insertion. Using the expected change in T_{ave} , the effective reactivity insertion was 76.2¢ with an equivalent temperature feedback of the reference design.

Table 4-19 Reference to Model Comparison for BLE-2

To provide a more direct comparison the data from [99] was extrapolated to the estimated equivalent

Magnitude (cents)	Peak Fuel Temp (K)	Peak Coolant Temp (K)
47.0	1386.6	1018.3
30	1372.0	1087.4

reactivity, the first row of Table 4-17. The last row is the hottest pin from the hottest channel, with the temperature adjusted for the higher core outlet temperature of the reference S-PRISM conditions of [102], 510 °C instead of 499.5°C. Because the core inlet temperature was not known, for the reference design accident scenario, it was assumed to be proportional to the change in core inlet temperature of the model plant. The modeled plant had core inlet temperature increase 185.5°C for a 267% power excursion. The reference plant had a 130% power excursion, which corresponded to a 90.4°C increase in core inlet temperature.

Once the difference in temperature feedback, α_T , is accounted for, the modeled plant's 30¢ UTOP corresponds to a 47¢ UTOP in the reference plant reported by [99]. For the purposes of safety analysis, a lower magnitude α_T , generally provides a more extreme power and temperature excursions and can be considered as being more conservative. There is one accident scenario, BE5-C a transient overpower, where the GEM reactivity can be offset by a more aggressive temperature response. One possible

explanation for the difference is that the reactivity feedback is only considered for two assembly groups, the average driver fuel and the average inner blanket. The hot inner blanket, hot driver fuel and average radial blanket are not considered. The blanket assemblies, because of their increased U-238 content will have a larger contribution to doppler feedback than the few driver assemblies that weren't considered. The impact on leakage from the central assemblies will be more pronounced because the radial blankets will absorb more neutrons that leave the core, reducing the fraction reflected, and will absorb more of the reflected neutrons.

Table 4-20 Full Power Fuel Assembly Bulk Coolant Outlet Temperatures

The peak channel outlet temperature for nominal full power reported in [102] of 594°C when adjusted for the change in core inlet temperature of the modeled S-PRISM which is based on that reported by [48] for the PRISM, the limiting assembly bulk coolant outlet temperature is 565°C. The orificing of the channels

	Temp (°C)
Ave Driver Fuel	509.1
Hot Driver Fuel	479
Ave Inner Blanket	492.9
Hot Inner Blanket	475.8
Ave Radial Blanket	548.2

mentioned earlier resulted in satisfactory performance as shown in Table 4-18, with the average radial blanket assemblies having the highest coolant outlet temperature of 548.2°C.

The PRISM reactor described in NUREG-1368 had a net prompt reactivity feedback of -0.88 pcm/K.[61] The BOC net prompt reactivity feedback of [90] was -0.23 pcm/K. When the fuel thermophysical properties were changed to those derived from [96], the model was not able to achieve steady state conditions and melted fuel for each core age after approximately 150 seconds for the BOC and MOC cases, and 123 seconds for the EOC cases. This change in core performance due to the change in core

thermophysical properties places the magnitude of the underestimate in the prompt reactivity feedback closer to 4 which is consistent with that observed with the NUREG-1368 PRISM core. To assess this impact, the thermophysical properties derived from [96] were combined with the fresh fuel configuration and the kinetics data from NUREG-1368. Figure 4-9 shows the response for this configuration. The peak power of 172% checks with that reported in NUREG-1368, however the time of the peak, 220 seconds, is well after the reported 30-seconds. Reactivity peaked at 10¢ occurring 11-seconds into the event. The settling time reported in NUREG-1368 was 100-seconds and was at 120%. Here the settling time was 1,000-seconds with power at 160%. One possible explanation for this difference is that the fuel's thermophysical properties may differ. Of note, the hot pool temperature reaches 607.9 °C. The maximum salt outlet temperature under this scenario is 578.2 °C, well below the long term decomposition limit of 600 °C.

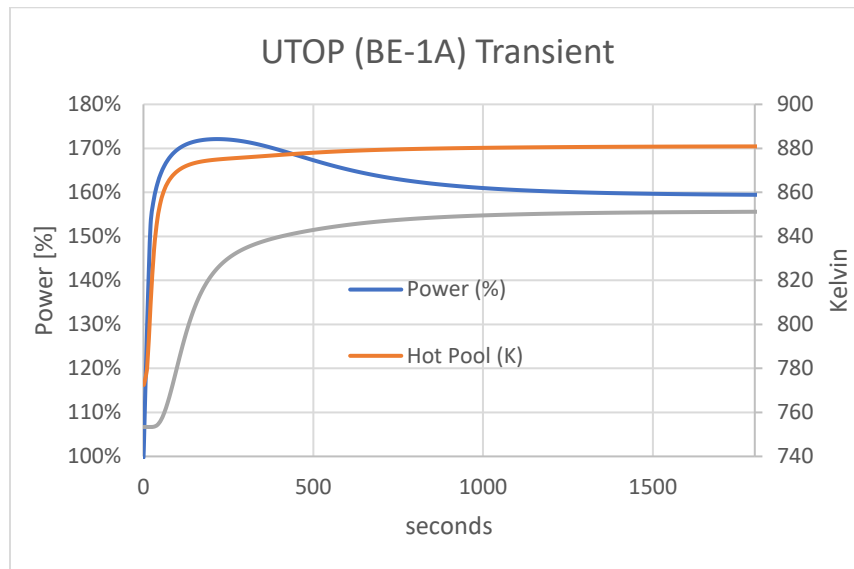


Figure 4-9 UTOP BE-1A using NUREG-1368 temperature feedbacks

Based on the two baseline events, the modeled plant is sufficiently close to the parameters of the reference design to be able to make reasonable and a generally

conservative approximation. All other parameters are within available operating limits for a nominal full power plant. Using the NUREG-1368 temperature feedback with the fuel thermophysical data derived in the present work, appears to adequately approximate the reported kinetic response.

6.2 Unprotected Accidents

The accident scenarios considered here were taken directly from NUREG-1368 and modified as needed to fit the modeled plant's design. Every accident scenario evaluated here performed at least as good as the reference design (where data was available for comparison). All analyzed scenarios did not exceed ASME Service Condition C structural temperature limits (922 K), fuel melting temperatures (1,228 K and 1,300 K for driver and blanket respectively), fuel clad eutectic formation (978 K), or the salt decomposition temperature (873 K). In most of the considered bounding events, the fuel and coolant did not exceed normal operating temperatures. And, for every bounding event considered, coolant temperatures never exceeded 600°C.

6.2.1 Unprotected Loss of Flow – ULOF

There were two events considered for the ULOF taken directly from NUREG-1368. The first event, BE4-A, was a nominal trip of a single RCP without protective action, N/F SCRAM. The second event was an instantaneous coastdown of a RCP during a reactor trip, BE4-B. The loss of flow for both scenarios was initiated by assuming that the RCP's power was instantaneously cut and that the normal coastdown mechanism was not available. This was simulated by changing the RCP time dependent junction to a single junction with the initial condition of the flow rate of the time dependent junction at the time of the pump trip. In both cases, flow reversed through the RCP in ~0.25 seconds.

This inserted ~\$1 of reactivity in under 2 seconds. This caused a rapid drop in core power, which fell faster than flow did in every channel, ensuring that fuel temperatures did not rise as reported in NUREG-1368. This suggests that the pressure response of the GEM is faster in the one modeled here than the one reported in NUREG-1368.

For BE4-A, the loss of 1 RCP with no plant trip, the grid plate pressure fell rapidly after initiation, causing an immediate negative reactivity insertion. Figure 4.10 shows the power, total reactivity and GEM reactivity. The response shown in Figure 4-10 is for the reference BOC core reported by [90]. When core thermophysical properties were modeled in more fidelity, the only change was the magnitude of the reactivity insertion, -\$1 for every core age, otherwise the responses were identical.

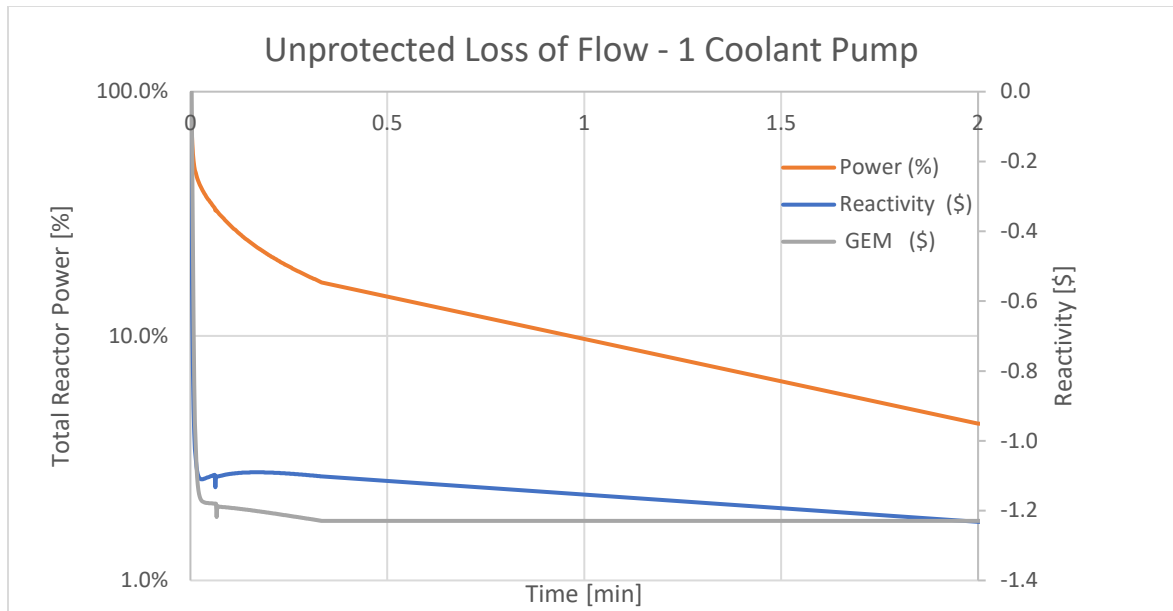


Figure 4-10 Reactivity and power response to a loss of 1 RCP without protective action

For BE4-A, the lower magnitude of α_T acts to make the transient less conservative. The total reactivity became less negative shortly after the event initiation, with a stronger temperature feedback, there would be more positive reactivity added. However, because of the initial large negative reactivity insertion, the temperature

feedback would not affect criticality until the plant had sufficiently cooled down, even with a 56% increase in $|\alpha_T|$, which is the estimated discrepancy.

The second unprotected loss of flow event occurred when a single RCP coastdown mechanism failed during a normal plant trip from full power, BE4-B. This event was evaluated for 10 minutes, the approximate time needed for the remaining RCP's to fully coast down. The fuel temperatures are well below thermal limits, but are elevated due to the reduced flow, Figure 4.11. Once, natural circulation is established, the fuel temperatures will return to normal during a plant trip.

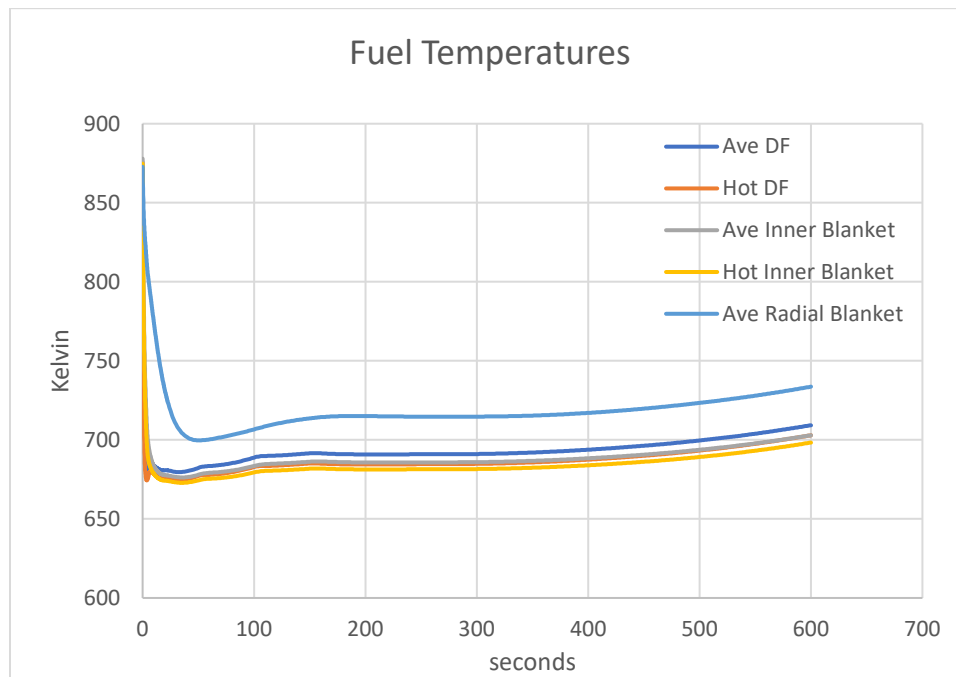


Figure 4-11 Fuel temperatures during a reactor SCRAM with 1 RCP failing to coastdown

6.2.2 LOHS

The only LOHS event considered was a modification to BE3-A of NUREG-1368, consisting of a complete blockage of RVACS for 12 hours with an indefinite loss of power and 1 ACS channel due to sabotage. This was the most temperature limiting of the events considered. Plant temperature peaked at 57 hours into the simulation at 583.7°C.

When comparing with the reported result in NUREG-1368, where temperature peaked at 699 °C 25-hours after the event initiated with RVACS 25% unblocked, the RVACS model used in the present study significantly underestimates the system's RHR at elevated temperatures as RVACS was considered fully unblocked at 12-hours.

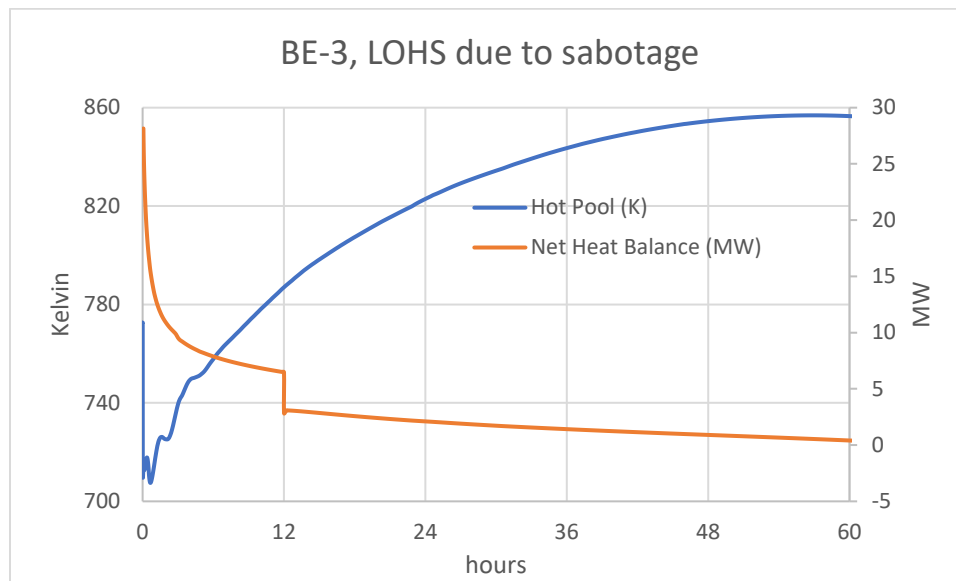


Figure 4-12 Loss of heatsink due to sabotage

6.2.3 ATWOS

The ATWOS was initiated with an indefinite SBO and a failure of control rods to unlatch for 12 hours. Figure 4.12 shows the first 12 hours of the ATWOS compared to the temperature profile of a reactor trip with a loss of both ACS channels. The loss of power to the RCP's caused a -1.4\$ reactivity insertion causing the reactor to immediately shut down. It is expected for the ATWOS to follow the same progression of the nominal reactor trip with a loss of both ACS channels, because the power removed by both functioning ACS channels is initially small in comparison to the magnitude of decay heat. The combined DHR capability of both ACS channels and RVACS, ~5 MW, exceeds decay heat after 59.5 hours. For this reason, BLE-1 under nominal conditions serves as an

upper limit on the peak coolant temperature, with temperature declining after 59.5 hours.

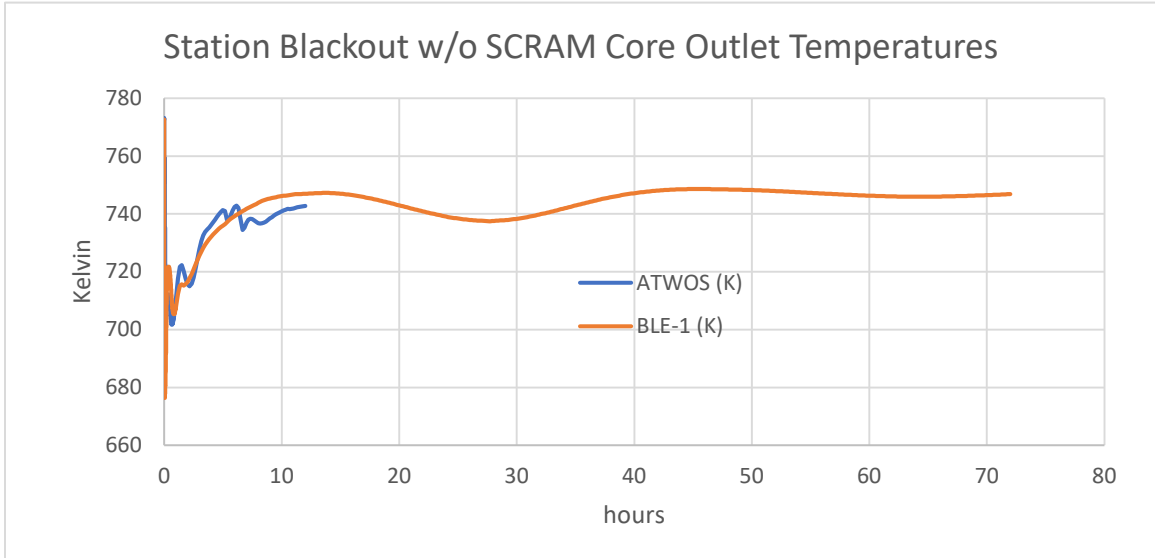


Figure 4-13 Core outlet temperature for ATWOS compared to nominal loss of both ACS channels

The large thermal inertia of the system and multiple paths for passive DHR, allows for a benign transient, especially when compared to the extended SBOs that can occur with LWRs, much less ones where the plant fails to SCRAM for 12-hours.

6.2.4 *UTOP*

Three different UTOP scenarios were evaluated. The first two are based on Bounding Events 1 A and B of NUREG-1368. The third was an over cooling event. BE-1A was previously discussed as BLE-2, during the evaluation of the core's temperature coefficient of reactivity.

BE1-B was simulated by preventing a reactor trip, but allowing a plant trip. Because, the negative period signal was not received the pumps tripped 10 seconds after receiving the N/F trip signal. The event was allowed to continue for 32.4 hours without any operator action. One channel of the ACS was inoperative (failed air damper). The N/F signal occurred 4.303 seconds into the event. The degraded fuel doppler performance

caused a larger power excursion due to reduced feedback. At the time the protection logic received the trip signal, total core power was 111%. When the RCP's tripped 10 seconds later, total reactor power was 172%. The highest fuel temperatures peaked with reactor power and were 1043 K and 1033 K for the driver and blanket assemblies respectively (melting temperatures correspondingly are 1,228 K and 1,300 K). The clad/fuel interface was 969 K, below the fuel clad interdiffusion melting temperature of 978 K for all assemblies and nodes. The Core Outlet temperature peaked approximately 26 seconds after rod withdrawal at 822 K.

Of the thermal limits, the clad fuel interface temperature was the most limiting. To properly assess the margin to Fuel Clad Thermal Interaction (FCTI), the average channel heat transfer coefficient needed to be adjusted to assess the thermal-hydraulic performance of the assembly corner pins. The results of taking into account local thermal-hydraulic performance is shown in Figure 4.13. While the pins do not fully liquify, the hottest corner pin fuel clad eutectic does melt, peak Fuel Clad Interface (FCI) temperature of 1021 K. This can simply be corrected by limiting the power overshoot, accomplished by shortening the delay of the pump trip from the reactor trip to 5 seconds, the FCI 5-sec curve in Figure 4-14. The remaining curves are for the 10 second time delay from a plant trip, since the shorter than a -80 second period trip did not actuate, due to the failure to SCRAM.

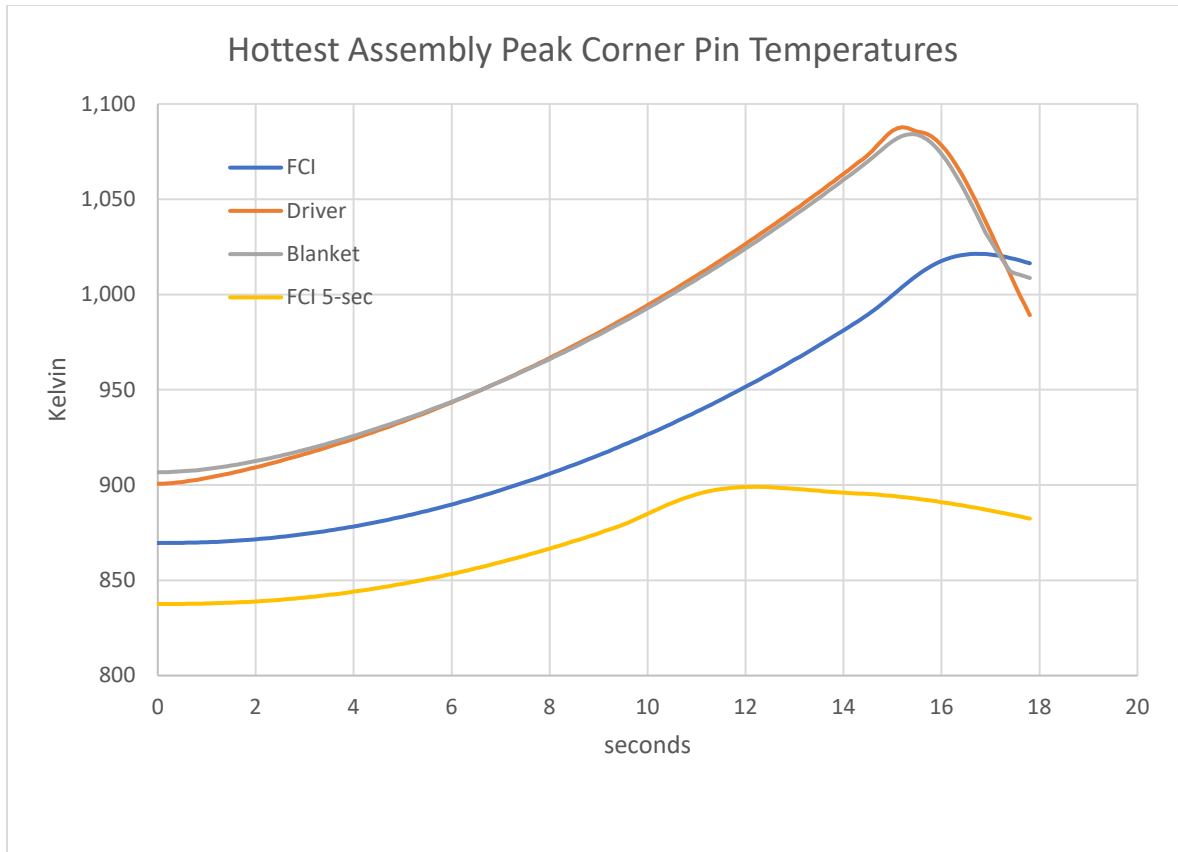


Figure 4-14 Hottest pin adjusted temperatures during protected transient over power

BE-1B was analyzed under 4 different conditions for varying temperature feedbacks and fuel models all with the 5-second pump trip delay. The NUREG scenario used the BOC fuel model with the temperature feedback model from NUREG-1368. It is considered the most accurate of the models due to its comparative correlation with published data in NUREG-1368.

Table 4-21 Core Age/Fuel Model Impact on UTOP

	Rx Trip (s)	Pump Trip (s)	Peak Driver (K)	Peak Blanket (K)	Peak FCI (K)	Peak Power	Time to Peak Power (s)
BOC	4.223	9.223	995.4	969.2	909.4	137.74%	9.6
MOC	4.406	9.406	1033.2	1014.8	912.6	135.23%	9.7
EOC	4.161	9.161	1007.8	1042.7	911.4	139.07%	9.5
NUREG	5.267	10.267	972.7	953.0	900.7	128.24%	10.5

The remainder of this event follows the general core outlet temperatures during a plant trip, with slightly elevated values due to the increased reactor power at the time of trip. This can be seen in Figure 4.14. After 34 hours, the core outlet temperature is approximately at normal operating temperature. This is with one channel of ACS disabled. The long term transient response did not measurably change other than by slight changes in the temperature due to different heat additions due to the magnitude of the initial power overshoot. What is shown in Figure 4-14, is the event that had the largest power overshoot for each of the different reactivity feedbacks and fuel configurations.

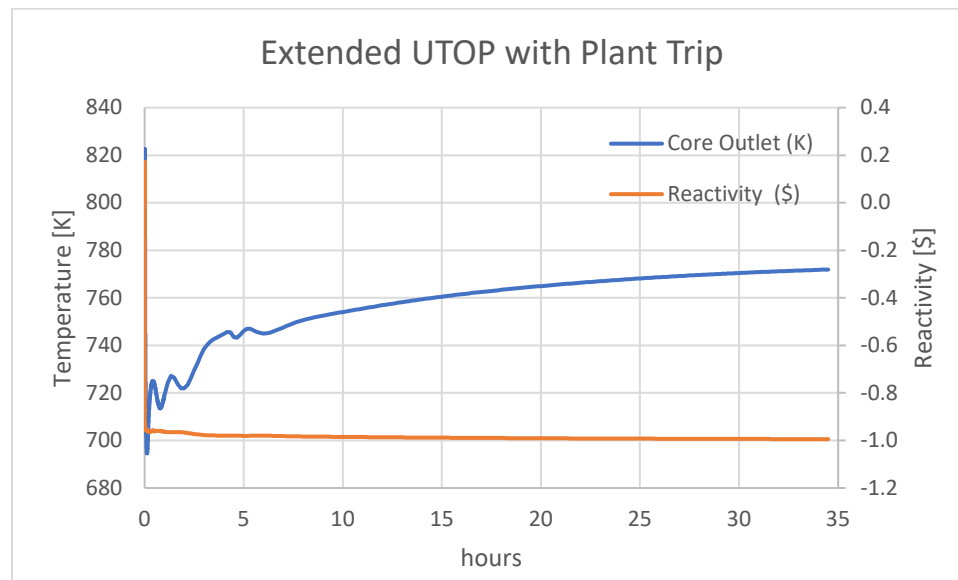


Figure 4-15 Extended UTOP with plant trip

The final unprotected transient over power event is the loss of control of the non-safety-grade Salt Coolant Pump. To simulate this event the plant was not allowed to trip, while the SCP speed increased from 100% flow to 200% flow in 8 seconds. shows the resulting transient. The increased cooling initially increased reactivity, but the extent of the cooling lowered the reactor vessel pressure which caused a negative reactivity insertion, which eventually overcame the temperature feedback. This was not the

anticipated response. What was expected was for the temperature coefficient of reactivity to dominate and cause the reactor to increase power, similar to what occurred in Part 3. The temperature reactivity having a lower magnitude than the actual plant, plus the deadband of the GEM were contributing to this event. To be able to more accurately model this phenomenon, these two items need more careful consideration.

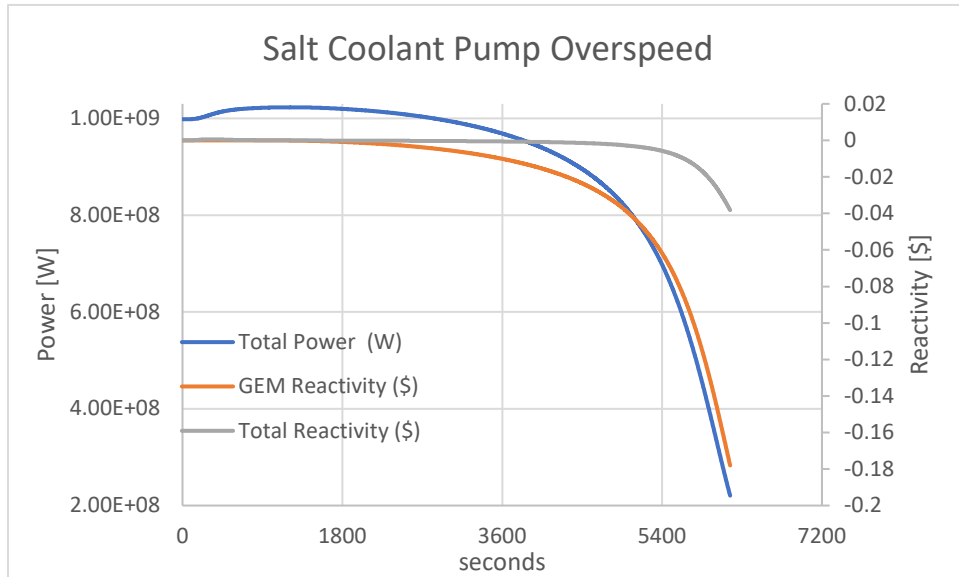


Figure 4-16 Salt Coolant Pump overspeed transient response using [90] BOC temperature feedbacks.

When the temperature feedbacks were taken from NUREG-1368, the general response was the same, but the power peaked more with the NUREG kinetics data, and did not fall off as quickly, Figure 4-16. This suggests that the GEM introduce non-linearities in the system's thermal response and that they need to be explicitly modeled in the integrated control system design. The contributing factor is the change in PHTS pressure due to the contraction of the larger cold pool relative to the smaller hot pool's expansion.

When analyzed at different time in core age the power would fall off similarly, those core ages that had lower magnitude temperature feedbacks, would fall off more

rapidly and have a lower positive power excursion. For this reason, failure in the salt pumps or their control logic are not expected to negatively impact reactor safety. Thus, keeping the salt pumps out of the safety envelope is justified. This will need to be confirmed with more detailed kinetic and GEM modeling.

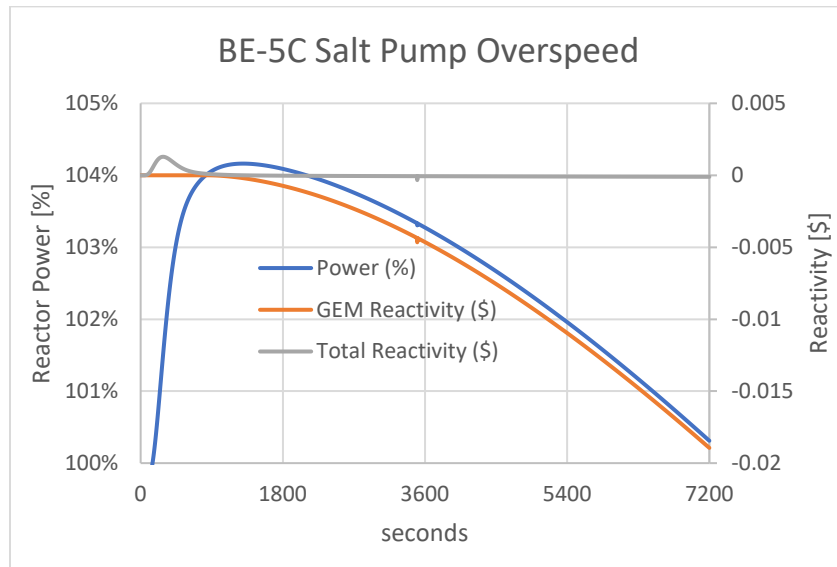


Figure 4-17 BE-5C Salt pump overspeed using NUREG-1368 temperature feedbacks

6.2.5 SBO

There were two scenarios considered for the SBO. The first, ATWOS, was discussed in section 6.2.4. The second is the unfaulted SBO. This corresponds with BE-2A. Here the problem was run until peak temperatures were reached or for 72-hours. The

hot pool temperature peaked at 42.25 hours at 481.3 °C. Figure 4-16 shows the hot pool temperature during the transient.

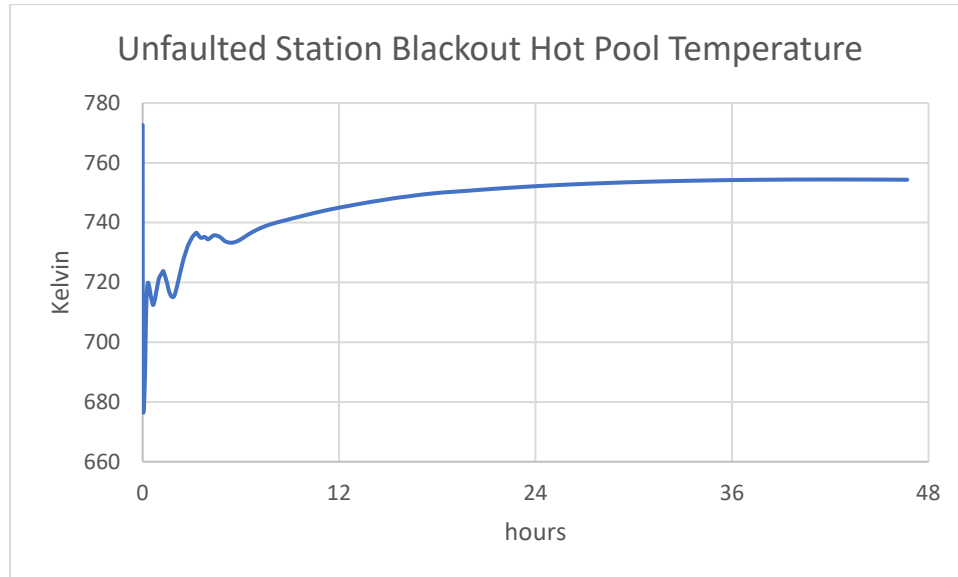


Figure 4-18 Unfaulted SBO transient Response

6.2.6 SHX Rupture

A SHX plate rupture and instantaneous catastrophic loss was simulated. In this event the reactor was tripped 20 seconds after initiation, no forced cooling was provided, the other ACS system and RVACS both performed nominally. This event was to simulate Bounding Event 5 of NUREG-1368. The simulation lasted for 12-hours of model time. The resulting core outlet transient is similar to the design basis accident and can be seen in Figure 4-17. After 12-hours, forced cooling to the operable AHX is assumed, terminating the event, well below normal operating temperatures.

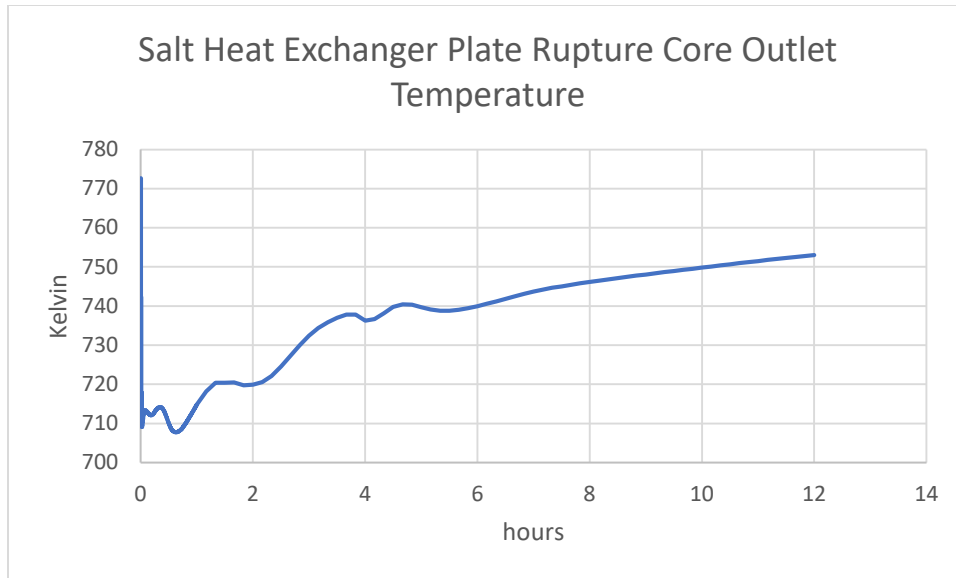


Figure 4-19 Core outlet temperature during a rupture of a single SHX heat exchanger

6.2.7 DBA

The design basis accident was a 36-hour SBO with failure of one ACS. The plant response closely mirrored that of BE-5A, SHX plate rupture, but with slightly lower temperatures due to the control rods inserting immediately during the SBO. Figure 4-17 shows the hot pool's temperature response.

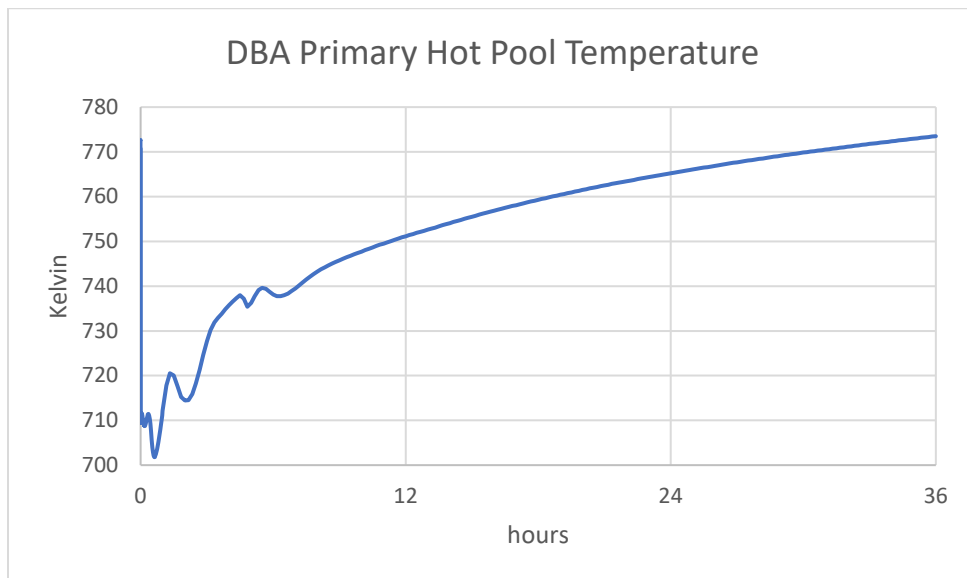


Figure 4-20 DBA Hot pool temperature response

CHAPTER 7 CONCLUSIONS

The addition of the SHTS to the S-PRISM, does not degrade safety related performance. In each of the considered bounding events, the modified system exceeded nominal plant performance for all published data. PRISM has a large thermal inertia limiting the overall plant heat up while the decay heat generation exceeds removal. This is further assisted by very little energy being stored in the fuel due to the fuels high thermal conductivity. Essentially, as reactor power is removed, so too is the heat. With oxide fuels, a significant amount of energy is stored in the fuel, leading to higher temperatures with degraded heat flow.

The addition of the SHTS increases the thermal inertia of the system and provides another redundant safety-grade path for DHR. In cases where both safety-grade ACS systems are available, complete DHR with no forced circulation is assured at normal operating temperatures 45-hours after a trip from full power. The use of fans in the ACS allows operators to remove as much decay heat as necessary under normal situations when fans and electrical power are available.

The extended duration of inaccessibility of forced cooling in many of the events considered, show that for this design forced cooling is a nicety, not a necessity to prevent exceeding normal operational temperatures, much less structural or fuel thermal limits. In all events considered, hot pool temperature did not exceed 600 °C.

The model presented here is limited in that is based entirely on engineering estimations of an actual design, not the actual design. Any further investigation or authoritative conclusions can only be gained by using actual engineering data. What this

model does show is the potential that it has for increasing the operational capability of pool-type reactors with the inclusion of thermal energy storage.

PART 5 – TECHNOLOGICAL IMPLICATIONS

CHAPTER 1 INTRODUCTION

The energy server concept allows for an entirely different business model for a utility. Part 4 showed how the safety of the reactor is not dependent upon the balance of plant and that the most severe accidents that can be induced by the balance of plant are entirely benign for the reactor. The possibilities that this creates are manifold.

The most obvious of the possibilities is the ability for nuclear technology to access every current electrical market from capacity to regulation mileage. Some not as intuitive market opportunities include synthetic fuels and other process heat applications.

While not as hot as needed for many synthetic fuel processes, the salt outlet temperature is close to that needed for hydromethanation of coal.[110] Higher temperature processes, e.g. conventional fixed bed Lurgi gasification, can be accessed by the addition of a high temperature heat pump.[111] It becomes entirely possible for the utility to be able to produce the fuel for its combustion turbines on site. But the molecular carbon monoxide and hydrogen, which are the products of gasification are the fundamental building blocks of the modern economy.

The site can produce any organic chemical, from liquid fuels to plastics. The heat from the reactors can even be used to aid in oil refining. Using inexpensive nuclear heat to provide the energy needed to drive the chemical reactions for these processes, instead of the expensive feedstock hydrocarbons. Applied to such technologies as Steam Assisted Gravity Drain, the salt can be used to transport heat significant distances allowing local generation of steam for oil recovery. In the SAGD model, there energy storage tanks are the multi-kilometers of piping. The piping, even though it is stainless steel, can be a

lower grade such as 316, and of much thinner walls because of the lack of pressure.

Combined with the high heat of the reactor, recovered bitumen can be upgraded to a more transportable form onsite, before being pumped to another location for final processing.

If the ultimate process is to close the material loop of the industrial economy, having an inexpensive enough fuel source is the only means to accomplish this, as recycling is fundamentally an energy intensive process. Garbage gasification, either with plasma gasifiers or with steam reformation can provide such an avenue forward.[112]

CHAPTER 2 UTILITY SIMULATION

To determine the technical efficacy of the nTES in electrical applications, the reference model, Figure 2.1, was applied to a multi-year study period of the Bonneville Power Administration. Two scenarios were considered, a conventional plant with no renewable resources and one with an increasing renewable energy fraction. The modeling technique was simply of maximizing the reactor output for a given energy demand. It included no forecasting or model predictive control. Model Predictive Control using forecasted information would result in a more optimized sizing ratio of reactors, to storage to PCS, to combustion turbines, 1.68 GW(t) nuclear: 1.80 GW(t)-hr storage: 914 MW(e) PCS: 253.2 MW(e) combustion turbines. Figure 5.1 shows the power profile of the

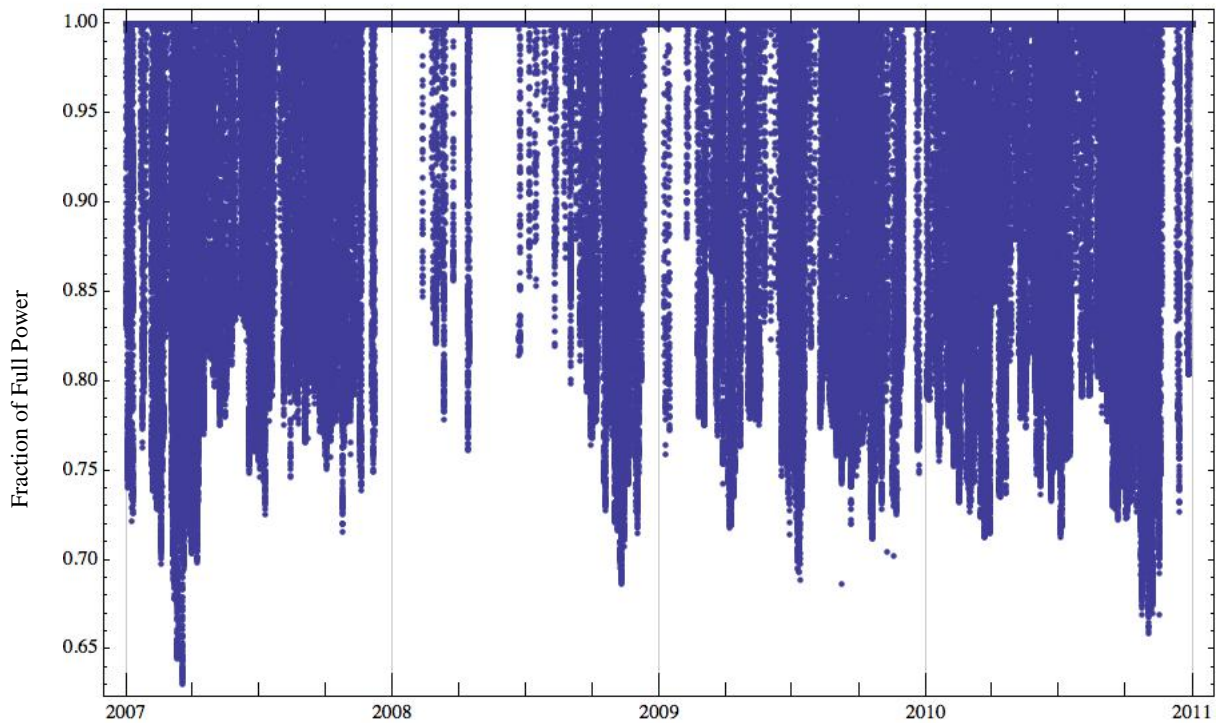


Figure 5-1 nTES integrated with Bonneville Power Administration

reactors integrated as described. The reactors including 1 month refueling outages on an 18-month schedule, had an average capacity factor of 92.3%. This allows for conventional economic recovery of the reactor supplying heat to the storage.

With an increase in the amount of renewable energy on the grid, the capacity factor of the nuclear plant went down. The best explanation for this trend is that the increased variability of renewable energy created a cost externality that was absorbed by the nuclear reactors. The amount of this cost was the value of the reduced revenue from the sale of heat from the reactor. If increased reactor utilization was desired the size of the storage and the PCS had to increase, and their utilization went down.

CHAPTER 3 NON-CONVENTIONAL APPLICATIONS

Nuclear energy has long been considered for applications associated with chemical processes.[113, 114] These have not materialized. The likely cause is having to prove to the regulator that the process doesn't negatively impact reactor operations. By using storage to buffer the various processes from the reactor, the proof to the regulator is that the buffering salt system won't negatively impact the reactor, which was done in Part 4 of the present work.

One of the interesting possibilities that isn't usually considered in nuclear licensing is the impact of chemical and process explosions. While missile hazards from the rotating equipment in a traditional turbine building are considered, chemical processes are not. The NRC under the current regulatory framework will consider non-conventional uses and issue guidance to applicants "in a time frame consistent with the licensing schedule".[115]

The process heat applications are significant users of energy. Using the 2006 Manufacturing Energy Consumption Survey from 2006 and a survey of the different processes used by each industry a rough distribution of energy and temperature are provided in Figure 5.2. As can be seen the bulk of process heat applications are below 1000 °C. These consist predominantly of iron refining applications. The uses around 500°C are for petroleum refining and nitrogen fixation for fertilizer production.

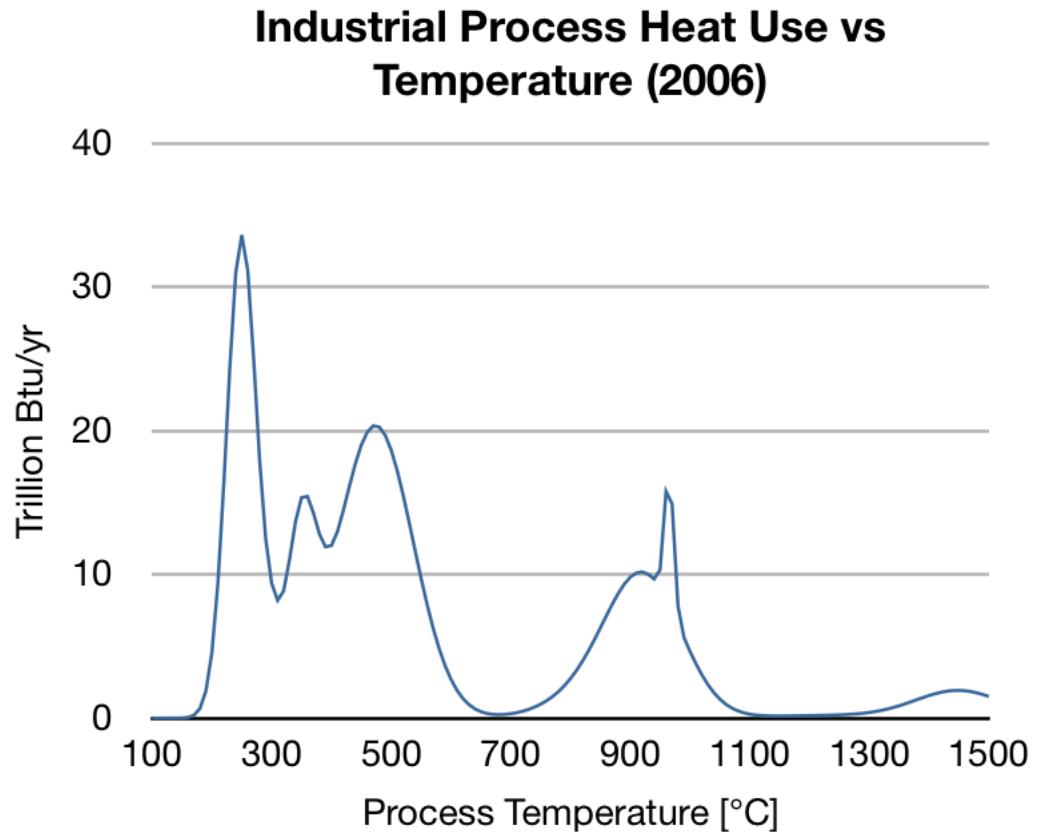


Figure 5-2 Estimated process heat distribution from MECS 2006

Being close to these temperatures the PRISM, can be an effective fit, especially if a heat pump is considered to amplify the temperature to the needed process, about 830°C is achievable with existing materials and technologies. This allows direct gasification of coal which can be used in the direct reduction of iron.[116] Further integration can be achieved with processes such as FINEX[®] or a modification of it to use the excess syngas from the reduction process to smelt the iron ore. By using the heat from the reactor to produce the syngas, more of the coal is used for reducing the iron.

The production of hydrogen ranges from 500 to 800. Steam Methane Reforming is a common method for hydrogen production and typically occurs between 700-1,000°C.[117] Raising the steam to 470°C and then using oxygen to combust some of the

methane to achieve the remaining heat for the reaction will limit reagent loss and maximize hydrogen production, or a heat pump can be used to make up the remaining needed temperature.[116]

CHAPTER 4 POLICY LIMITATIONS

Even with the technological development of the current work, it remains to be seen if the NRC will allow flexibility with collocating additional technologies. Because the process can now be located “off-site”, adjacent to the nuclear facility, the external events considered in the Bounding Events needs to include such risks. Jurisdictions that allow greater flexibility in plant siting and collocation will see more development of process heat applications. The process heat facilities are on par with the nuclear facility regarding capital costs, thus regulatory risks will be much higher.

4.1 Non-Light Water Reactor Licensing

While the NRC has never licensed a non-light water reactor, Clinch River Breeder Reactor was the closest, they have the regulatory ability to be able to do so.[118] There is no standardized guidance on how to license a reactor, such as the General Design Criteria. NUREG-1368 proposed how to go about modifying those GDC to provide more general design guidance to simplify the licensing process. The revised standardized licensing has not been issued, but is actively being developed. Similarly, the American Nuclear Society is in the process of updating its fast reactor standards, which are used by the NRC in determining regulations.

4.2 Price Anderson and Liability

Smaller reactors, but still above 100MW(e) are required to carry the maximum insurance available under the Price-Anderson Act. This has been identified by many SMR developers as an impediment to the future licensing of smaller reactors as the insurance premiums are based on much larger reactors and adversely affect the

economics of the smaller reactors.[119]There does not exist a solution to this problem and will require further regulatory consideration and potentially a revision to the statutes.[119]

CHAPTER 5 RECOMMENDATIONS/CONCLUSIONS

While the technology developed in the present work creates new possibilities for the application of nuclear energy. It is not without limitations. These limitations are regulatory and statutory. Many of these limitations are due to nobody ever trying them and the regulators developing regulations only for what they have regulated not what they potentially might.

What occurs then is a chicken and egg problem. If the regulator hasn't regulated something in the past and how they would rule on it is unknown and costs money to obtain a ruling that may not be favorable, tends to make overcoming such natural regulatory barriers to innovation very difficult, unless one has deep pockets and the wherewithal to risk losing money on a less than favorable regulatory decision, very little will change. In many ways, regulators maintain the world in which they were created, stifling innovation and protecting the status quo.[120]

The simplest approach to solve this problem is to do the technological deployment in a country that does not have the same regulatory burden. If that is not an option due to technology export restrictions under the Atomic Energy Act of 1954, then it is to put the least amount of money at risk to move forward, and to spread the risk to a more manageable amount.

After the cessation of the V.C. Summer expansion project, utilities are going to be weary of building a new technology, unless it is something that meets a need that they don't currently have fulfilled or creates new market opportunities. Thermal storage and PRISM presents such an opportunity for utilities across the country. It also opens the

potential to have direct “off site” customers of the heat produced and stored by the reactor. It enables these customers to build their own sub-grid using the salt to provide all of their energy services.

While untested in the real world, the paper design created in this current work, represents a potential to fulfill many of the needs of utilities in the United States. True progress on the policy front will not occur unless there is a broad enough support for the deployment of the technology. But there is hope and tomorrow is another day.

APPENDIX A: INSTRUCTIONS FOR RELAP5-3D

Because of the size of the input files to be able to run the various scenarios, they are included electronically with the dissertation and are available for download from the Georgia Institute of Technology. Because of the complexity of the system studied and especially because of the problems that RELAP has with non-condensable gases and the small volumes used in the counter-flow heat exchangers, the inputs had to be carefully constructed to be able to run.

There are a number of restart decks that are not included. These input decks were used to tweak parameters to achieve the proper steady state conditions or used in situ to restart cases that had aborted due to failure. Their inclusion would only complicate the explanation of how to generally run this model.

As a note to users, the models included here were developed using APT Model Editor for RELAP5-3D v 4.3.4. They will have errors in the loop check of the IHTS loops if run under a different version. I am not sure why this is, but if you are using any version other than 4.3.4 plan on needing to fix the loop elevations. On the same note, none of the included models will pass the preliminary loop check of Model Editor.

A.1 Reference Design Initialization

The initial input deck concurrently starts up the steam generator and reactor. It does this using a programmed reactor power with a linear ramp, programmed PHTS and IHTS pump speed linear ramps, and a PI controller for the feedwater flow control. Additionally, the kinetics data and fuel thermophysical properties do not match that of the

nTES. If a direct comparison is needed, the data in the reference design needs to be adjusted to that of the nTES design.

To create a steady state restart file:

1. Run “Reference S-PRISM Initialization.i”
2. Using the restart file from 1, run “Reference S-PRISM Optimization.i”
3. Using the restart file from 2, run “Reference S-PRISM Kinetics.i”

The resulting restart file from step 3 can be used to establish 100% power history needed for the accident analysis. This can also be used to provide an initial condition to evaluate operational transients.

A.2 nTES Design Initialization

The initialization of the nTES S-PRISM design is similar, except that the “Optimization.i” is replaced with a file that adjusts the fuel properties based on core age. This is then allowed to come to equilibrium and the next restart file implements the kinetics. Because of the complexity of the problem and the time needed to run the initialization, there may be some things that are implemented in the subsequent restarts that should be in the initialization file. To the maximum extent possible, if there was a change needed, I would update the initialization file so that the change would propagate all the way through, and then remove the short term patch from the later restart file. But because it takes 18-hours to run the initialization, there may be some redundancy/overlap/not fully implemented changes.

There are four different fuel scenarios: BOC, MOC, EOC, and NUREG. The BOC represents fresh fuel and beginning of cycle conditions. MOC represents the middle of cycle, and uses fuel that has swelled completely and is logged with sodium inside its

pores. EOC is the same as MOC but with end of cycle kinetics. NUREG is fresh fuel (100% theoretical density) but uses the kinetic data taken from NUREG-1368.

To create a steady-state restart file with kinetics, do the following:

1. Run “nTES S-PRISM Initialization.i”
2. Using the restart file from 1, run “nTES S-PRISM Mod IC ____i”
3. Using the restart file from 2, run “nTES S-PRISM Kinetics ____i”

For the NUREG kinetics use the BOC Mod IC input deck in step 2.

A.3 Testing and Initialization

To test the various features of the nTES S-PRISM, each of the subsystems, e.g. IHTS, PHTS, RVACS, ACS, SHTS, were modeled as independent and standalone systems. One of the difficulties in starting a problem is to have the appropriate pressures, temperatures and flow rates. To simplify this, each initialization problem began with the reactor in a quiescent shutdown state at 613.0 K. This approach left only pressures needing to be determined for the appropriate elevation. This was especially important for the counterflow heat exchangers that had a very fine nodalization scheme. To assist in accurately determining these pressures, these subsystem testing files were created to establish the necessary quiescent state, by allowing a smaller system to come quickly into long-term equilibrium.

The ACS system was set to run in two modes. The first mode was with flow secured to the UHS (air dampers CLOSED) and the PHTS IHX wall heat flux set to zero. To simulate natural circulation operations, the air damper was opened and the IHX primary side wall temperature set to the desired temperature.

A.4 Bounding Events

The bounding baseline events were broken up into two main categories. First were those that relied upon an unfaulted reactor trip as the event initiator and those that did not. To run the bounding events, the restart file from the appropriate initial condition (reactor tripped or the reactor at full power) was used with the event's input deck. For those cases that the initial condition was not the full power condition, the event also needed the previous file's plot file, so that a contiguous plot file output could be made for the entire event duration.

For events that are numbered the run order goes 1, 2, 3 and then the file with just the event name. In a few cases there may be a "C" file, this is the continuation file for that bounding event and was usually needed because the final event run terminated prematurely or had some additional needed tweak to get the problem to properly run.

REFERENCES

1. Sider, B.O.a.A. *Wall Street Cash Pumps Up Oil Production Even as Prices Sag*. 2017 July 7, 2017 Available from: <https://www.wsj.com/articles/wall-street-cash-pumps-up-oil-production-even-as-prices-sag-1499419801?tesla=y&mod=e2fb>.
2. DOE, *Staff Report to the Secretary on Electricity Markets and Reliability*, U.S.D.o. Energy, Editor. 2017. p. 187.
3. Polson, J. *Why Nuclear Power, Once Cash Cow, Now Has Tin Cup*. 2017 [cited 2017 July 14, 2017]; Available from: <https://www.bloomberg.com/news/articles/2017-07-14/why-nuclear-power-once-cash-cow-now-has-tin-cup-quicktake-q-a>.
4. NRC, *State-of-the-Art Reactor Consequence Analysis (SOARCA) Report*, in *NUREG 1935*. 2012, Office of Nuclear Regulatory Research: Washington DC.
5. Warr, R.U.A.a.B., *The Economic Growth Engine: How Energy and Work Drive Material Prosperity*. 2009, Northhampton, MA: International Institute for Applied Systems Analysis.
6. EIA, *Electric Power Monthly*. 2018.
7. *Electric Power Monthly*. 2013 23 September 2013]; Available from: http://www.eia.gov/electricity/monthly/epm_table_grapher.cfm?t=epmt_5_6_a.
8. Jenkins, J.D., *What's Killing Nuclear Power in US Electricity Markets?: Drivers of Wholesale Price Declines at Nuclear Generators in the PJM Interconnection*. MIT Center for Energy and Environmental Policy Research, 2018.
9. Sotkiewicz, P.M. *Market Report*. 2016 July 25, 2016]; Available from: <http://www.pjm.com/-/media/committees-groups/committees/mc/20160725-webinar/20160725-item-07a-markets-report.ashx>.
10. Agency, N.E., *Technical and Economic Aspects of Load Following with Nuclear Power Plants*. 2011.
11. Adams, R. *Texas Nuke Plant Stays Online Amid Harvey. Give Credit To Resilient Operators, Robust Design And A Plan*. 2017 August 30, 2017]; Available from: <https://www.forbes.com/sites/rodadams/2017/08/30/nuke-plant-could-close-but-didnt-give-credit-to-resilient-operators-robust-design-and-a-plan/#538e76696f87>.
12. Pablo Antolin, S.S.a.J.Y., *The Economic Impact of Protracted Low Interest Rates on Pension Funds and Insurance Companies*. OECD Journal: Financial Market Trends, 2011. **2001**(1).
13. Gopinath, C.N.a.S. *U.S. shale firms more exposed to falling oil prices as hedges expire*. 2017 June 13, 2017 June 13, 2017]; Available from: <https://www.reuters.com/article/us-usa-oil-hedges/u-s-shale-firms-more-exposed-to-falling-oil-prices-as-hedges-expire-idUSKBN1940IL>.
14. EIA, *Natural Gas Prices*.
15. Paul Denholm, J.C.K., Charles F.Kutcher, Paul P.H.Wilson, *Decarbonizing the electric sector: Combining renewable and nuclear energy using thermal storage*. Energy Policy, 2012. **44**: p. 301-311.
16. NYISO, *POWER TRENDS 2016 the changing energy landscape*, ed. N.Y.I.S. Operator. 2016: NYISO.

17. Jessica R. Lovering, A.Y., Ted Nordhaus, *Historical construction costs of global nuclear power reactors*. Elsevier, 2016(91): p. 12.
18. Baldwin, E.J.C.a.L.A., *Toxicology rethinks its central belief*. Nature, 2003. **421**(6924): p. 691-692.
19. S. T. Cantril, H.M.P., *The Tolerance Dose*, A.N. Laboratory, Editor. 1945, United States Atomic Energy Commission.
20. T. C. Carter, M.F.L., Rita J. S. Phillips, *Genetic Hazard of Ionizing Radiations*. Nature, 1958. **182**(409).
21. Calabrese, E.J., *Muller's Nobel lecture on dose–response for ionizing radiation: ideology or science?* Archives of Toxicology, 2011. **81**(4): p. 1495-1498.
22. Calabrese, E.J., *Muller's Nobel Prize Lecture: When Ideology Prevailed Over Science*. Toxicological Sciences 2011
23. Rockwell, T., *The Realism Project Reconciling Nuclear Power and Radiation Policies With The Real World*. 2006.
24. Smith, A. *Fukushima evacuation has killed more than earthquake and tsunami, survey says*. 2013 [cited 2013 September 10, 2013]; Available from: <https://www.nbcnews.com/news/other/fukushima-evacuation-has-killed-more-earthquake-tsunami-survey-says-f8C11120007>.
25. Times, J. *After weathering nature's worst, Fukushima nuclear evacuees ostracized by society*. 2017 March 18, 2017 March 17, 2017]; Available from: <https://www.japantimes.co.jp/news/2017/03/17/national/social-issues/weathering-natures-worst-fukushima-nuclear-evacuees-ostracized-society/#.WayDyYokq8U>.
26. Nations, U., *Report of the United Nations Scientific Committee on the Effects of Atomic Radiation*, U. Nations, Editor. 2012, United Nations. p. 21.
27. Pradhan, D.A.S. *On the risk to low doses (<100 mSv) of ionizing radiation during medical imaging procedures - IOMP policy statement*. 2013 [cited 2013; Available from: <https://www.ncbi.nlm.nih.gov/pmc/articles/PMC3683301/>.
28. Adams, R. *Root cause of Vogtle and VC Summer delays*. 2014 [cited 2014 November 12, 2014]; Available from: <http://ansnuclearcafe.org/2014/11/12/root-cause-of-vogtle-and-vc-summer-delays/#sthash.s6Og0cTa.fLaBDHkD.dpbs>.
29. Platts. *Delays in pouring concrete for new US nuclear units ending: Westinghouse, SCE&G*. 2013 14 Feb 2013]; Available from: <https://www.platts.com/latest-news/electric-power/washington/delays-in-pouring-concrete-for-new-us-nuclear-6157988>.
30. Dickson, J.A.A.a.H.W., *What is ALARA?*, in *Edison Electric Institute's Health Physics Committee Meeting*. 1981, U.S. Government: Hartford, Connecticut.
31. Chen, W.L., et al., *Effects of Cobalt-60 Exposure on Health of Taiwan Residents Suggest New Approach Needed in Radiation Protection*. Dose Response, 2007. **5**(1): p. 63-75.
32. Matanoski, G.M., *Health effects of low-level radiation in shipyard workers*. 1991, Johns Hopkins Univ., Baltimore, MD (United States). Dept. of Epidemiology.
33. Sponsler, R. and J.R. Cameron, *Nuclear shipyard worker study (1980–1988): a large cohort exposed to low-dose-rate gamma radiation*. International Journal of Low Radiation, 2005. **1**(4): p. 463-478.
34. Roser, M. *Life Expectancy*. Our World in Data 2016 [cited 2018; Available from: <https://ourworldindata.org/life-expectancy>.

35. Hayek, F.A., *The Use of Knowledge in Society*. JSTOR, 1945. **35**(4): p. 13.
36. Loewen, E.P., *Is ALARA reform needed?* ANS, 2011: p. 14.
37. NRC, U.S. *Post 9/11 Information*. August 11, 2017; Available from: <https://www.nrc.gov/security/post-911.html>.
38. NEI, *Nuclear Costs in Context*. 2017, Nuclear Energy Institute.
39. INPO, *Special Report on the Nuclear Accident at the Fukushima Daiichi Nuclear Power Station*. 2011, Institute of Nuclear Power Operations.
40. Rudy J. M. Konings, T.W.O.B. *Predicting material release during a nuclear reactor accident*. 2015 [20 February 2015]; Available from: <http://www.nature.com/nmat/journal/v14/n3/full/nmat4224.html?foxtrotcallback=true>.
41. EPRI, *The Path to Zero Defects: EPRI Fuel Reliability Guidelines*. 2008.
42. Agency, N.E., *Leaking Fuel Impacts and Practices*. 2014. **NEA/CSNI/R(2014)10**.
43. Lewis, P., *France Set to Build Reactors*. New York Times, 1981.
44. NRC, *10 CFR Part 52: Licenses, Certifications, and Approvals for Nuclear Power Plants*, NRC, Editor. 2017, Office of the Federal Register p. 85.
45. Davis, W., *Incompetence at every level*, C. Abel, Editor. 2017.
46. A, D. *The Wind Is Fickle*. 2012 [cited 2012 June 2012]; Haiku]. Available from: <https://helloworldpoetry.com/poem/210147/the-wind-is-fickle-haiku/>.
47. EIA, *Annual Energy Outlook 2013*, E.I. Agency, Editor. 2013.
48. Brian S. Triplett, E.P.L., and Brett J. Dooies *PRISM: A Competitive Small Modular Sodium-Cooled Reactor*. Nuclear Technology, 2010. **178**(2): p. 186-200.
49. Sackett, J., *Operating and test experience with EBR-II, the IFR prototype*. Progress in nuclear energy, 1997. **31**(1): p. 111-129.
50. Yandle, A.S.a.B., *Bootleggers and Baptists*. 2014: CATO Institute.
51. Walsh, B. *Exclusive: How the Sierra Club Took Millions From the Natural Gas Industry—and Why They Stopped [UPDATE]*. 2012 [cited 2012 Feb. 02, 2012]; Available from: <http://science.time.com/2012/02/02/exclusive-how-the-sierra-club-took-millions-from-the-natural-gas-industry-and-why-they-stopped>.
52. Stone, R., *Pandora's Promise*. 2013.
53. Don Boudreaux, M.M., and Russ Roberts. *EconTalk Episode with Don Boudreaux, Michael Munger, and Russ Roberts* 2017 [cited 2017 JUNE 12, 2017]; Available from: http://www.econtalk.org/archives/2017/06/don_boudreaux_m.html.
54. Warner, E.S. and G.A. Heath, *Life Cycle Greenhouse Gas Emissions of Nuclear Electricity Generation: Systematic Review and Harmonization*. Journal of Industrial Ecology, 2012. **16**(S1): p. S73-S92.
55. Council, N.R., *Hidden Costs of Energy: Unpriced Consequences of Energy Production and Use*, N.R. Council, Editor. 2007, National Academies Press: Washington DC. p. 373.
56. EPA, *Standards of Performance for Greenhouse Gas Emissions from New Stationary Sources: Electric Utility Generating Units*, in *40 CFR Part 60*. 2013, Environmental Protection Agency: United States.
57. CBO, *Nuclear Power's Role in Generating Electricity*, C.B. Office, Editor. 2008.

58. Mills, A.D., *The Cost of Transmission for Wind Energy: A Review of Transmission Planning Studies*. 2009.
59. EIA. *About U.S. Natural Gas Pipelines - Transporting Natural Gas* Natural Gas 2013 20 September 2013]; Available from: http://www.eia.gov/pub/oil_gas/natural_gas/analysis_publications/ngpipeline/develop.html.
60. EIA. *Factors Affecting Natural Gas Prices*. Natural Gas 2013 20 September 2013]; Available from: http://www.eia.gov/energyexplained/index.cfm?page=natural_gas_factors_affecting_prices.
61. NRC, *Preapplication Safety Evaluation Report for the Power Reactor Innovative Small Module (PRISM) Liquid-Metal Reactor*. 1994, U.S. Nuclear Regulatory Commission.
62. Engel, M.D.S.a.J.R., *Survey of Technology for Storage of Thermal Energy in Heat Transfer Salt*. 1977, Oak Ridge National Laboratory: Oak Ridge, TN. p. 32.
63. Forsberg, C.W. *Gigawatt-Year Geothermal Energy Storage Coupled to Nuclear Reactor an Large Concentrated Solar Thermal Systems*. in *Thirty-Seventh Workshop on Geothermal Reservoir Engineering*. 2012. Stanford, California.
64. Michael Green, P.S., Michael George Mckellar, Su-Jong Yoon, Cal Abel and Bojan Petrovic, *Nuclear Hybrid Energy System: Molten Salt Energy Storage*. 2013, Idaho National Laboratory. p. 51.
65. Kearney, D., et al., *Assessment of a Molten Salt Heat Transfer Fluid in a Parabolic Trough Solar Field*. *Journal of Solar Energy Engineering*, 2003. **125**(2): p. 170-177.
66. SENER, *Andasol 1 & 2 50 MW, 7 hrs molten salt heat storage*, in *NREL Trough Technology Workshop*. 2007: Dencer, CO.
67. Moore, R., et al., *Design considerations for concentrating solar power tower systems employing molten salt*. Sandia Report SAND2010-6978. Available to the public from US Department of Commerce National Technical Information Service, 2010. **5285**: p. 51.
68. Jacob Edwards, H.B.a.P.S., *Exergy analysis of thermal energy storage options with nuclear power plants*. Elsevier, 2016.
69. Dubberley, A.E., et al. *S-PRISM Fuel Cycle Study For Session 3: Future Deployment Programs and Issues*. in *ICAAP*. 2003. Córdoba Spain.
70. WNA. *Uranium Markets*. 2017 July 2017; Available from: <http://www.world-nuclear.org/information-library/nuclear-fuel-cycle/uranium-resources/uranium-markets.aspx>.
71. Greider, W. *Uranium Cartel Stirs Questions Of Energy Policy*. 1977 [cited 1977 May 8, 1977]; Available from: https://www.washingtonpost.com/archive/politics/1977/05/08/uranium-cartel-stirs-questions-of-energy-policy/c22c6a3d-6b43-457b-93fd-1a26a09792f0/?utm_term=.4e53c5e1b65d.
72. IEA, *World Energy Investment Executive Summary*. 2017, International Energy Agency.
73. Forum, D.N.E.R.A.C.a.t.G.I.I., *A Technology Roadmap for Generation IV Nuclear Energy Systems*. 2002, U.S. DOE. p. 97.

74. Heatric. *Typical diffusion-bonded heat exchanger characteristics*. http://www.heatric.com/typical_characteristics.html 2012 May 31, 2012].
75. ASM, *Nickel, Cobalt, and Their Alloys*. ASM Specialty Handbook, ed. J.R. Davis. 2000, Materials Park OH: ASM International. 425.
76. Walters, L., et al., *Sodium Fast Reactor Fuels and Materials: Research Needs*, in *Sodium Fast Reactor Safety and Licensing Research Plan–Volume II*. 2010, Sandia national Laboratories: Albuquerque, New Mexico. p. 119.
77. Furukawa, T., S. Kato, and E. Yoshida, *Compatibility of FBR materials with sodium*. *Journal of Nuclear Materials*, 2009. **392**(2): p. 249-254.
78. Natesan, K., et al., *Sodium effects on mechanical performance and consideration in high temperature structural design for advanced reactors*. *Journal of Nuclear Materials*, 2009. **392**(2): p. 243-248.
79. Henry, J.F., *Growing experience with P91/T91 forcing essential code changes*. *Combined Cycle Journal*, 2005. **2005**(1Q): p. 8-17.
80. Riyas, A. and P. Mohanakrishnan, *Studies on physics parameters of metal (U–Pu–Zr) fuelled FBR cores*. *Annals of Nuclear Energy*, 2008. **35**(1): p. 87-92.
81. Konovalenko, F.D. and S.I. Kondrashov, *Experimental analysis of liquid-metal reactor scram rod kinematic characteristics*. *Journal of Physics*, 2017.
82. Dewson, D.S.a.S.J. *Innovative Compact Heat Exchangers in International Congress on Advances in Nuclear Power Plants*. 2010. San Diego, CA.
83. Rao, Y., et al., *Development of a butterfly check valve model under natural circulation conditions*. *Annals of Nuclear Energy*, 2015. **76**: p. 166-171.
84. Ryan Burnett, D.C., Justin Tang, *Fluidic Diode Development and Optimization*. 2010, University of California, Berkeley. p. 36.
85. Kays, W.M. and A.L. London, *Compact heat exchangers*. 3rd ed. 1984, New York: McGraw-Hill. xv, 335 p.
86. Hesselgreaves, J.E., *Compact heat exchangers: selection, design and operation*. First ed. 2001: Access Online via Elsevier.
87. *Data for BPA Balancing Authority Total Load, Wind Gen, Wind Forecast, Hydro, Thermal, and Net Interchange*. 2012, Bonneville Power Administration: <http://transmission.bpa.gov/business/operations/wind/>.
88. Suzuki, K., J. Shimazaki, and Y. Shinohara, *Application of H Infinity Control Theory to Power Control of a Nonlinear Reactor Model*. *NUCLEAR SCIENCE AND ENGINEERING*, 1993. **115**: p. 10.
89. Xing Luo, X.G., Meiling Li, Wilfried Roetzel, *Dynamic behaviour of one-dimensional flow multistream heat exchangers and their networks*. *International Journal of Heat and Mass Transfer*, 2003. **46**: p. 11.
90. Sumner, T., *Effects of fuel type on the safety characteristics of a sodium cooled fast reactor*, in *Woodruff School of Mechanical Engineering*. 2010, Georgia Institute of Technology.
91. C.E. Boardman, A.E.D., M. Hui, K. Iwashige, *Containment performance of S-prism under severe BDB conditions* *INIS*, 2001. **33**(16).
92. Murray, R.M., Z. Li, and S. Sastry, *A mathematical introduction to robotic manipulation*. 1994, Boca Raton: CRC Press. 474.
93. Weaver, L.E., *Reactor Dynamics and Control*. 1968: American Elsevier Publishing Company.

94. Ferri, R., A. Cammi, and D. Mazzei, *Molten salt mixture properties in RELAP5 code for thermodynamic solar applications*. International Journal of Thermal Sciences, 2008. **47**: p. 1676-1687.
95. Alibaba. *Solar Salt*. Available from: https://www.alibaba.com/trade/search?fsb=y&IndexArea=product_en&CatId=&SearchText=solar+salt+fluid.
96. Hofman, G.L., et al., *Metallic Fuels Handbook*, D.o. Energy, Editor. 1985: Argonne, IL.
97. Fink, J.K. and L. Leibowitz, *Thermodynamic and Transport Properties of Sodium Liquid and Vapor*. 1995, Argonne National Laboratory.
98. Sabharwall, P., et al., *Molten Salts for High Temperature Reactors: University of Wisconsin Molten Salt Corrosion and Flow Loop Experiments – Issues Identified and Path Forward*. 2010.
99. A. E. Dubberley, A.J.L., C. E. Boardman, T. Wu. *SuperPRISM Metal Core Margins to Severe Core Damage*. in *ICONE 8*. 2000. Baltimore, MD.
100. Charles E. Boardman, A.E.D., T. Wu and K. Yoshida. *SuperPRISM Oxide and Metal Fuel Core Designs*. in *ICONE 8*. 2000. Baltimore, MD.
101. Charles E. Boardman, M.H., Douglas G. Carroll, Allen E. Dubberley. *Economic Assessment of S-PRISM Including Development and Generating Costs*. in *ICONE 9*. 2000. GE Nuclear Energy Division.
102. Boardman, C.E., et al. *A Description of the S-Prism Plant*. in *ICONE 8*. 2000. Baltimore, MD: ASME.
103. CRANE, *Flow of Fluids: Through Valves, Fittings and Pipe*. 2013: CRANE Co.
104. Hiroyuki OTA , K.K., Minoru Funato , Junzo Taguchi , Alan W. Fanning , Yoshihiro Doi , Nobuaki Nibe , Masahiro Ueta & Tatsutoshi Inagaki *Development of 160 m³/min Large Capacity Sodium-Immersed Self-Cooled Electromagnetic Pump*. Journal of Nuclear Science and Technology, 2004. **41**(4): p. 13.
105. Passerini, S., R. Ponciroli, and R.B. Vilim, *Impact of Active Control on Passive Safety Response Characteristics of Sodium-Cooled Fast Reactors: I—Theoretical Background*. Nuclear Technology, 2017. **199**(1): p. 1-15.
106. Ponciroli, R., S. Passerini, and R.B. Vilim, *Impact of Active Control on Passive Safety Response Characteristics of Sodium-Cooled Fast Reactors: II—Model Implementation and Simulations*. Nuclear Technology, 2017. **199**(1): p. 18.
107. Sun, P., et al., *Robust Control of Once-Through Canadian Supercritical Water-Cooled Reactors*. Nuclear Technology, 2017. **199**(1): p. 35-46.
108. Energy, G.H.N., *GE Hitachi Nuclear Energy PRISM Technical Brief*. 2013, General Electric Hitachi Nuclear Energy.
109. London, R.K.S.a.A.L., *Flow Forced Convection Heat Transfer and Flow Friction in Straight and Curved Ducts A Summary of Analytical Solutions*. 1971, Stanford University: Stanford, CA. p. 311.
110. Rappas, A.S., *Coal Compositions for Catalytic Gasification*, USPTO, Editor. 2009: United States. p. 9.
111. Abel, C., *Nuclear Powered Facility that Generates Consumable Fuels*, USPTO, Editor. 2012, US Patent 20,120,039,430: USA. p. 15.

112. Holcroft, P.C.a.G., *Plasma Resource Recovery Technology: Converting Waste to Energy and Valuable Products*, in *13th North American Waste to Energy Conference*. 2005, ASME: Orlando Florida. p. 71-79.
113. USPTO, *Patent App. No. 13/584,034*, C. Abel, Editor. 2015: U.S. p. 2.
114. USPTO, *Patent App. No. 13/210,518*, C. Abel, Editor. 2015: U.S.
115. Borchardt, R.W., *Potential Policy, Licensing, and Key Technical Issues for Small Modular Nuclear Reactor Designs*. 2010, U.S. Nuclear Regulatory Commission. p. 38.
116. Burkhart, J.A., *Ultra-High-Efficiency Engines and Corresponding Thermodynamic System*, USPTO, Editor. 2014, Burkhart Technologies, LLC: U.S. p. 48.
117. Cheremisinoff, J.R.a.N.P., *Gasification Technologies*, ed. H. Heinemann. 2005, Boca Raton, Fl: Taylor and Francis 336.
118. NRC, *NRC Vision and Strategy: Safely Achieving Effective and Efficient Non-Light Water Reactor Mission Readiness*. 2016, U.S. Nuclear Regulatory Commission. p. 25.
119. Johnson, M.R., *Insurance and Liability regulatory requirements for Small Modular Reactor Facilities*. 2011. p. 6.
120. Yandle, B., *The Political Limits of Environmental Regulation: Tracking the Unicorn*. 1989, Westpoint, Connecticut: Quorum Books. 180.